

A Position Optimization of a Powertrain Mounting System for a Commercial Vehicle in terms of Vibration Isolation

Submitted to the Graduate School of Natural and Applied Sciences
in partial fulfillment of the requirements for the degree of

Master of Science

in Mechanical Engineering

by

Sinan Yıldırım

ORCID 0000-0001-7008-8739

February, 2022

This is to certify that we have read the thesis **A Position Optimization of a Powertrain Mounting System for a Commercial Vehicle in terms of Vibration Isolation** submitted by **Sinan Yıldırım**, and it has been judged to be successful, in scope and in quality, at the defense exam and accepted by our jury as a MASTER'S THESIS.

APPROVED BY:

Advisor: **Prof. Dr. Mehmet Çevik**
İzmir Kâtip Çelebi University

Committee Members:

Assoc. Prof. Levent Aydın
İzmir Katip Çelebi University

Assist. Prof. Dr. Saim Kural
Manisa Celal Bayar University

Date of Defense: February 03, 2022

Declaration of Authorship

I, **Sinan Yıldırım**, declare that this thesis titled **A Position Optimization of a Powertrain Mounting System for a Commercial Vehicle in terms of Vibration Isolation** and the work presented in it are my own. I confirm that:

- This work was done wholly or mainly while in candidature for the Master's degree at this university.
- Where any part of this thesis has previously been submitted for a degree or any other qualification at this university or any other institution, this has been clearly stated.
- Where I have consulted the published work of others, this is always clearly attributed.
- Where I have quoted from the work of others, the source is always given. This thesis is entirely my own work, with the exception of such quotations.
- I have acknowledged all major sources of assistance.
- Where the thesis is based on work done by myself jointly with others, I have made clear exactly what was done by others and what I have contributed myself.

Date: 24.01.2022

A Position Optimization of a Powertrain Mounting System for a Commercial Vehicle in terms of Vibration Isolation

Abstract

Controlling vibration on vehicles have been one of the most popular issues in automotive sector for durability and customer satisfaction. Likewise, a powertrain mounting system (PMS) is one of the main systems to be studied for vibration control in a vehicle. That is used both for the connection of the powertrain system to the vehicle body and for the isolation of engine-induced vibration. Sometimes, it may not be an economical solution to provide a mount configuration with different stiffness and damping values for each different engine-transmission group. Therefore, the most suitable positioning of mount according to the static and dynamic loading conditions in a desired vibration isolation rate is the one that offers an economical alternative.

In this study, it is aimed to optimize the position of each engine-transmission mount within the PMS of a public bus considering static loading cases, roll mode frequency around the Torque Roll Axis (TRA), vibration transmissibility ratio and dimensional constraints in the early design phase of the bus.

Considering the approach of the study, a finite element (FE) model was first set and then validated by static and modal tests on a reference real public bus. Utilizing the validated FE model, a new PMS design for another public bus was investigated. Mount locations were randomly initialized provided that there will be no interference with other components within the vehicle. First analyses were conducted as pre-optimization calculations in terms of static and dynamic requirements of the study.

A Plackett-Burmann design was conducted as a Design of Experiment study using the pre-optimization results. The design was developed to screen the behavior of response functions by means of changing each location as a parameter.

Multi-Objective Genetic Algorithm was applied into pre-optimization FE model using the software Hyperstudy 2021.2. As a result of our study, the vibration isolation ratio of the PMS, which was 33% before the parametric optimization, was increased to 72%.

Keywords: Vibration control, parametric optimization, vibration transmissibility, powertrain mounting system, finite element analysis

Ticari Bir Aracın Güç Grubu Montaj Sisteminin Titreşim İzolasyonu Açısından Konum Optimizasyonu

ÖZ

Araçlardaki titreşimi kontrol etmek, otomotiv sektöründe dayanıklılık ve müşteri memnuniyeti için en çok aranan konulardan biri olmuştur. Aynı şekilde, bir güç aktarma montaj sistemi (PMS), bir araçta titreşim kontrolü için çalışılacak ana sistemlerden biridir. Bu, hem güç aktarma sisteminin araç gövdesine bağlanması hem de motor kaynaklı titreşimin izolasyonu için kullanılır. Bazen her farklı motor-şanzıman grubu için farklı sertlik ve sönüm değerlerine sahip bir takoz konfigürasyonu sağlamak ekonomik bir çözüm olmayabilir. Bu nedenle montajın statik ve dinamik yükleme koşullarına göre istenilen titreşim izolasyon oranında en uygun şekilde konumlandırılması ekonomik bir alternatif sunmaktadır.

Bu çalışmada, statik yükleme durumları, Tork Dönme Eksenini (TRA) etrafındaki yuvarlanma modu frekansı, titreşim geçirgenlik oranı ve erken aşamadaki boyutsal kısıtlamalar dikkate alınarak bir halk otobüsünün PMS'indeki her bir motor-şanzıman yatağının konumunun otobüsün ön tasarım aşamasında optimize edilmesi amaçlanmaktadır.

Çalışmanın yaklaşımı göz önünde bulundurularak, öncelikle bir sonlu elemanlar (FE) modeli kurulmuş ve daha sonra bu model referans gerçek bir halk otobüsü üzerinde statik ve modal testler ile doğrulanmıştır. Doğrulanmış FE modeli aracılığıyla, başka bir halk otobüsü için yeni bir PMS tasarımı araştırılmıştır. Montaj yerleri, araç içindeki diğer bileşenlerle etkileşim olmaması şartıyla rastgele başlatılmıştır. İlk analizler, çalışmanın statik ve dinamik gereksinimleri açısından ön optimizasyon hesaplamaları olarak yapılmıştır.

Ön optimizasyon sonuçları kullanılarak bir Deneysel Tasarım çalışması olarak Plackett-Burmann tasarımı yapılmıştır. Tasarım, her bir lokasyonun bir parametre olarak değiştirilmesine göre tepki fonksiyonlarının davranışının görüntülenmesini sağlayacak şekilde gerçekleştirilmiştir.

Hyperstudy 2021.2 yazılımı kullanılarak optimizasyon öncesi FE modeline Çok Amaçlı Genetik Algoritma uygulanmıştır. Çalışmamızın sonucunda, parametrik optimizasyon öncesi %33 olan PMS'nin titreşim izolasyon oranı, %72'ye yükseltilmiştir.

Anahtar Kelimeler: Titreşim kontrolü, parametrik optimizasyon, titreşim izolasyonu, güç aktarım organları, sonlu elemanlar analizi

For the Sake of the Butterfly Effect...

Acknowledgement

I am thankful to BMC Otomotiv San. ve Tic. A.Ş. for hardware, software and data support, to my supervisor Prof. Dr. Mehmet evik for any support, to my family, my friends, my team leader Ufuk oban, my colleagues, and to NVH test engineer Onur elikkan for motivational support during the thesis process.

Table of Contents

Declaration of Authorship	ii
Abstract	iii
Öz	v
Acknowledgment	viii
List of Figures	xii
List of Tables.....	xvi
List of Abbreviations.....	xvii
List of Symbols	xviii
1 Introduction	1
2 Mechanical Vibrations in the Automotive Industry	6
2.1 A Mechanical Vibration System.....	6
2.2 Modal Analysis of a Vibrating System.....	14
2.2.1 Frequency Response Functions (FRF) in Relation with Modal Analysis	17
2.2.2 Modal Decoupling	19
2.3 Vibration Control	19
3 The Role of the Powertrain System in Vibration Control	24
3.1 Internal Combustion Engine and Transmission as Vibration Sources.....	24
3.2 Powertrain Mounting System (PMS) as a Vibration Isolator	26
4 Finite Element Method	30
5 Design of Experiments and Parametric Optimization	32
5.1 Design of Experiments.....	32
5.2 Parametric Optimization	35

6	Materials and Methods	39
6.1	Materials	41
6.2	Methodology	41
6.2.1	Validation of the Finite Element Model	42
6.2.1.1	Finite Element Model of the Reference Powertrain System	48
6.2.1.2	Physical Test of the Reference Powertrain System	52
6.2.2	Pre-optimization Model Analysis for Conceptual PMS	60
6.2.2.1	Static Analyses	66
6.2.2.2	Modal Analysis	68
6.2.2.3	Transmissibility Analysis	68
6.2.3	DoE and Optimization Studies	70
6.2.3.1	DoE Study	70
6.2.3.2	Parametric Optimization	73
6.2.3.3	Post-Optimization Analyses	74
7	Results and Discussion	75
7.1	Validation Results of the Reference Powertrain System	75
7.1.1	FEA Results of the Reference PMS	75
7.1.1.1	Results of the Static Analysis	75
7.1.1.2	Results of the Modal Analysis.....	77
7.1.2	Physical Test Results	81
7.2	Pre-optimization Results of the Conceptual PMS	83
7.2.1	Results of the Static Analysis	83
7.2.2	Results of the Modal Analysis.....	85
7.2.3	Results of the Transmissibility Analysis	89

7.3 DoE and Parametric Optimization Results	90
7.3.1 DoE Results	90
7.3.2 Parametric Optimization Results	92
8 Conclusion.....	102
References	104
Curriculum Vitae	109

List of Figures

Figure 2.1	Scotch yoke mechanism [22]	10
Figure 2.2	Free vibration graph for $\xi \neq 0$	12
Figure 2.3	Effect of damping on resonance	13
Figure 2.4	Vibration control in powertrain system	19
Figure 2.5	Representation of the vibration isolator in terms of a vehicle	21
Figure 2.6	The transmissibility T_f curve in relation with frequency ratio “r” [22] ..	23
Figure 3.1	The local coordinate system for a powertrain system.....	25
Figure 3.2	A representation of engine mounts [28].....	26
Figure 3.3	A force versus displacement curve for an elastomeric mount [32].....	29
Figure 4.1	A spring model with 1 element and 2 nodes [46]	30
Figure 4.1	Element types for FEM [40].....	31
Figure 5.1	An I/O scheme of a design process [42]	32
Figure 5.2	Flowchart of MOGA [42]	37
Figure 6.1	Venn diagram of the study	40
Figure 6.2	The flowchart of the overall methodology	42
Figure 6.3	The flowchart of the FE model validation procedure	43
Figure 6.4	The reference commercial vehicle	44
Figure 6.5	The reference powertrain system and PMS highlighted	44
Figure 6.6	CAD image of the reference PMS.....	45
Figure 6.7	Nomenclature of the reference engine mounts.....	45
Figure 6.8	Axial static stiffness plot of the reference mount A of the engine side ..	47
Figure 6.9	Axial static stiffness plot of the reference mount B of the transmission side	48
Figure 6.10	Schematic representation of a PMS with 4 mounts.....	49

Figure 6.11 FE model of the reference PMS	50
Figure 6.12 Element types used in the FE model of the reference PMS	51
Figure 6.13 Reference powertrain lay-out	52
Figure 6.14 Triaxial accelerometer used for modal test	53
Figure 6.15 Accelerometer instrumentation for P ₁ , P ₂ and P ₃	54
Figure 6.16 Accelerometer instrumentation for P ₄	54
Figure 6.17 Accelerometer instrumentation for P ₅	55
Figure 6.18 Accelerometer instrumentation for P ₆	55
Figure 6.19 Accelerometer instrumentation for P ₇	56
Figure 6.20 Accelerometer instrumentation for P ₈	56
Figure 6.21 Accelerometer instrumentation for P ₉	57
Figure 6.22 Accelerometer instrumentation for P ₁₀	57
Figure 6.23 Accelerometer instrumentation for P ₁₁	58
Figure 6.24 Accelerometer instrumentation for P ₁₂	58
Figure 6.25 Impact hammer used for modal test	59
Figure 6.26 Calibration points for modal measurements	59
Figure 6.27 Nomenclature of PMS in optimization study	61
Figure 6.28 Determination of control volume according to conceptual design stage	62
Figure 6.29 Nomenclature of control volume	62
Figure 6.30 Axial static stiffness plot of the conceptual PMS for mount A of the engine side	65
Figure 6.31 Axial static stiffness plot of the conceptual PMS for mount B of the transmission side	65
Figure 6.32 FE model for static analysis	67
Figure 6.33 FE model for static analysis 2	67
Figure 6.34 FE model for modal analysis	68
Figure 6.35 FE model for FRF transmissibility analysis: Dynamic excitation node is shown with number 5	69
Figure 6.36 FE model for FRF transmissibility analysis	70
Figure 6.37 Parameter definition in Hyperstudy software	71
Figure 6.38 Internal relations among parameters defined in Hyperstudy software	72
Figure 6.39 Response functions	72
Figure 6.40 Objective functions for responses	73

Figure 7.1	Static analysis result for global X-axis of the reference PMS.....	75
Figure 7.2	Static analysis result for global Y-axis of the reference PMS.....	76
Figure 7.3	Static analysis result for global Z-axis of the reference PMS	76
Figure 7.4	Mode 1, Pitch at 4.45Hz.....	78
Figure 7.5	Mode 2, Trans-Y at 6.58Hz.....	78
Figure 7.6	Mode 3, Bounce at 7.64Hz.....	79
Figure 7.7	Mode 4, Trans-X at 8.13Hz.....	79
Figure 7.8	Mode 5, Yaw at 10.03Hz	80
Figure 7.9	Mode 6, Roll at 14.45Hz	80
Figure 7.10	Modal test results	82
Figure 7.11	Results for gravity loading case	84
Figure 7.12	Results for maximum torque loading case	84
Figure 7.13	Mode 1, Fore aft on Y-axis at 7.82Hz.....	85
Figure 7.14	Mode 2, Bounce on Z-axis at 10.49Hz	86
Figure 7.15	Mode 3, Pitch around Y-axis at 12.82Hz.....	86
Figure 7.16	Mode 4, Fore-Aft on X-axis at 13.25Hz	87
Figure 7.17	Mode 5, Yaw around Z-axis at 17.37Hz.....	87
Figure 7.18	Mode 6, Roll around X-axis at 24.59Hz	88
Figure 7.19	Transmissibility ratio vs. frequency plot.....	89
Figure 7.20	Transmissibility ratio vs. natural frequency of the roll mode	93
Figure 7.21	Comparison of optimal results according to all responses.....	94
Figure 7.22	Comparison of vibration isolation in terms of cumulative force reaction and the force reaction received by M_1	95
Figure 7.23	Comparison of vibration isolation in terms of cumulative force reaction and the force reaction received by M_2	95
Figure 7.24	Comparison of vibration isolation in terms of cumulative force reaction and the force reaction received by M_3	96
Figure 7.25	Comparison of vibration isolation in terms of cumulative force reaction and the force reaction received by M_4	96
Figure 7.26	Absolute reaction force distribution of M_1	98
Figure 7.27	Absolute reaction force distribution of M_2	98
Figure 7.28	Absolute reaction force distribution of M_3	99

Figure 7.29 Absolute reaction force distribution of M_4	99
Figure 7.30 Transmissibility ratio of the post-optimization analysis	101

List of Tables

Table 1.1	Percent contribution of vibration sources to total noise in a motor vehicle	2
Table 2.1	Damping ratio ξ for several arrangements in literature.....	9
Table 6.1	Mechanical properties of engine and transmission of the reference commercial bus	46
Table 6.2	Mechanical properties of rubberlike engine mounts.....	47
Table 6.3	Coordinates of calibration points for the modal test	60
Table 6.4	Positional limits of each control volume (units in mm).....	63
Table 6.5	Mount initial coordinates of selected hardpoints	63
Table 6.6	Mechanical properties of engine and transmission for the optimization model	64
Table 6.7	Mechanical properties of the engine mounts for the optimization model	64
Table 6.8	Loading scenarios for static analysis.....	66
Table 7.1	Absolute displacement results for standing loading case.....	77
Table 7.2	Modal analysis results for the reference PMS.....	81
Table 7.3	Comparison of test results with analysis outputs	82
Table 7.4	Comparison of modal analysis and modal test results	83
Table 7.5	Static analysis results	85
Table 7.6	Modal analysis results	89
Table 7.7	Correlation table between design variables and response functions	91
Table 7.8	Correlation table within response functions.....	92
Table 7.9	Coordinates of the best positional configuration of the PMS according to specs and scope of the study	100
Table 7.10	Percent change in responses by means of parametric optimization	101

List of Abbreviations

CG	Centre of Gravity
CV	Control Volume
DoE	Design of Experiments
DoF	Degree of Freedom
FEA	Finite Element Analysis
FEM	Finite Element Method
FRF	Frequency Response Function
MOGA	Multi-objective Genetic Algorithm
NVH	Noise Vibration and Harshness
PB	Plackett-Burman
PMS	Powertrain Mounting System
R&D	Research and Development
SDoF	Single Degree of Freedom
TRA	Torque Roll Axis

List of Symbols

c	Damping coefficient
x	Position [m]
k	Stiffness [N/m]
ω_n	Natural frequency [Hz]
F	Force [N]
m	mass [kg]
ξ	Damping ratio
ϕ	Phase angle [rad]
X_0	Amplitude [m]
r	Frequency ratio
T_f	Transmissibility ratio
rpm	revolutions per minute
f	frequency [Hz]

Chapter 1

Introduction

People's interest on controlling vibration started probably when the first musical instrument was invented. The inventor – who can be classified as a pioneer vibration engineer – managed how to vibrate the same material in different conditions. Then, s/he possibly recognized how to tune the vibration on a stretched skin or a string by performing some modifications on the musical instrument. Consequently, how a failure happens because of undesired vibration was also experienced.

Coming up with the contemporary life, vibration is still one of the captivating phenomena. People invest effort on controlling vibration to take precaution against earthquakes, mechanical failures in various machines and sound pollution. Similarly, mechanical vibrations are taken seriously in automotive industry as well.

Making improvement of mechanical vibrations in automotive sector is an effort of prevention against the initiation of any plastic deformation or fracture propagation due to the vibration on components on a vehicle, which ends up with a failure of those components. Moreover, an enhancement on noise and harshness – which are associated with vibration – helps engineers prevent potential accidents by increasing and facilitating the driver's focus on the road. Therefore, Noise, Vibration and Harshness (NVH) are combined as a discipline to increase safety in various systems, sub-systems and component of a vehicle.

Beyond the mechanical concerns, NVH performance of a vehicle directly affects the sales and aftermarket in automotive industry. The majority of people would prefer more comfortable travel in any case. Whole body vibration may cause adverse effects on several failures in either micro or macro levels in human body, which is proven by relevant studies [1]. For instance, the natural frequency of a seated human body is

between 4-8Hz [2] and if one of the natural frequencies of the vehicle coincides with the body modal frequency, then passengers may experience nausea due to the resonance. In another aspect, if the steering wheel is vibrated more than driver can bear up, then sales of the vehicle may not hit the market. For NVH characteristics of a vehicle, there are international regulations and standards to be applied [3].

There are two important sources of vibration in motor vehicles. One is the engine-transmission couple built within the powertrain system and the other is the vibration transmitted from the tires to the vehicle body due to the road profile [4]. In a motor vehicle, percent contribution of vibration sources to total noise is shown in Table 1.1 [5].

Table 1.1: Percent contribution of vibration sources to total noise in a motor vehicle

#	Source	% Contribution
1	Engine	22 to 30
2	Exhaust System	25 to 35
3	Intake system	5 to 15
4	Fan and cooling system	7 to 15
5	Transmission	12 to 15
6	Tyres	9 to 15

Engine-induced vibration is caused by gas pressure and unbalanced forces [6]. There are two ways of how engine-induced vibration is propagated: One is the direct transfer to the system equipment which are mechanically in contact with the powertrain of a vehicle which is called structure-borne vibration. The second is air-borne vibration [7].

Controlling vibration by directly regulating vibration sources in a vehicle may not be always an easy solution. For example, as a vibration source in vehicles, regulating the vibration characteristics of the engine according to different vehicles will not be a budget and easy solution. Instead, improvements can be made on powertrain mounting systems. Therefore, positioning a vibratory equipment within a vehicle becomes a complex problem.

What is more, the geometric integration of a vehicle may not always allow engineers to design a system in ideal conditions since there might be geometrical interactions among systems of a vehicle, which is ended up with that some components might not be located in a desired place. Considering this possibility of interaction, it is actually challenging to ideally design and position each system, sub-system or component within a vehicle. For instance, geometrically offset engine mounts may alter the performance of the corresponding system in terms of static and dynamic characteristics. This may lead engineers to work on several neighboring systems more such that

- A more expensive powertrain mounting system may be chosen.
- A stiffer chassis design may come up.
- Dynamic characteristics of cabin suspension system may need to be enhanced (for trucks).
- Different types of noise isolators may be invested on the vehicle.
- Steering wheel may be redesigned in terms of vibration control.

Therefore, how the connection between the engine and the chassis is done is one of the important factors to be considered at the early stage of a vehicle design [8].

Positioning engine mounts in a proper place is a remarkable duty in terms of NVH since an exceeding level of vibration may cause failures in any kind of equipment on a vehicle by resonating them or by vibration fatigue. Thanks to a proper positioning of engine mounts in a vehicle, the distribution of kinetic energy, reaction forces & moments and the level of vibration transmitted to other sub-systems of the vehicle can be kept in desired levels. In order to achieve a good result, the mounting system should be evaluated in terms of both static and dynamic characteristics of the powertrain system [7].

Considering the concerns told above, the aim of this study is to position the Powertrain Mount System (PMS) of a commercial vehicle at the most suitable location to assemble the engine-transmission group to the chassis regarding NVH parameters of the mount reaction forces, natural frequency and transmissibility targets, in a way that vehicle integration can be preserved at the same time.

The current literature reveals that the main approach to vibration isolation system design is through analysis and optimization techniques [9, 10, 11, 12, 13, 14, 15].

In the study of Karagöz et al., powertrain mount system was investigated via MSC Adams, which is a Multi Body Dynamics software. An optimization study was performed in terms of the positions of the mounts. Moreover, different damping ratio and stiffness values were also investigated within the optimization in order to achieve desired levels of natural frequency, kinetic energy distribution. By this, transmissibility of the system reduced as much as possible, which was specified as an enhanced vibration performance was seen in the finished vehicle [7].

In the study of Erdelyi et al., the powertrain mount positions and stiffness values of a vehicle were investigated at the early design stage of the vehicle. The optimization was performed in order to determine the best values for position and stiffness values [8].

In the study of Ooi et al., for a two-stroke engine, the optimum positions and orientation angles of each engine mount was determined by a process of dynamic optimization which was associated with the minimum force transmissibility over a range of frequency. According to the optimization process of the study, there seen 45% reduction in the mean force transmissibility in the vertical direction [16].

In the study of Naseri et al., an optimization approach to a PMS was introduced. Based on Torque Roll Axis (TRA), modal shapes of the engine-transmission group having 6 degree of freedom (DoF) were tried not to coincide with the idle frequency of the engine. By the optimization approach set up with the genetic algorithm, PMS was repositioned and stiffness values were enhanced regarding the system specs. Setting up the optimization process, the laminating positions were taken into the account because of the geometric integration of the vehicle within which a control volume can be logically created. According to the output of the study, transmitted force was reduced 50% compared with the base design. However, the geometric limits of repositioning mounts restrained the ideal decoupling of modal shapes [17].

Jeong and Singh performed an optimization approach of engine TRA decoupling method. Providing an analytical solution for a complete decoupling of TRA mode, they investigated that decoupling only TRA mode was enough to decouple the

complete system. The author also revealed the necessary condition of decoupling and analytical solution satisfied the overall study [18].

Xu et al. verified an optimization approach using genetic algorithm and fusion robustness analysis. Considering decoupling rate and modal frequency of mounts in each direction as objective function, stiffness of three mountings were optimized according to the objective function. Testing the optimized configuration with the base design, vibration noise test data demonstrated that the performance of the vibration isolation system was remarkably improved more than 10% [19].

Liang et al. proposed an optimization study of which the natural frequency of the powertrain mounting system was used as the objective function while translational stiffnesses of the mount was taken as a design variable of the optimization problem. Using Sequential Quadratic Programming algorithm, the output of the optimization process revealed that the maximum natural frequency was less than the excitation frequency, which was $f_{idle}/\sqrt{2}$. The optimization process was found sufficient as the objective function was satisfied [20].

Rossi de Sa et al. studied a sensitivity analysis of small deviations in positioning for PMS. Different types of mounts were interacted with the study and the model allowed to analyze different mounting configurations. Results showed the variations in stiffness, damping and positions of each mount, which may have caused a remarkable impact in the system. Consequently, an appropriate configuration was selected considering the dynamic behavior of the engine-transmission group and the vehicle [21].

Chapter 2

Mechanical Vibrations in the Automotive Industry

In automotive industry, NVH performance of a vehicle affects the performance of durability, maintenance, comfort, and sales of the vehicle. In this section, the concept of vibration and its control is discussed.

2.1 A Mechanical Vibration System

A system is vibrated when its potential energy is transmitted into kinetic energy and vice versa. If the system is damped, some percent of the current energy is transmitted into other types of energy such as heat and sound. This occurrence reduces the total mechanic energy of the system which must be maintained by an external energy source so that the system can work in steady cyclic vibration [22].

Vibrating systems are characterized by their degrees of freedom. The number of degrees of freedom (DoF) of a system is determined by the minimal number of independent coordinates necessary to determine all system locations at all moments. A simple pendulum and a single spring-mass system are examples of a single DoF (SDoF) system. In an SDoF system, all motion is bounded to the only independent parameter (radial or linear). The greater DoF a system has, the greater number of independent parameters is evolved in the system. Coming up with multi DoF systems, an engine of a vehicle –for instance– as a non-deformable rigid body can be considered having six DoF [7].

The motion of a vibrating system can be mathematically characterized using time-dependent coordinates or generalized displacements. Differential equations of motion govern these coordinates, which are derived from fundamental physical laws such as Newton's laws. Dynamic characteristics of a vibrating system can be visualized by a general second order differential equation of motion, which is

$$m\ddot{x}(t) + c\dot{x}(t) + kx(t) = F(t) \quad (2.1)$$

where x, \dot{x}, \ddot{x} represent displacement, velocity, acceleration, respectively and define the state of the system. $m, c,$ and k are system parameters that denote the mass, damping coefficient, and stiffness of the spring, in order, and $F(t)$ is the input excitation force operating on the mechanical vibration system.

A mass element describes total mass and moment of inertia of a system –which associates to the difficulty of a body starting from rest or changing velocity– as a function of the vehicle's position. In conjunction with the center of gravity (CG), the mass element is inextricably linked to a system's fundamental properties, as it affects the system's mechanical energy. The mass matrix of a system has a direct effect on inertial forces in all translational and rotational directions. Therefore, the system acts differently in terms of NVH characteristics if the mass matrix is changed [22, 23, 24].

Considering a system in real life, it may not always be easy to inspect the mass matrix in regards to complex systems such as heavy machines or an engine. Measurements such as determination of CG, moment of inertia and mass properties of a system should be taken seriously in industry since those affect many outputs of a project such as fuel consumption, durability, manufacturability, NVH characteristics, etc. [22, 23, 24].

A spring element is a form of mechanical connection that is considered to have minimal mass and damping in most applications. The spring constant “ k ”, which is also described as stiffness, exists whether there is a spring or not in a system. Any component within a system has its own stiffness matrix described with 6 DoF.

A spring is assumed to be linear according to the Hooke's Law shown in equation (2.2) where

$$F = kx \quad (2.2)$$

Damping refers to the phenomenon by which the vibrational energy is eventually transformed to heat or sound. Although the quantity of energy transferred to heat or sound may be negligible, damping becomes critical for an accurate forecast of vibration response of a system. The damping coefficient “c” should be determined for each individual system.

Natural frequency, alternatively referred to as eigenfrequency, is the frequency at which a system oscillates in the absence of any driving or damping force. The normal mode is the motion pattern of a system oscillating at its inherent frequency. Consequently, each member of the system oscillates sinusoidally at the same frequency. If an external force is applied to an oscillating system at the frequency at which the amplitude of its motion is highest, this frequency is referred to as the resonant frequency. Additionally, this phenomenon also occurs at neighboring frequencies of the natural frequency of the system. Therefore, considering the automotive industry, it is desired to avoid from resonance frequency.

Considering that natural frequency (ω_n) and damping factor (ξ) are dependent properties of a mechanical vibration system, they are calculated based on physical parameters, specifically mass, stiffness, and damping coefficients. These two parameters are proper to visualize the behavior of a vibration system.

$$\omega_n = \sqrt{\frac{k}{m}} \quad (2.3)$$

$$\xi = c/2m\omega_n \quad (2.4)$$

Substituting equation (2.3) and (2.4) into equation (2.1), it becomes,

$$\ddot{x} + 2\xi\omega_n\dot{x} + \omega_n^2x = F_{(t)}/m \quad (2.5)$$

Considering literature knowledge, equivalent viscous damping ratio exists for some materials and conditions specified in Table 2.1.

Table 2.1: Damping ratio ξ for several arrangements in literature [22]

Structural Arrangement	Equivalent Viscous Damping Ratio, (%)
Welded Design	1-4
Bolted Connection	3-10
Steel Frame	5-6
Unconstrained viscoelastic layer on steel-concrete girder	4-5
Constrained viscoelastic layer on steel-concrete girder	5-8

For $\xi = 0$ and $F_{(t)} = 0$, a free vibration of an undamped SDoF system can be visualized by the Scotch Yoke Mechanism, which is a good example for the demonstration of a harmonic behavior of the vibration (Figure 2.1). A crank with a radius of A spins around the point O in this mechanism. The other end of the crank, P , is inserted into a slotted rod that reciprocates within the vertical guide R . When the crank rotates at an angular velocity v , the slotted link's end point S and therefore the spring-mass system's mass m are displaced by an amount x from their middle locations (in time t) given by

$$x = A \sin\theta = A \sin \omega t \quad (2.7)$$

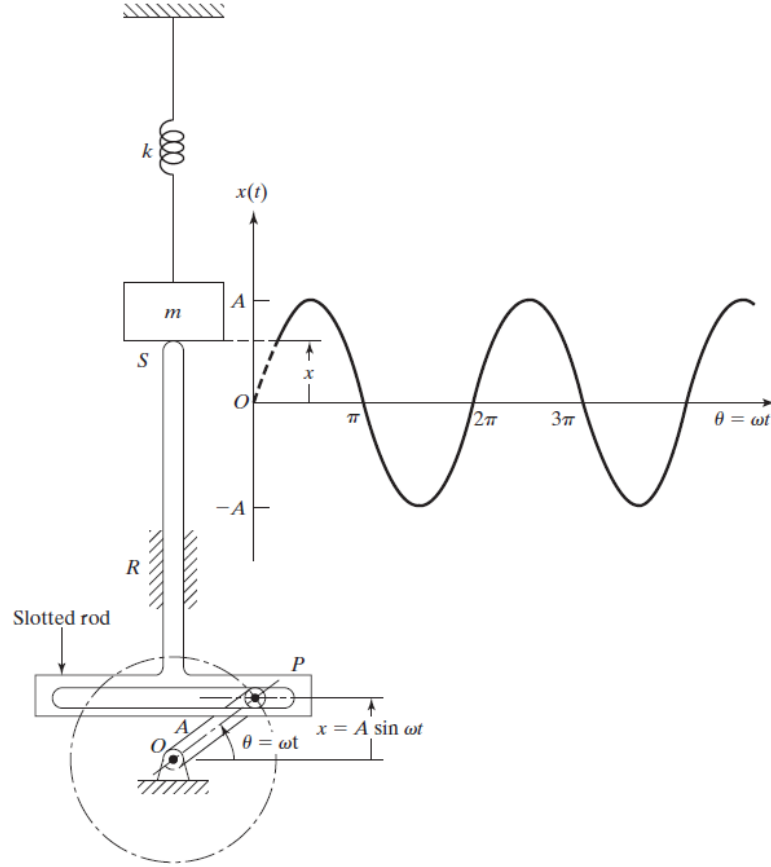


Figure 2.1: Scotch Yoke mechanism [22]

Therefore, recalling equation (2.5), the equation of motion in this situation becomes

$$m\ddot{x}(t) + kx(t) = 0 \quad (2.8)$$

While there is an initial displacement $x(0) = x_0$. Equation (2.8) leads to the eigenvalue problem assuming $x(t) = ue^{i\omega t}$.

$$\omega^2 mu = ku \quad (2.9)$$

Equation (2.9) promotes n eigenvalues:

$$\det(-\omega_k^2 m + k) = 0 \quad (2.10)$$

where ω_k refers to the natural frequencies of the system. In accordance with ω_k , the eigenvector \vec{u}_k denotes a certain distribution of displacements and is referred to as the

mode shape. Coming up with the pair (ω_k, \vec{u}_k) defining k^{th} mode of vibration of the system by:

$$x_k(t) = (A_k \sin \omega_k t + B_k \cos \omega_k t) \vec{u}_k \quad (2.11)$$

Undamped vibration is a purely theoretical term due to the inevitability of damping [25].

On the other hand, if $\xi > 0$ and $f_c(t) = c\dot{x}(t)$ where “ c ” is damping coefficient in kg/s, the viscously damped system appears as denoted in equation (2.1). Assuming $x(t) = Ae^{\lambda t}$ and $F(t) = 0$ for the free vibration of an underdamped system, the characteristic equation becomes

$$m\lambda^2 + c\lambda + k = 0 \quad (2.12)$$

The roots of the system become

$$\lambda_{1,2} = -\xi\omega_n \pm i\sqrt{1 - \xi^2}\omega_n \quad (2.13)$$

For $0 < \xi < 1$, the roots are complex; therefore, the response of the system is

$$x(t) = e^{-\xi\omega_n t} (A \sin \omega_d t + B \cos \omega_d t) \quad (2.14)$$

A and B are the terms determined by initial conditions. Moreover, the term ξ and ω_n are combined by the expression denoted beneath to give frequency of damped oscillation “ ω_d ”.

$$\omega_d = \omega_n \sqrt{1 - \xi^2} \quad (2.15)$$

If $\xi > 1$, then the system is overdamped since both roots are real and negative. In this case, amplitude of the system decays with no oscillation (Figure 2.2).

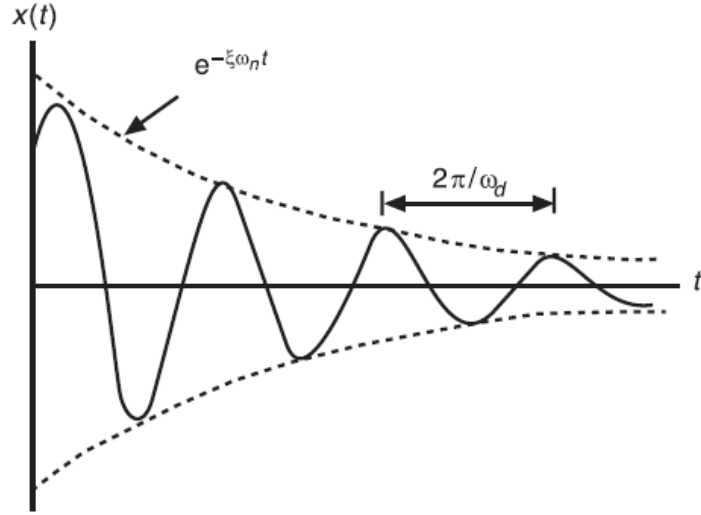


Figure 2.2: Free vibration graph for $\xi \neq 0$

Coming up with a forced vibration, the forced vibration is the motion of a vibrating system caused by external forces. A forced vibration generally has two components: a transient reaction that fades away and a steady-state response that persists after the brief response fades away [26].

Considering a SDoF system, which is denoted as

$$m\ddot{x}(t) + c\dot{x}(t) + kx(t) = F_0 \sin \omega t \quad (2.16)$$

where ω is the excitation frequency or forcing frequency; moreover, the system's steady-state response $x_{ss}(t)$ is considered sinusoidal,

$$x_{ss}(t) = X_0 \sin(\omega t + \phi) \quad (2.17)$$

Substituting equation (2.17) into equation (2.16) so that the amplitude and the phase angle could be found:

$$X_0 = \frac{F_0}{k} \frac{1}{\sqrt{(1-r^2)^2 + 4\xi^2 r^2}}, \quad \phi = \tan^{-1}\left(\frac{2\xi r}{1-r^2}\right) \quad (2.18)$$

where “r” is the frequency ratio $r = \omega/\omega_n$. As the excitation approaches the undamped natural frequency, the amplitude increases. The peak increases with decreasing damping ratio. Coming up with the underdamped case, the amplitude becomes

$$x(t) = e^{-\xi\omega_n t}(A \sin \omega_d t + B \cos \omega_d t) + X_0 \sin(\omega t + \phi) \quad (2.19)$$

Equation (2.19) resembles equation (2.14) in terms of the transient response since larger values of t makes the equation converge to zero.

Without damping, the amplitude given in the equation (2.18) approaches infinity; see Figure 2.3. The unbounded response is termed “resonance”, and the resonance condition is $\omega = \omega_n$. However, the expression in equation (2.17) cannot represent the steady increase in amplitude.

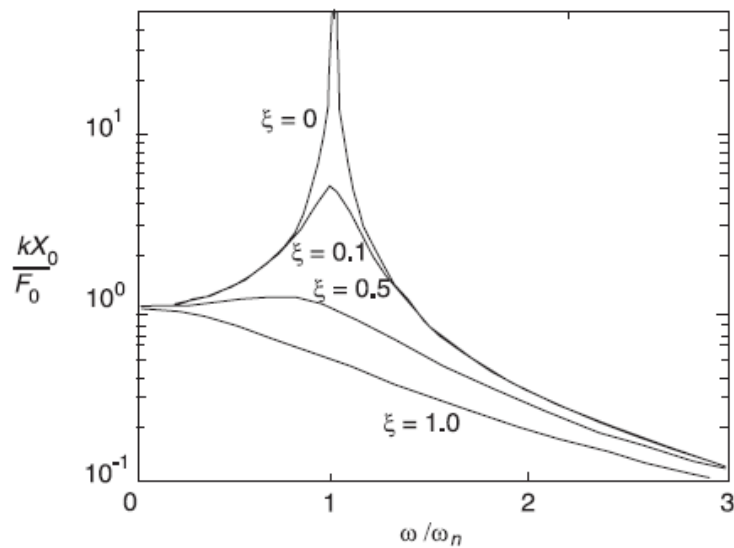


Figure 2.3: Effect of damping on resonance

The resonant response to the harmonic excitation $F_0 \sin \omega_n t$ is:

$$x(t) = \frac{F_0}{2m\omega_n} t \sin \omega_n t \quad (2.20)$$

In real life, the amplitude cannot expand since the spring is broken after a certain amount of deflection.

In a wide variety of engineering applications, the control of resonant vibration is essential. Among the methods for resonance control that are often employed are the following:

- passive or active dampening, which lowers resonance peaks (see Figure 2.3, ratio r);
- frequency tuning, in which natural frequencies are shifted away from stimulation frequencies; and
- dynamic vibration absorption, in which the vibration energy is contained inside an additional vibrating subsystem called a vibration absorber.

2.2 Modal Analysis of a Vibrating System

Modal analysis is a computational way for comprehending the dynamics of a vibrating system through the characteristic eigenvalues and eigenvectors [27]. By this, fundamental properties of a vibrating system, such as natural frequencies, damping factors, and mode shapes can be determined, which help engineers develop models in design and problem-solving abilities. There are some advantages that modal analysis provides, described beneath [26]:

- **Structural modification:** Modal analysis provides engineer a comprehension on structural modification by simulation and predictions of dynamic characteristics of a structural design. Therefore, changes in mechanical and geometric properties in design stage is allowed to be altered by modal analysis.
- **Sensitivity analysis:** A sensitivity analysis can be performed with respect to modal analysis in order that which physical change can be most effective to a suggested modal parameter change like shifting a natural frequency. Considering this, the sensitivity analysis is directly related with the structural modification.

- **Forced response prediction:** Another aspect is that prediction of vibration responses to a given force can be calculated performing modal analysis. For instance, considering that the vehicle's modal model is known, vibration measurements on the test track can be used to forecast the vehicle's response on the track prior to driving. The superposition concept can also be used to forecast the reaction to many forces. Often, the challenge with this application is precisely calculating or quantifying the forces.
- **Force identification:** In reality, the forces that cause a system to vibrate are not always measurable. However, they may be identified using response measurement and a system's modal model. Identification of forces that causes significant vibration is critical in some applications. For example, a loose bearing inside a turbine engine may generate an excitation force that results in excessive vibration. Additionally, this excitation force has the potential to cause catastrophic structural collapse.
- **Response prediction:** For a modal model of a structure, it is possible to predict its reaction to any coalition of input forces. This establishes a scientific foundation for the investigation of structural integrity in a known dynamic environment. When structural vibration responses take the form of dynamic strain, response prediction can be extremely useful in forecasting the fatigue life of the structure. A modal model derived experimentally typically includes damping parameters for a structure, which are critical for proper response prediction.
- **Vibration control:** Traditionally, a vibration control procedure is relied on a credible vehicle model to deduce control laws from observers. On the other hand, as each different system is unique on its own, it is critical for vibration control of a vehicle as a structure to have an accurate mathematical model that denotes its dynamic features. Being a thesis statement of this study, a novel way for vibration control can be proposed using modal analysis and its variances.

Modal analysis depends on the existence of a specific orthogonality within eigenvectors (mode shapes) of a system. This orthogonality is used to decouple the

actual equations of vibration into a group of independent differential equations. The solution of the decoupled equations results in a sequence of system eigenvectors containing the response. This method is often referred to as “modal expansion” or “eigenfunction expansion”. The fundamental idea of modal analysis is discussed as follows:

Initially, considering an undamped vibration system with distinct mass and stiffness matrices, eigenvectors denoted by $x_{(t)} = \vec{u}e^{i\omega t}$ share the orthogonality:

$$\vec{u}_k^T M \vec{u}_l = 0 \text{ and } \vec{u}_k^T K \vec{u}_l = 0 \text{ for } k \neq l \quad (2.21)$$

Typically, eigenvectors fulfilling the above relations are referred to as orthogonal or normal modes. The eigenvectors can be normalized in the following manner, which is called normalization factor:

$$\vec{u}_k^T M \vec{u}_k = 1 \quad (2.22)$$

The orthogonal relations open a proper path to demonstrate a dynamic response of arbitrary excitations. Giving an example, let the solution be denoted by a series of system eigenvectors:

$$x(t) = \sum_{k=1}^n q_{k(t)} \{\vec{u}_k\} \quad (2.23)$$

where $q_{k(t)}$ are called modal coordinates. The equation (2.23) demonstrates a real transformation from global coordinates to modal coordinates for each instance. Substituting equation (2.23) into the undamped equation of vibration using the orthogonal relations denoted in equation (2.21) and normalization factor denoted in equation (2.22), there combine n independent second-order differential equations:

$$\ddot{q}_k(t) + \omega^2 \dot{q}_k(t) = \vec{u}_k^T f(t), \quad k = 1, 2, \dots, n \quad (2.24)$$

which can be determined by various methods. Thanks to a determined $q_k(t)$, a closed-form modal expansion of the overall response can be stated by equation (2.23).

Secondly, considering a damped vibration system, the system is proportionally damped if $\mathbf{KM}^{-1}\mathbf{C} = \mathbf{CM}^{-1}\mathbf{K}$ is satisfied. Eventually, demonstrating the orthogonality and satisfying $\bar{\mathbf{u}}_k^T \mathbf{C} \bar{\mathbf{u}}_l = 0$ for $l \neq k$, the modal expansion denoted in equation (23) can be directly implemented to decouple the equation of damped vibration system:

$$\ddot{q}_{k(t)} + 2\xi_k \omega_k \dot{q}_{k(t)} + \omega_k^2 q_{k(t)} = \bar{\mathbf{u}}_k^T \mathbf{f}(t), \quad k = 1, 2, \dots, n \quad (2.25)$$

where ξ_k is called ‘‘modal damping ratio’’. The equation (2.25), which promotes the proportionally damped condition, is valid only if eigenvalues are complex but eigenvectors are real. In contrast, if the vector equation $\mathbf{KM}^{-1}\mathbf{C} = \mathbf{CM}^{-1}\mathbf{K}$ is not satisfied, both eigenvalues and eigenvectors are complex. Therefore, the system is called non-proportionally damped in that case. Furthermore, complex modes may cause gyroscopic forces induced by mass transport or Coriolis acceleration and circularity forces [25]. Such forces are usually assumed as non-orthogonal which cause a collapse in linear modal expansion. In that sense, a complex modal analysis must be performed, which is not dealt in this study.

2.2.1 Frequency Response Functions (FRF) in Relation with Modal Analysis

Considering a SDoF vibration system, the system reaction to a harmonic force $f(t) = F(\omega)e^{i\omega t}$ is $x(t) = X(\omega)e^{i\omega t}$, where $X(\omega)$ is a complex amplitude. By substituting them into the structural damping model's equations of motion, we get the following ratio:

$$\frac{X(\omega)}{F(\omega)} = \frac{1}{k - \omega^2 m + jc} \quad (2.26)$$

This ratio, indicated as $\alpha(\omega)$, is the system's frequency response function (FRF). The FRF is defined as the ratio of force to reaction. When damping is zero, the complex FRF function becomes real.

Displacement is used as the response of the defined FRF. Additionally, the vibration response can be in the form of velocity or acceleration. By substituting velocity and acceleration for the displacement response into FRF, mobility (velocity per unit force) and Accelerance (acceleration per unit force) can be defined as follows:

$$\text{Mobility FRF for structural damping: } Y(\omega) = \frac{\dot{X}(\omega)}{F(\omega)} = \frac{j\omega}{k - \omega^2 m + jc} \quad (2.27)$$

$$\text{Accelerance FRF for structural damping: } A(\omega) = \frac{\ddot{X}(\omega)}{F(\omega)} = \frac{-\omega^2}{k - \omega^2 m + jc} \quad (2.28)$$

Considering equation (2.26), equation (2.27) and equation (2.28), it can be seen that they are interchangeable. $\alpha(\omega)$, $Y(\omega)$ and $A(\omega)$ are complex functions of frequency. Their amplitudes have the relationship $|A(\omega)| = \omega|Y(\omega)| = \omega^2|\alpha(\omega)|$

FRFs of a vibration system can be used for proper physical significance and for modal analysis as a tool, which are:

$$\text{Dynamic stiffness: } \frac{1}{\alpha(\omega)} = \frac{\text{force}}{\text{displacement}} \quad (2.29)$$

$$\text{Mechanical impedance: } \frac{1}{Y(\omega)} = \frac{\text{force}}{\text{velocity}} \quad (2.30)$$

$$\text{Apparent mass: } \frac{1}{A(\omega)} = \frac{\text{force}}{\text{acceleration}} \quad (2.31)$$

Examining such equations, dynamic characteristics of a structural design can be enhanced and vibration can be controlled.

2.2.2 Modal Decoupling

Decoupling engine mounting system is a good starting point for proper vehicle design. In many publications, a high performance NVH characteristics requires a modally decoupled powertrain mounting system for 6 DoF, where the level of decoupling is associated with the kinetic energy distribution for each mode [18, 29, 30, 31].

Moreover, as the torque roll axis (TRA) is the major excitation axis for any kind of engine-transmission sub-system, the roll mode of any kind of powertrain mount system should be eliminated at the first step of the powertrain mounting system design [8].

2.3 Vibration Control

A vibration isolation system should be designed to control the vibration source so that a feasible level of vibration can be achieved. By this, the rest of the system can experience a minimal vibration transmitted from the vibration source [32]. It is good to mention that the main vibration sources are engine and transmission in this study (Figure 2.4). Consequently, vibration isolation is inspected with respect to modal analysis and transmissibility ratio [33].

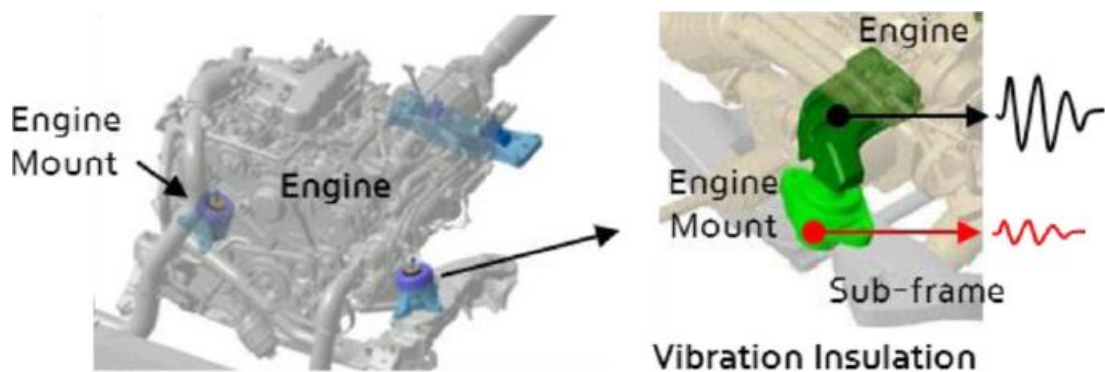


Figure 2.4: Vibration control in powertrain system

Since the vibration affects any component on the vehicle, a highly transmissible vibration isolator may cause additional engineering studies for other subsystems on

the vehicle (mirrors, interior trim components such as dashboard, steering column connection, cabin suspension, sheet metal cabin, doors and closures, etc.). Therefore, the vibration isolation system designed for the vibration source should be the least transmissible as much as it can be.

In general, the methods of how a vibration is controlled can be listed as follows [22]:

- Managing the system's natural frequencies and preventing resonance in response to external excitations.
- By including a damping or energy-dissipating mechanism, the system's reaction is prevented from becoming excessive, even at resonance.
- By using vibration isolators, reducing the transmission of excitation forces from one area of the machine to another.
- Modifying the system's reaction by including an auxiliary mass neutralizer or vibration isolator.

Vibration control is classified as active and passive in general. Active vibration control attempts to prevent the propagation of vibration generated by equipment into the surrounding environment. In contrast, the objective of passive control is to shield sensitive devices from external vibrations. For both classifications, the vibration source is surrounded by elastic supports, which is also called mounting systems. This is referred to the oscillatory system, which consists of the fundamental mass of the machine and its base, as well as the components (springs) that elastically support it [27]. It is good to mention that passive rubberlike vibration isolators are taken into the account in this study.

Vibration isolation is applied to systems in two different situations. The first situation refers to a system where the base of a vibration source is buffered against largely unbalanced forces. The second one is applied when a precision device is desired to buffer against structure-borne vibration transmitted from the base. For this study, the first situation is valid (Figure 2.5).

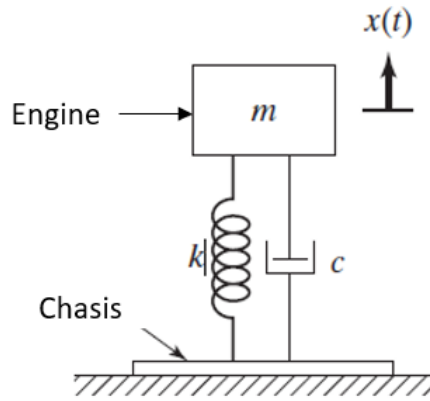


Figure 2.5: Representation of the vibration isolator in terms of a vehicle

Considering how the force transmitted to the chassis of the vehicle is to be reduced, here are the followings:

Bolting an engine directly to the chassis of a vehicle, the chassis is exposed to a harmonic load caused by the unbalanced force existing in the engine in addition to the static load caused by the engine's weight. Thus, an isolator (alternatively referred to as a resilient member) is mounted between the engine and the chassis to decrease the force transferred to the chassis. As shown in Figure 2.5, the system may then be idealized as an SDoF system. It is assumed that the isolator has both elasticity and damping characteristics.

Assuming the harmonic force is described by $F(t) = F_0 \cos \omega t$, the equation of motion of the vibrating engine can be expressed in terms of an underdamped SDoF vibration system. The steady-state determination of the system then becomes

$$x(t) = X \cos(\omega t - \phi) \quad (2.32)$$

where “X” and “ ϕ ” are

$$X = \frac{F_0}{\sqrt{(k - m\omega^2)^2 + \omega^2 c^2}}, \quad \phi = \tan^{-1} \frac{\omega c}{(k - m\omega^2)} \quad (2.33)$$

The force $F_t(t)$ transmitted to the chassis through the isolator is denoted by

$$F_t(t) = kx(t) + c\dot{x}(t) = kX \cos(\omega t - \phi) - c\omega X \sin(\omega t - \phi) \quad (2.34)$$

The magnitude of the transmitted force is

$$F_T = \sqrt{(kx)^2 + (c\dot{x})^2} = X\sqrt{k^2 + \omega^2 c^2} \quad (2.35)$$

The transmissibility of the isolator (T_f) is described by a ratio of the magnitude of the transmitted force to the magnitude of the exciting force, which is:

$$T_f = \frac{F_t}{F_0} = \sqrt{\frac{k^2 + \omega^2 c^2}{(k - m\omega^2)^2 + \omega^2 c^2}} \quad (2.36)$$

Knowing that “ r ” is the frequency ratio of the excitation frequency (idle frequency for the engine) of the engine to the natural frequency of the system, also denoted by $r = \omega/\omega_n$ as stated in equation (2.18), equation (2.36) becomes

$$T_f = \sqrt{\frac{1 + (2\xi r)^2}{(1 + r^2)^2 + (2\xi r)^2}} \quad (2.37)$$

So that the isolation phenomenon can be achieved, the force transmitted to the chassis should be less than the excitation force of the engine. As seen in Figure 2.6, the frequency ratio has to satisfy the condition $r > \sqrt{2}$ so as to achieve the isolation within the system. If $r = \sqrt{2}$, then neither isolation nor amplification happens. In the condition where $r < \sqrt{2}$, natural frequency of the system starts affecting the transmitted force which is resulted with the amplification of the transmissibility (Figure 2.6).

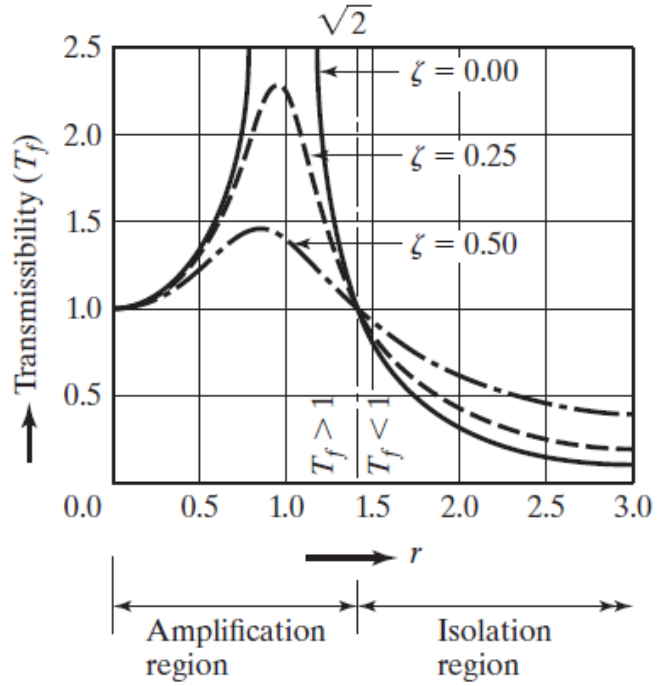


Figure 2.6: The transmissibility T_f curve in relation with frequency ratio “r” [22]

In another word, considering the TRA of the powertrain system of a vehicle, the target roll mode frequency has to be

$$f_{TRA} < \frac{f_{idle}}{\sqrt{2}} \quad (2.38)$$

where f_{TRA} is the roll mode frequency through the TRA and f_{idle} is the idle frequency of the engine.

Considering Figure 2.6 in terms of damping ratio, greater isolation values can be achieved as ξ increases while $r > \sqrt{2}$. In contrast, transmissibility increases as ξ increases while $r < \sqrt{2}$.

Lastly, transmissibility can also be approximated by the given equation below:

$$T_f \approx \frac{1}{r^2 - 1} \text{ or } r^2 \approx \frac{1 + T_f}{T_f} \quad (2.39)$$

Chapter 3

The Role of the Powertrain System in Vibration Control

A powertrain is an assembled system within a vehicle, which provides the kinematic properties of the vehicle. As a source of power generation, the system is combined with various subsystems providing vehicle to initiate and pursue motion, transmit the motion within it and suspend loads and vibrations to maintain the drive comfort as well as the durability of the vehicle. On the other hand, initiated and pursued motion causes vibration to be controlled. Therefore, in this section, the powertrain system is discussed in terms of engine-induced vibration control.

A powertrain system is composed of engine, transmission, driveshaft, axles, and differential. However, since engine, transmission and PMS are considered. These subsystems in terms of vibration control will be introduced in this section.

3.1 Internal Combustion Engine and Transmission as Vibration Sources

The engine is responsible for the majority of the vehicle's performance; therefore, it is critical to get familiar with its behavior prior to conducting vehicle research. Considering the engine as a vibration source, main causes of engine-induced vibration are [34, 35]

- Variable gas pressure stemming from combustion process
- Moment of inertia of equipment within the engine itself during translational and rotational motions

- Mechanical design of the engine, i.e. distribution of mass and CG

To prevent the system against excessive vibration, various components could be added onto engine-transmission and some enhancements could be generated on vibration characteristics of an engine by this operation [34, 35].

Dealing with the transmission, the purpose of the transmission is to transfer engine power to the vehicle's driving wheels [36]. The transmission involves the set of gears that modify the speed of the vehicle by changing gear ratio on the go. As the transmission is directly connected to the engine output, the mass and inertial matrix of the transmission as well as the CG become one of the leading factors in design and positioning it within the vehicle. Coupled with the engine, those factors lead engineer to handle with durability and vibration issues within engine room of the vehicle.

Cartesian coordinates are used for the powertrain as seen in Figure 3.1. X-axis is called the torque roll axis (TRA), on which the crank shaft rotates. Y-axis is placed in transverse direction of the engine. Consequently, Z-axis denotes the vertical positioning of the engine.

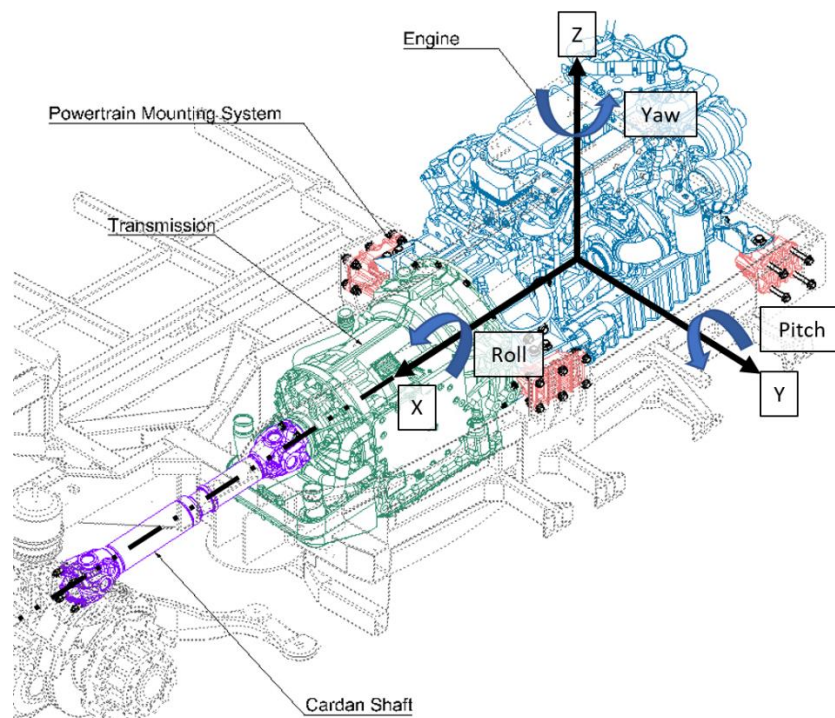


Figure 3.1: The local coordinate system for a powertrain system

Simulations on vibration responses of powertrain systems is very essential for the contemporary engineering approaches as powertrain systems are complex enough to estimate anything without any advanced calculation.

3.2 Powertrain Mounting System (PMS) as a Vibration Isolator

A PMS is a subsystem of the powertrain system and connects the system to the rest of the vehicle. In this way, PMS is a supporting sub-system by limiting the excessive displacements on powertrain and by isolating vibration excitation [17].



Figure 3.2: A representation of engine mounts [28]

Within the PMS, a mount (or more commonly engine mount) can be defined as a vibration isolator (Figure 3.2). The main purpose of the mount design is to reduce the dynamic response of the powertrain system under specified conditions of vibration excitation. Without any vibrational excitation coming from the vibration source, no mount can perform its function, but they only carry the static load of the powertrain system [22].

A mount performs resistance to deflection between the terminals in all translational and rotational directions and follows a non-linear stiffness. Each mounting within PMS has 6 DoF (3 translational and 3 rotational) [17, 23]. Having stiffness and damping matrix in three translational axes, the mathematical model of a mount can be set.

Mathematically modelling a mount, frequency range changes the approach. At a low-frequency range, the mass of the mount can be negligible as the greatest importance is vibration isolation. However, at the high frequency range, the body of the mount can be affected by vibration transmissibility and wave resonances. In that sense, the mass of the mount could be considered [23].

By a mathematical model, the minimum stiffness of a powertrain mount can be determined by the limit of elastic deformation of the mount according to different load cases, and the dynamic characteristics of the isolated object such as the idle frequency, the number of cylinders of the engine, weight, moment of inertia and CG of the engine and transmission. The maximum displacement of the vibration source induces shock loads such as rocking and this behavior of the system leads mounts to a reduction in bench life and to working out of isolation criteria [23].

During an impact motion, displacement may be larger in linear conditions, in which the mount may not handle such a large displacement. This may be resulted by neglecting the isolated vibration. To prevent this occurrence, instead of coming across any large displacement on mounts due to high acceleration, end stop bumpers are often positioned at the extreme points of a mount travel [32]. Consequently, a mount having this force versus displacement curve should be kept in the linear region.

Engine mounts can be designed according to active, semi-active and passive work principle. Active engine mounts can be controlled via a software and generates large actuating force. By this, a counter force occurs which results an active damping against the vibration. Semi-active mounts can handle the duty of vibration isolation by adjusting interior parameters of the mount such as damping in order to dissipate vibration energy. Hydrostatic and hydrodynamic properties can be applied into semi-active mounts. Passive engine mounts are the most common type in use. They work with specific damping and stiffness properties.

A passive engine mount consists of a resilient member (stiffness) and an energy dissipator (damping). Examples of passive isolators include metal springs, cork, felt, pneumatic springs, and elastomer (rubber) springs [22].

The material selection for the flexible components of vibration isolators is critical since it determines, to a great degree, the performance characteristics of the isolators. Here are main parameters affecting the material selection [37]:

- Ratio between dynamic and static stiffness
- Damping
- Frequency and amplitude dependencies of stiffness and damping
- Creep resistance
- Stability within the desired temperature range
- Flexibility in design and production

An elastomer is a natural rubber or a synthetic rubberlike polymer having elastoplastic mechanical properties [38]. Considering the material selection criteria, the reason why elastomeric materials are widely in use in engine mount systems is as beneath [7, 37, 38]:

- Elastomers can be easily molded in different shape configurations.
- They perform a remarkable energy absorption.
- Elastomeric mount can provide a wide range of stiffness and good stiffness tuning.
- They require relatively less space and weight.
- They provide more damping ratio than metallic springs.
- Inserting a metallic flange onto the rubber, they can be easily assembled to the vibration source.
- Lower cost.

Elastomeric mounts are usually manufactured in shape of cylindrical discs or rectangular prisms. The center of the mount is generally hollow, which provides an increase in dimension of mount without changing the stiffness. This feature allows the mount to resist against tilting [23].

Figure 3.3 shows a stiffness graph of an elastomeric rubberlike passive vibration isolator. The isolator, described by the graph, works reciprocally (compression and tension). Curved section designates the plastic deformation region which engineers should prevent to be within it.

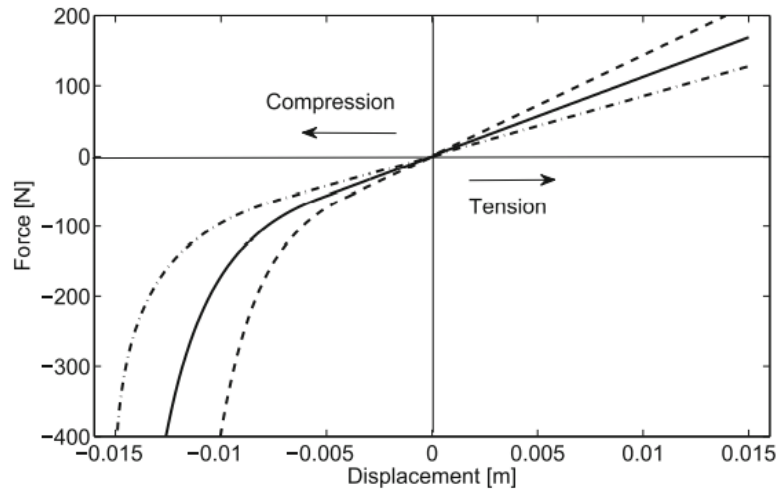


Figure 3.3: A force versus displacement curve for an elastomeric mount [32]

In machinery industry, mounts exist with a rated load in the range of 1-25 kN [23]. However, some special applications may require a different range of rated load.

Coming up with engine mount configuration, the positioning of the engine mount depends on the engineering calculations considering vibration and static characteristics of the vehicle [8]. The number of engine mounts is also associated with the static and dynamic characteristics of a powertrain. A PMS may involve 3-point, 4-point or more engine mounts.

The advantage of PMS with 4 engine mounts is that lower mount forces can be achieved respectively than PMS with 3 engine mounts. On the other hand, the drawback of the triple configuration is that they can be more expensive and more sensitive to mounting tolerances [8].

Triple configuration is often used in lightweight vehicles and gasoline-powered engines. On the other hand, ternary configuration is often used in large and diesel commercial vehicles [39].

Chapter 4

Finite Element Method

Without a doubt, investing significant time and money on prototyping and employing a trial and error strategy in current development activities is not cost effective. In the automobile industry, employing virtual simulations through the use of complex mechanical software is a typical practice. With this regard, the finite element method is a numerical technique used in engineering and mathematical physics to analyze systems. The finite element approach may be used to solve a variety of problems in engineering and mathematical physics, including structural analysis, heat transfer, fluid flow, mass transport, and electromagnetic potential.

When a geometric region is divided into a series of discrete and smaller parcels, each parcel is finite and called an element. Each element is connected to each other at discrete locations called nodes. Further, the finite element method is basically based on the relationship among nodes within an algebraic calculation.

As seen in Figure 4.1, a spring is modelled with 2 nodes and 1 element. The spring with the stiffness k and the length L is displaced from node 2. Developing a relationship between displacement and force gives the stiffness matrix given in Equation (4.1).

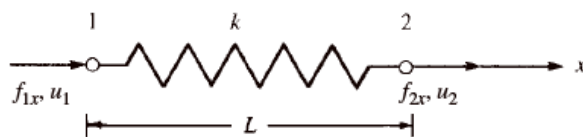


Figure 4.1: A spring model with 1 element and 2 nodes [46]

$$\begin{bmatrix} f_{1x} \\ f_{2x} \end{bmatrix} = \begin{bmatrix} k_{11} & k_{12} \\ k_{21} & k_{22} \end{bmatrix} \begin{bmatrix} u_1 \\ u_2 \end{bmatrix} \quad (4.1)$$

For a determined stiffness matrix [k], unknown reaction forces or displacement can be determined.

Different element types can be used in FE models shown in Figure 4.2. Increasing the number elements can increase the precision of the model as well as an increase occurs in computational cost.

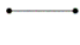





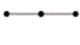

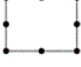

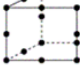

	1D Elements	2D (Shell) Elements		3D (Solid) Elements		
	Beams	Triangles	Quadrilaterals	Tetrahedrons	Hexahedrons	Pentahedrons
First Order Elements	 1-noded	 3-noded	 4-noded	 4-noded	 8-noded	 6-noded
Quadratic Elements	 3-noded	 8-noded	 8-noded	 10-noded	 20-noded	 12-noded

Figure 4.2: Element types for FEM [40]

Further, mass and rigid elements can be applied into a FE model. A mass element is a nodal element that involves the mass and inertial properties. This element is used in general to symbolize a component that is unnecessary to be modelled but its only function is mass and inertial properties.

A rigid element is an element of which stiffness matrix is extremely high. Therefore, this kind of rigid elements just transmit force from one node to another node with a negligible displacement [41].

Chapter 5

Design of Experiments and Parametric Optimization

5.1 Design of Experiments

In an actual environment of a system, there can be numerous design variables affecting the output. Controllable design variables can be included into a simulation-based design process. The more design variables are considered, the more accurate results can be achieved. In this way, the numerical model of the design evolves towards its original form. On the other hand, dealing with parameters that do not have a great effect on the design creates the so-called computational cost, which is an important constraint on the time criterion of the study. That's why the behavior of significant parameters in a design is studied with Design of Experiments (DoE).

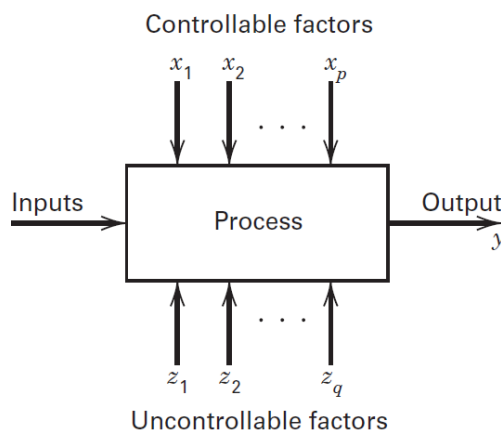


Figure 5.1: An I/O scheme of a design process [42]

As seen in Figure 5.1, a process or a system has both controllable and uncontrollable factors – which is also called noise– affecting the output performance. A process can generally be visualized as a combination of operations of machines, methods, or resources that transform inputs into outputs.

Knowing that experiments are generally performed to demonstrate the performance of a process/system, following questions can be answered by DoE study:

- Which design variables are most effective on response of the system?
- How are design variables set so that the response of the system can always converge to the desired level?
- How are design variables set so that minimum variance can be achieved in the response of the system?
- How are controllable design variables set so that uncontrollable variables affect system less?

In this regard, the DoE approach provides the number of design approaches and is classified according to the functional applications denoted beneath:

- DoE for Screening: It provides a main comprehension of the overall system such that which variable is changed according to which variable is observed. The screening provides the researcher to investigate the number of parameters to be reduced. However, screening DoE approaches have lower precision and may have relatively high computational cost. Main DoE approaches for screening are full factorial design, fractional factorial design and Plackett-Burman design.
- DoE for Response Surface Methodology: The purpose of DoE studies is to evenly distribute the design points in the design space in order to input into a fit technique for accurate prediction of the model behavior. The investigations are conducted using a limited number of parameters in order to produce higher order response surfaces. This fitting function may then be utilized for optimization, stochastic analysis, and rapid what-if analysis. Main DoE approaches for Response Surface Methodology are Box-Behnken design, Central Composite Design (CCD), Latin Hypercube Design, Hammersley and Taguchi Design.

This study deals with DoE for screening; therefore, it is beneficial to discuss the related technique.

Among DoE types for screening, the only type consisting three level design is the full-factorial design. Let's propose that n^k symbolizes the full factorial design where "n" is the level factor and "k" is the number of design variables as the power of level. Considering a lower number of design variables such as three, two-factorial design requires 8 experiments while three-factorial design requires 27 experiments. Having more design variables means more computational time for the full factorial design. Thus, if the number of design variable is, for instance, higher than three, screening may result a much higher computational cost.

Fractional factorial design is the fractional form of the full factorial design. A fractional design is one in which just a subset, or "fraction," of the runs in a full factorial design are conducted. Because fractional factorial designs need fewer runs than full factorial designs, they are a useful choice when resources are limited or the number of components in the design is considerable. Since a fractional factorial design employs a subset of the variables in a full factorial design, some of the main effects and two-way interactions are confounded and cannot be distinguished from the effects of other higher-order interactions. Typically, experimenters are ready to make a minor assumption about higher-order effects in order to obtain information on the main effects and low-order interactions with fewer runs.

Plackett-Burman (PB) designs are utilized for screening tests because they minimize the confounding effect of two-factor interactions on main results. For example, the PB design with 12 runs may be utilized for an experiment including up to 11 components. This means that PB design is by far the most economical way to screen design variables. The most apparent drawback of this design is that PB design cannot be used for 3 or a greater level design but only for 2 level design. The output of the PB design may not show the optimal solution but reveals the behavior of interaction between response functions and design variables.

5.2 Parametric Optimization

The concept "design optimization" refers to the use of a collection of mathematical processes that assists engineers in achieving the most flawless, functional, or effective design feasibly. Converting a design challenge to an optimization problem entails three processes. These are [45]

- Design variables are identified so that system parameters can be modified to enhance the system performance such as geometric dimensions, hard-point positions, stiffness and damping properties etc.
- Objective functions to be maximized or minimized are identified such as mass, displacement, reaction forces, natural frequency, cost, etc.
- Constraint functions are identified so that the system requirements are described in mathematical way. These functions constrain design variables.

According to the characteristics of the design variables, objective functions, and constraints, optimization issues may be characterized as constrained problems, discrete problems, multi-objective problems, reliability and robustness-based design challenges, and so on.

In general, optimization strategies are classified as iterative or exploratory. Iterative approaches can be classified as local or global approximation techniques. Local approximation approaches need sensitivity analysis of the design and are best suited for linear static, dynamic, and multi-body simulations. Global approximation approaches are the most efficient for nonlinear situations. Finally, while exploratory approaches are optimal for discrete issues and nonlinear simulations, they are costly due to the enormous number of analysis runs required.

For studies having large amount of design variables, constraint functions and response functions, Multi-objective Genetic algorithm (MOGA) is one of the most efficient optimization algorithms. As the name of the algorithm states, it is well-suited for tackling issues involving multi-objective optimization, as it is capable of exploring various parts of the solution space. It is feasible to search for a varied collection of solutions with a greater number of variables that may be optimized concurrently.

MOGA is a heuristic technique which is a problem-solving approach that makes use of a practical method or a variety of shortcuts to develop answers that are not ideal but are adequate, given a constrained period or deadline.

The MOGA method begins with a population that was generated randomly. A random binary number is used to generate the initial population. Each chromosome is a collection of binary codes that encode the answer. The chromosome's length, L , equals the number of bits in the string. There are 2^L potential solutions for selection, each of which is encoded in the L -bit binary coding of chromosome C . The optimization process began with the establishment of a chromosome with the desired properties. The following is a generic illustration:

$$C_k = [X_{k1}, X_{k2}, \dots X_{kn}] \quad (5.1)$$

$$C_k = [|110 \dots 00|, |101 \dots 1|, \dots |110 \dots 11|] \quad (5.2)$$

where X are the design variables to be optimized.

The flowchart of the MOGA is shown in Figure 5.2.

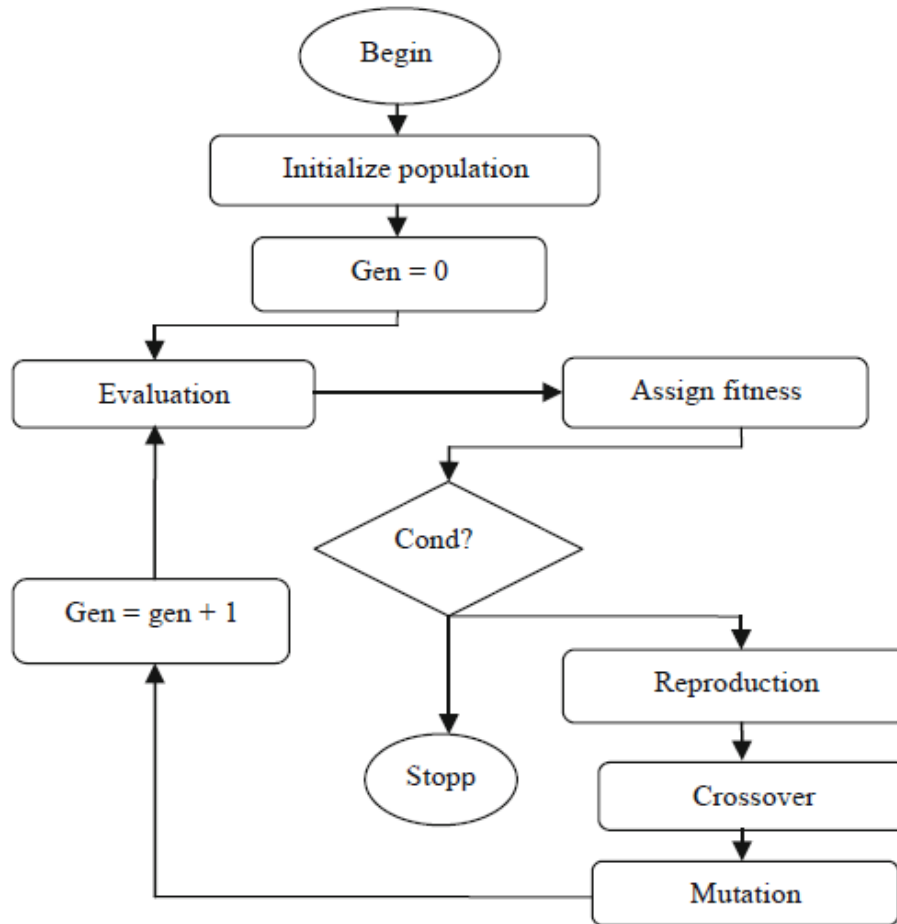


Figure 5.2 Flowchart of MOGA [42]

The procedure is as follows [45]:

- Chosen design variables are encoded from real number to a binary system.
- A chromosome is constructed via the combination of a number of genes, each of which is employed for crossing and mutation.
- The operator of the crossover will unite two chromosomes from the population to create a new chromosome called offspring. The offspring chromosome is predicted to have more genes than the parent chromosome. As a result of the crossover operator, the desirable chromosome will arise in the population, providing an overall desirable solution.
- Mutation is the process that occurs following crossing. The mutation operator will insert random chromosomes into a string. The mutation process will aid in overcoming local minima trapping.

- The chromosome assessment is determined by encoding the binary codes of the chromosome into values for machining parameters that may be used to estimate the machining performance.
- The objective function, also known as the fitness function, is the function that must be optimized or minimized throughout the machining procedure. This function must include all arguments that require optimization. The fitness function values can be used to determine whether or not to optimize the settings.
- The algorithm will continue to iterate until a stopping condition is established. One of the most often utilized halting criterion is when the value of the previous generation's fitness function is less than 1×10^{-7} in the succeeding generation.

Chapter 6

Materials and Methods

As stated previously, this study deals with the determination of the optimum position of each engine mount within the PMS of a commercial vehicle. In this context, the specs and scope of the study are explained in detail below:

- Using rubberlike elements as passive vibration isolators, the methodology of the study is performed without changing the type of the rubberlike engine mount. In other words, the stiffness matrix and damping ratio of PMS within the optimization problem are fixed.
- The number of engine mounts used in PMS is fixed as 4 within the optimization problem for positioning.
- For engine and transmission as vibration sources, mechanical properties such as mass and inertia matrices and CGs are fixed. Wherever the powertrain is located in the vehicle, origin of the system is always positioned at the CG of the engine.
- The idle frequency of the engine and the maximum torque created by the engine are fixed during the optimization problem solving.
- Any type of internal combustion engine can be used in order to apply the methodology through other problems.

Thanks to these specs and scope, the remaining variables are just the Cartesian coordinates of the hardpoints of each engine mount.

Objective functions of the study are

- Minimizing static reaction forces coming onto engine mounts due to different loading conditions

- Minimizing the natural frequency of the last mode, specifically the roll mode of the powertrain system regarding the torque roll axis (TRA).
- Minimizing the transmissibility of the PMS

Constraint functions of the study are

- $F_{reaction} < F_{plastic}$ which means that static reaction forces of different loading conditions should not exceed the elastic limits of any rubberlike engine mount.
- $f_{TRA} < \frac{f_{idle}}{\sqrt{2}}$ where f_{TRA} is the highest natural frequency of the roll mode in the system and f_{idle} is the idle frequency of the engine, explained in Section 2.3 “Vibration Control” and equation 2.38.
- Considering TRA, $T < 0.4$ where T is the transmissibility ratio of the PMS in TRA. In other words, vibration isolation rate of the system should be at least 60%. The target value is designated generically.

The functionality of the study concept is designated by a Venn diagram as seen in Figure 6.1. Neglecting any requirement causes a side-effect in the system.

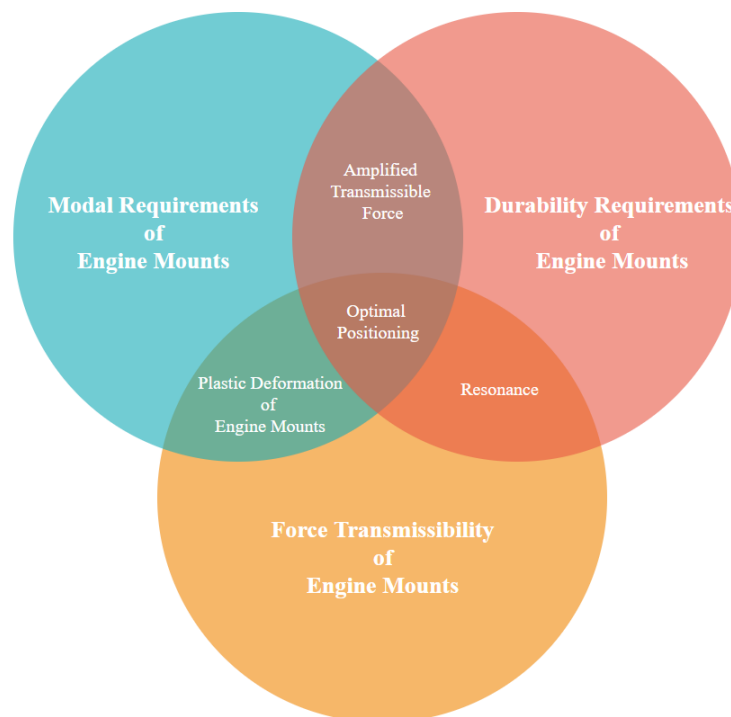


Figure 6.1: Venn diagram of the study

6.1 Materials

Commercial vehicles that are mentioned in this study were produced by BMC Otomotiv. The study is mainly based on finite element analysis which was performed via the software “Altair Hyperworks version 2021” for FEA and the software “Altair Hyperstudy version 2021” for DoE and parametric optimization problem, which were provided by BMC Otomotiv.

For the validation of the finite element model, physical tests were performed within Test & Validation Department of BMC Otomotiv.

6.2 Methodology

The methodology was stated as a flowchart shown in Figure 6.2. Initially, a reference powertrain system was taken into consideration so that FE model of the reference PMS could be validated by a physical test. Afterwards, another powertrain system was taken into consideration, whose vehicle design was at the early stages, so called conceptual design. By the conceptual study, the pre-optimization analysis was initially performed. The output of the pre-optimization model became the input of the DoE study and parametric optimization afterwards. Outputs of parametric optimization were evaluated and the most appropriate result was selected. The selected coordinates of each engine mount within the conceptual powertrain system were implied into FE model of the PMS and a post-optimization analysis was performed to make a final correction.

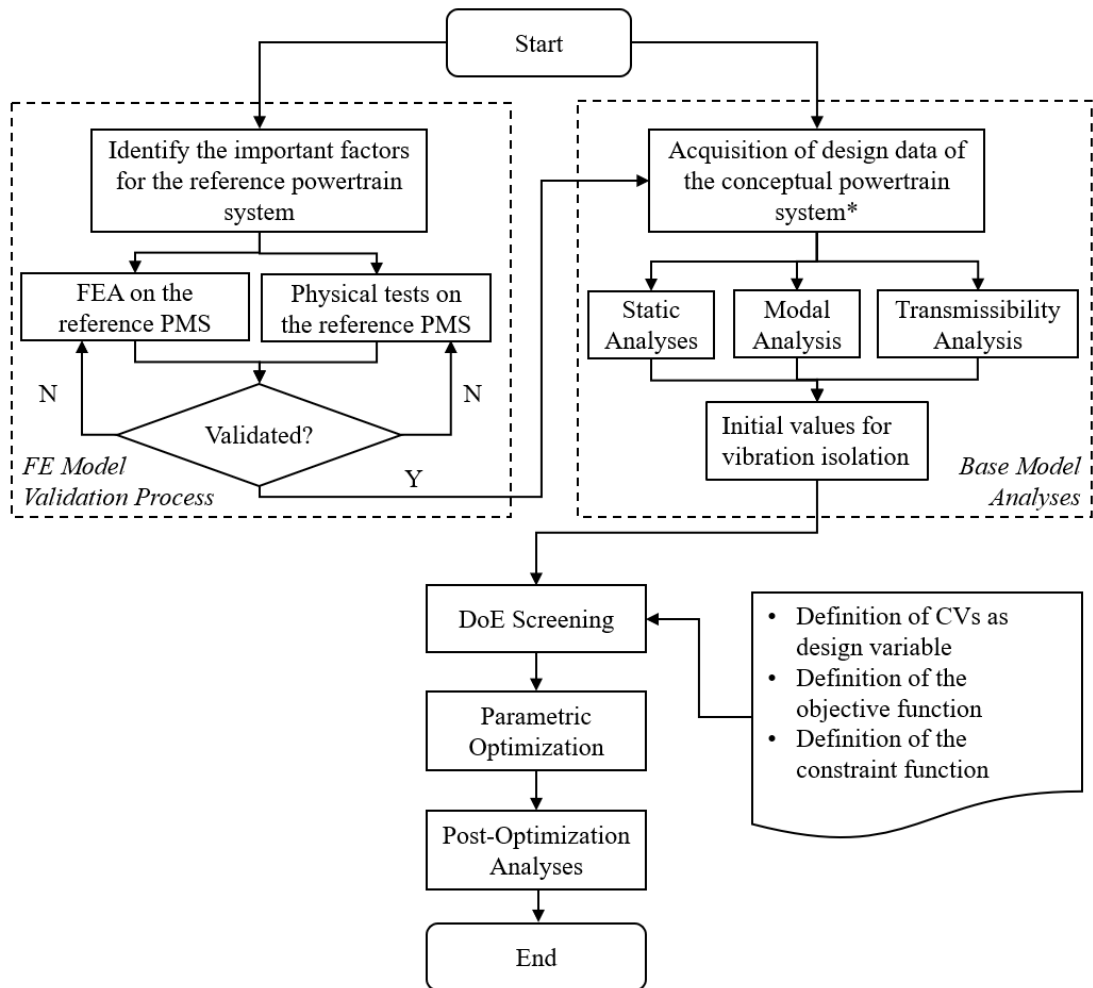


Figure 6.2: The flowchart of the overall methodology

6.2.1 Validation of the Finite Element Model

It is important to validate the FEA outputs with a physical test. By a validated model, further analyses via finite element method can be correct. To do so, as seen in Figure 6.3, a validation procedure was implemented at the beginning of the study.

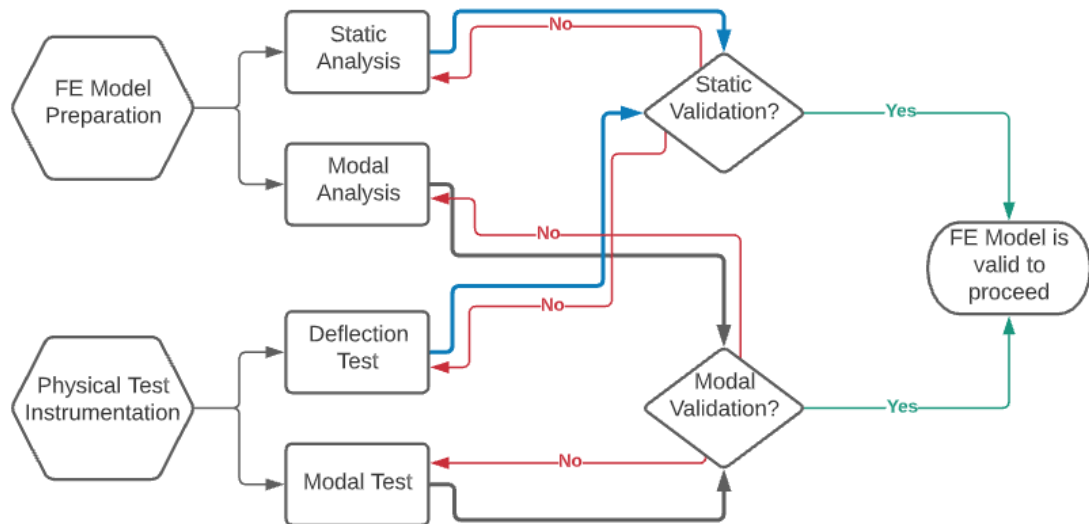


Figure 6.3: The flowchart of the FE model validation procedure

The procedure was as follows: Both virtual and physical models were prepared to perform static and dynamic (modal) measurements. The outputs of both physical tests and FEA were supposed to be correlated to each other for each subcase, which were static and modal validations. If any of two subcases didn't give a proper correlation between virtual and physical tests, then both virtual and physical tests were repeated for the unsuccessful subcase. If both of two subcases were validated, then the FE model of the system was accepted to be validated. Consequently, there existed a validated FE model methodology to be used in further similar problems.

For the validation, a reference commercial vehicle –whose PMS was positioned based on previous conventional experiences– was chosen. The diesel public bus –as the reference commercial vehicle– is demonstrated in Figure 6.4. The powertrain system was located at the rear of the vehicle.



Figure 6.4: The reference commercial vehicle

The powertrain system was connected to the body of the reference vehicle by PMS highlighted in Figure 6.5.

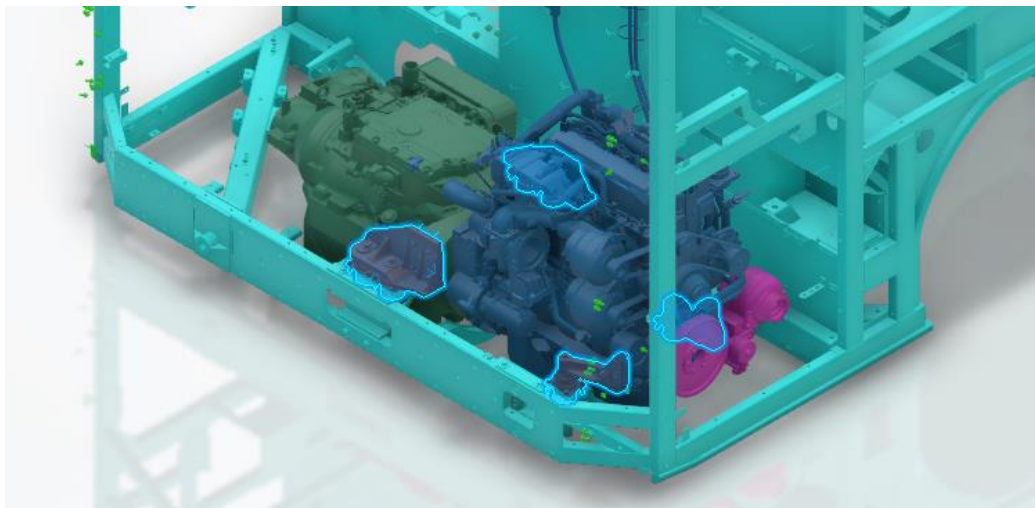


Figure 6.5: The reference powertrain system with PMS highlighted

The PMS of the vehicle can be seen in Figure 6.6, where engine brackets and engine mounts can be seen in assembly. Stated that engine brackets within PMS were not taken into the scope of this study, and knowing that bracket design stage would be the next stage after the positions of engine mounts were decided, those brackets were assumed as rigid bodies integrated with the engine-transmission coupling.

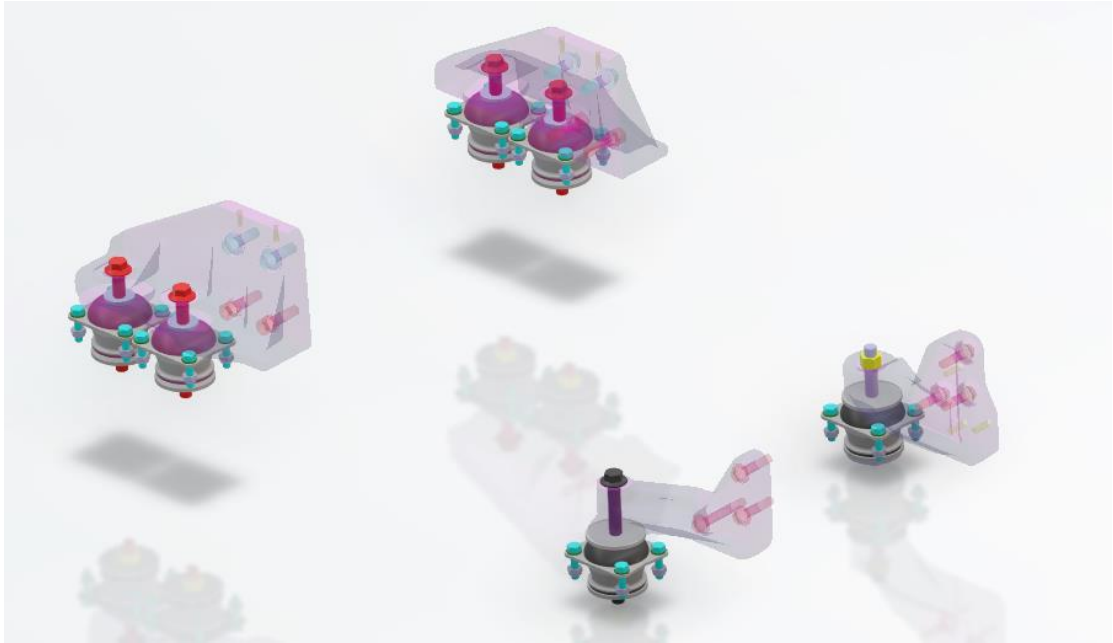


Figure 6.6: CAD image of the reference PMS

Before any operation, it is good to declare the nomenclature of the reference engine mounts. As seen in Figure 6.7, a local Cartesian coordinate system was specialized for the PMS and the origin was located at the CG of the engine. The front side was the engine side and the rear side was the transmission side, where the cardan shaft or an angle drive takes the mechanical power at the end of the transmission. Each mount was named with “M” and numbered starting from 1. The rear mounts were doubled; therefore, numbering was sectioned.

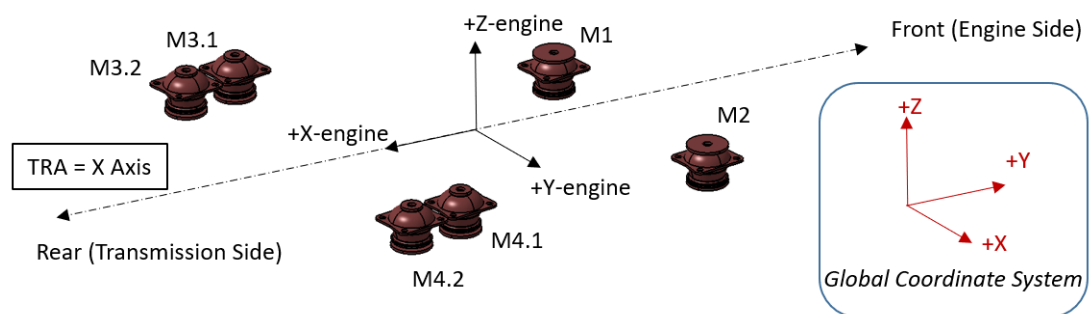


Figure 6.7: Nomenclature of the reference engine mounts

It is noted that global coordinate system is used to allocate mounts for optimization study. Local coordinate system of the engine is used only for the nomenclature of each modal shape, which has no effect on calculations. (Figure 6.7).

Mechanical properties of the engine and the transmission of the reference commercial bus are given in Table 6.1. The engine used in the bus has 4 stroke and its idle speed is 700rpm. It is known that an engine having n stroke has the greatest impact on n/2th firing order. In this case, considering the second firing order has the greatest disturbance on the TRA, the idle frequency becomes 23.34Hz which comes from

$$f_{idle_ref_PMS} = \frac{rpm_{idle}}{60s} \times (firing\ order) = \frac{700rpm}{60s} \times 2 = 23.34Hz$$

Table 6.1: Mechanical properties of engine and transmission of the reference commercial bus

Component	Moment of Inertia [kg.m ²]	CG [mm]			Weight [kg]
		X	Y	Z	
Engine	$\begin{bmatrix} 28.70 & & \\ & 29.90 & \\ & & 16.00 \end{bmatrix}$	0	0	0	400.00
Transmission	$\begin{bmatrix} 38.00 & & \\ & 14.00 & \\ & & 35.00 \end{bmatrix}$	-23.82	-906.94	-116.10	520.00

The PMS has only one type of rubberlike engine mounts (Figure 6.7). A total of 6 mounts are positioned where 2 of them are at the engine side and the rest are at the transmission side.

Mechanical properties of rubberlike engine mounts are given in Table 6.2 where only translational stiffnesses are given for the engine mounts. Damping ratio of the rubberlike specimen is taken as 0.05 [22].

Table 6.2: Mechanical properties of rubberlike engine mounts

Mount Type	Location	Number in Use	Static Stiffness [N/mm]			Dynamic Stiffness [N/mm]		
			Trans-X	Trans-Y	Trans-Z	Trans-X	Trans-Y	Trans-Z
Mount A	Engine	1+1	210	415	192	250	535	230
Mount B	Transmission	2+2	260	530	270	355	740	355

Force vs. displacement plots of the used engine mount are given in Figures 6.8 and 6.9. According to these plots, static force reaction must be within the elastic region in each translational direction.

The feasible lengths of both Mount A and Mount B were 22.2mm.

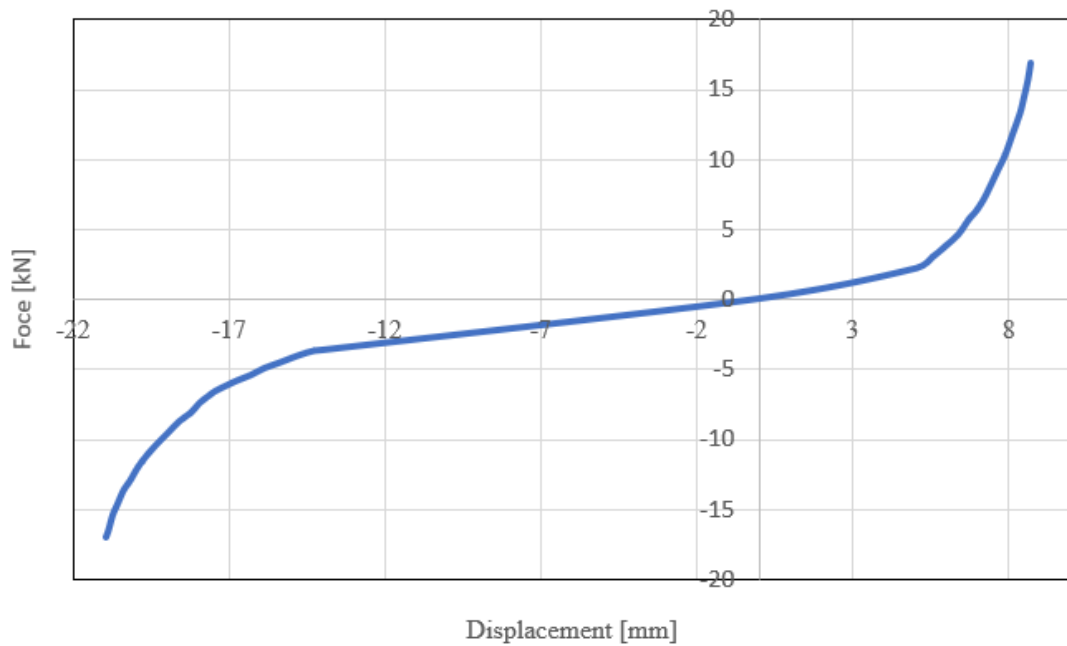


Figure 6.8: Axial static stiffness plot of the reference mount A of the engine side

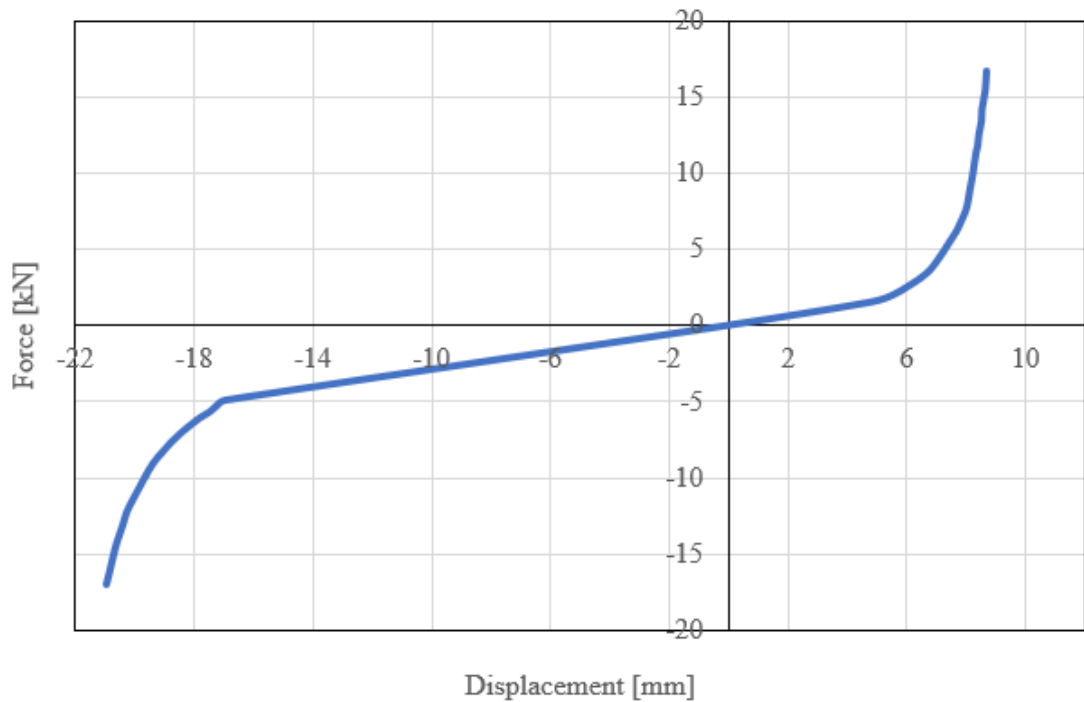


Figure 6.9: Axial static stiffness plot of the reference mount B of the transmission side

6.2.1.1 Finite Element Model of the Reference Powertrain System

The finite element model of the study was based on as follows:

According to this study, engine and transmission are represented by point masses with mass and inertial properties on its own. Eventually, engine and transmission are assumed to be rigid bodies in the finite element model.

Further, it is important to state that the brackets within PMS providing the connection between engine mounts and engine-transmission coupling are also assumed as rigid bodies since the study dealt with the determination of the hardpoints of each engine mount and the design stage of those brackets is performed according to the determined hardpoints of the engine mounts. The scope of the study doesn't cover the design stage of the engine brackets. In this sense, PMS brackets are represented by RBE2 elements, which are nondeformable 1D connections.

Coming up with engine mounts within PMS, they are represented by 1D bushing elements having stiffness matrices for 3 translational axes (Figure 6.10). The powertrain is supported by mounts with rotational stiffness negligible compared to the translational stiffness forces. As denoted before, engine mounts are considered to have no mass since the study deals with low frequency ranges.

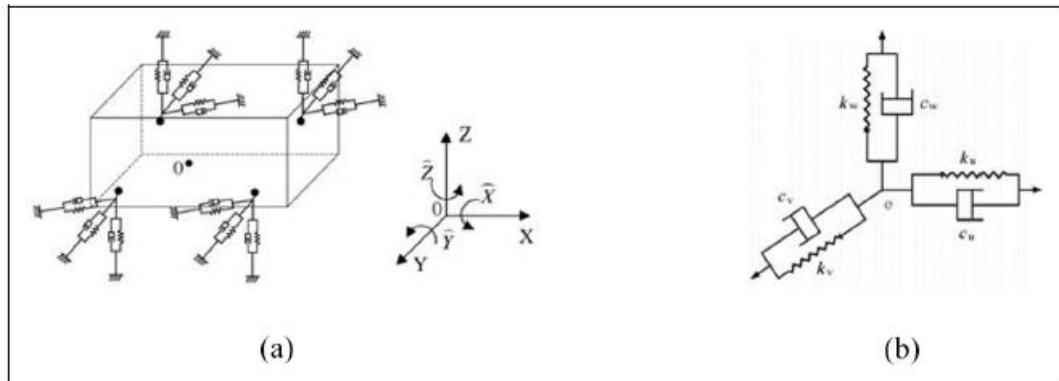


Figure 6.10: Schematic representation of a PMS with 4 mounts [20]

In this concept, consequently, the finite element model of the powertrain system of the demonstration vehicle is set as denoted in Figures 6.11 and 6.12. The FE model is created via Altair Hyperworks 2021.1. Engine and transmission are put as point masses having the values in Table 6.1. Each mount is modelled with 1D bushing elements involving 3 translational stiffness values designated in Table 6.2.

For rear mounts, as there are 2 mounts at each side, an equivalent spring stiffness value is calculated considering parallel connection of springs. Consequently, total number of bushing elements is reduced to 4.

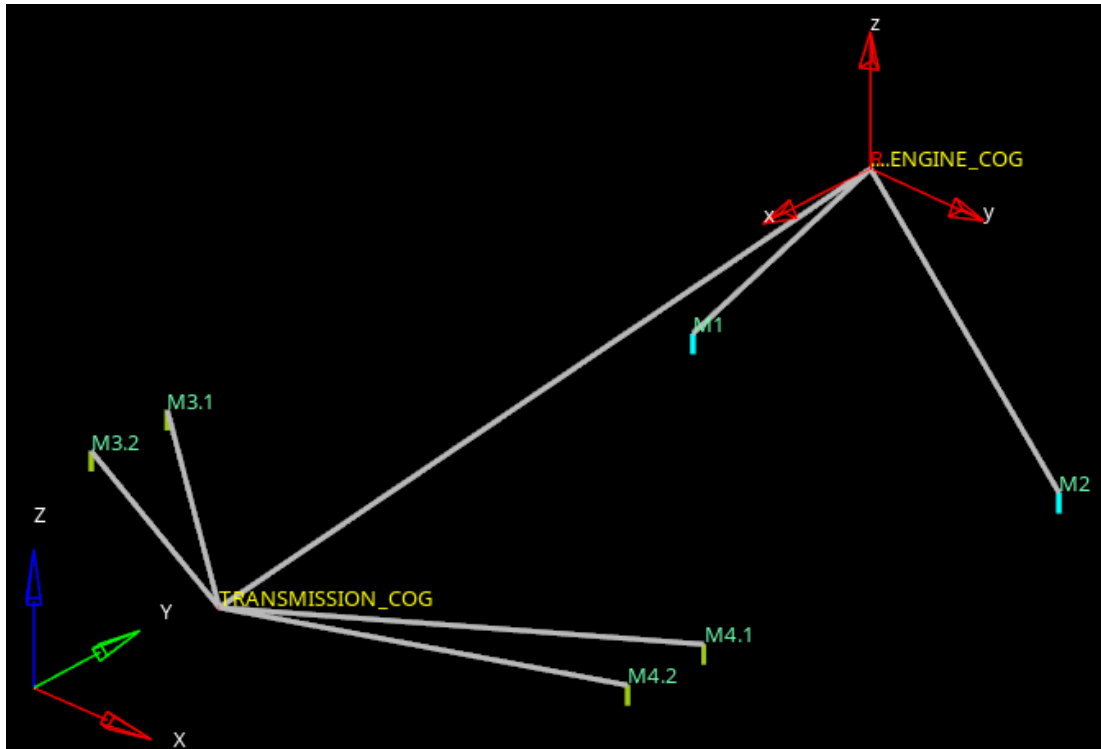


Figure 6.11: FE model of the reference PMS

In Figure 6.12, element types are described. CONM2 (Concentrated Mass Element-2) represents point mass elements, RBE2 (Rigid Body Element-2) for the engine brackets that are assumed rigid bodies, and CBUSH represents engine mounts.

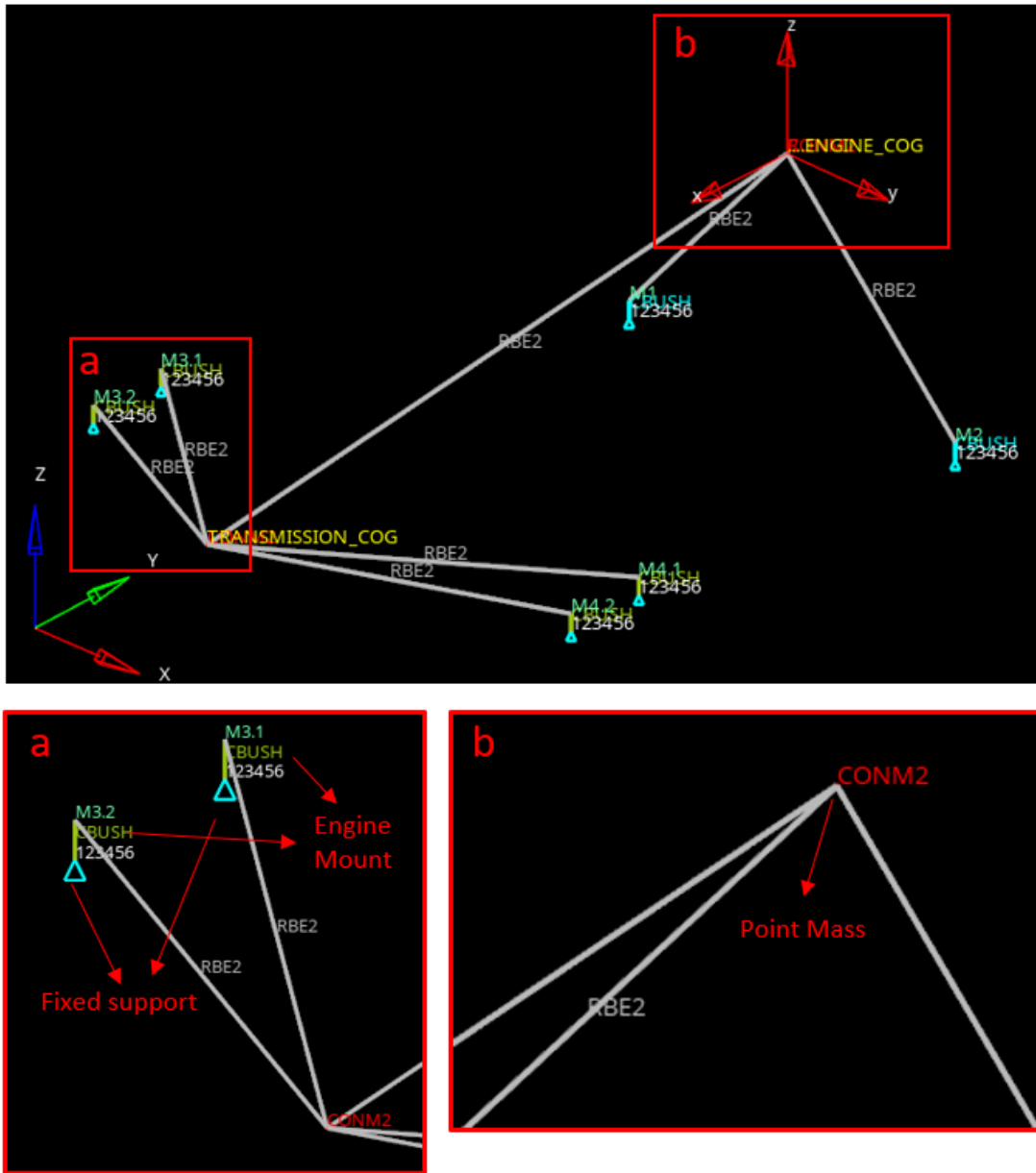


Figure 6.12: Element types used in the FE model of the reference PMS

Considering boundary conditions, Cyan colored triangles (Figure 6.12) depicted on the CBUSH elements reveals that the system is fixed to the ground in all DoF nodally. Since CBUSH element is not rigid like RBE2, and the rest of the system is assumed as a rigid body, the DoF of the system remains six.

For static analysis, the only loading scenario was attained at the basic gravity in $-Z$ direction, gravitational acceleration was taken 9.81kg/m^2 .

For modal analysis, Lanczos modal solver was used since Lanczos method directly solves modal analysis for limited number of modal results; hence, a faster solution is acquired. The Lanczos method is used for a frequency range of 0-50Hz. All normal modes were required to be seen. The result file was printed out in H3D file format.

6.2.1.2 Physical Test of the Reference Powertrain System

Static loading and modal tests were performed to validate the FE model of the reference PMS. Instrumentation and testing processes were performed at 25 °C of environmental temperature on an unheated engine-transmission.

For static loading test, the length of each mount was compared with the original length by a caliper. The difference gave the displacement on each engine mount due to the compressive force of the engine-transmission group (Figure 6.13). Eventually, the displacement stemming from the total weight distribution of engine-transmission was compared with displacement found in FEA.



Figure 6.13: Reference powertrain lay-out

For modal test, accelerations were measured with a PCB Piezotronics brand and 356A33 model ICP®, triaxial accelerometer (Figure 6.14) [43].



Figure 6.14: Triaxial accelerometer used for modal test

12 measurement points were decided to be enough so that the test software Siemens Simcenter Testlab version 2021.2 can evaluate all modal shapes. Each accelerometer was located at each corner of the engine-transmission in order to represent the volume in virtual environment (Figure 6.15-24).

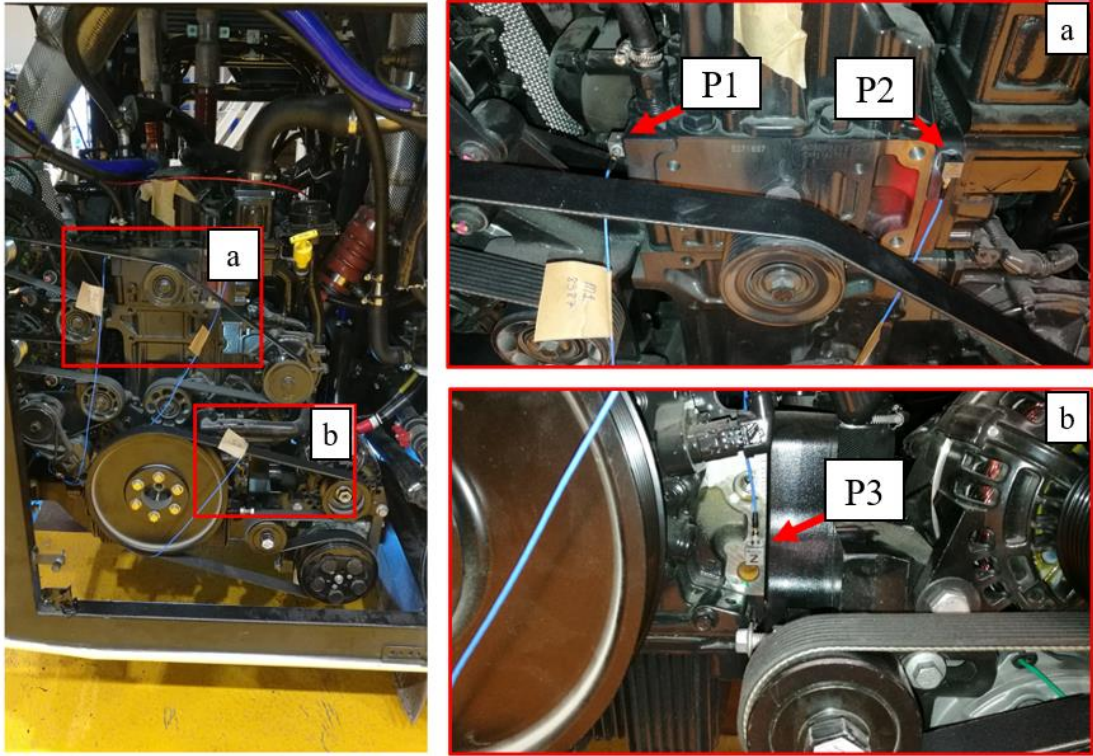


Figure 6.15: Accelerometer instrumentation for P₁, P₂ and P₃

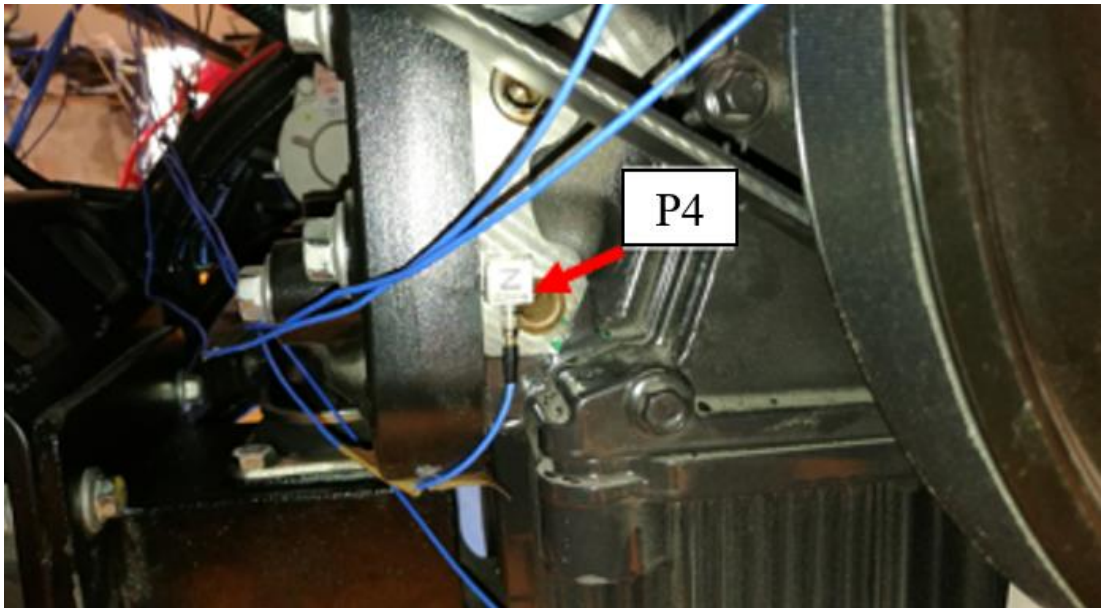


Figure 6.16: Accelerometer instrumentation for P₄



Figure 6.17: Accelerometer instrumentation for P₅

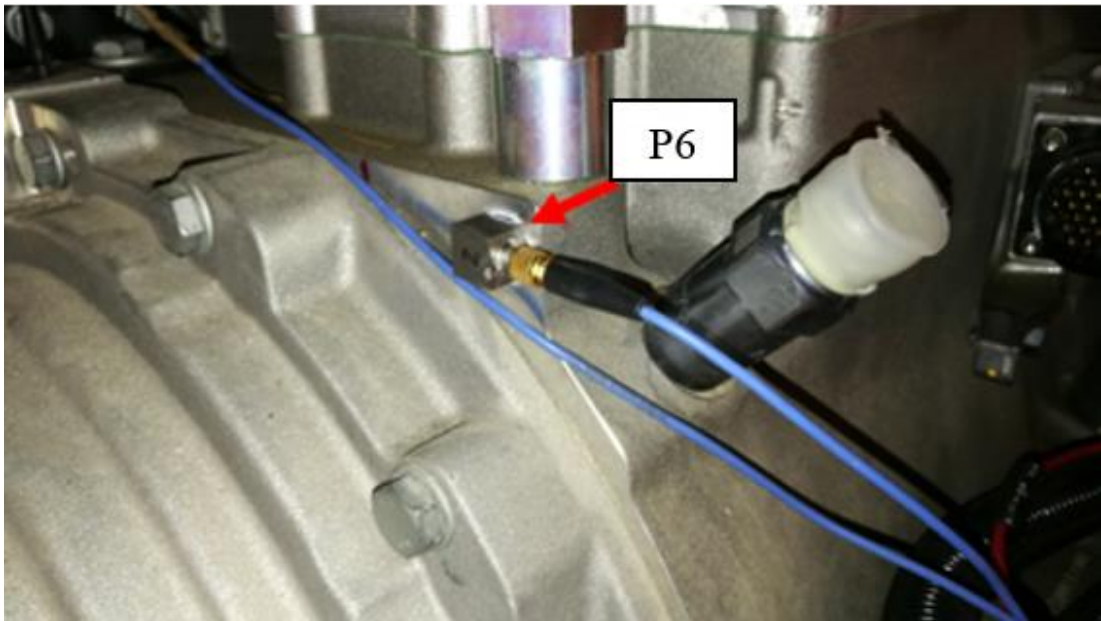


Figure 6.18: Accelerometer instrumentation for P₆

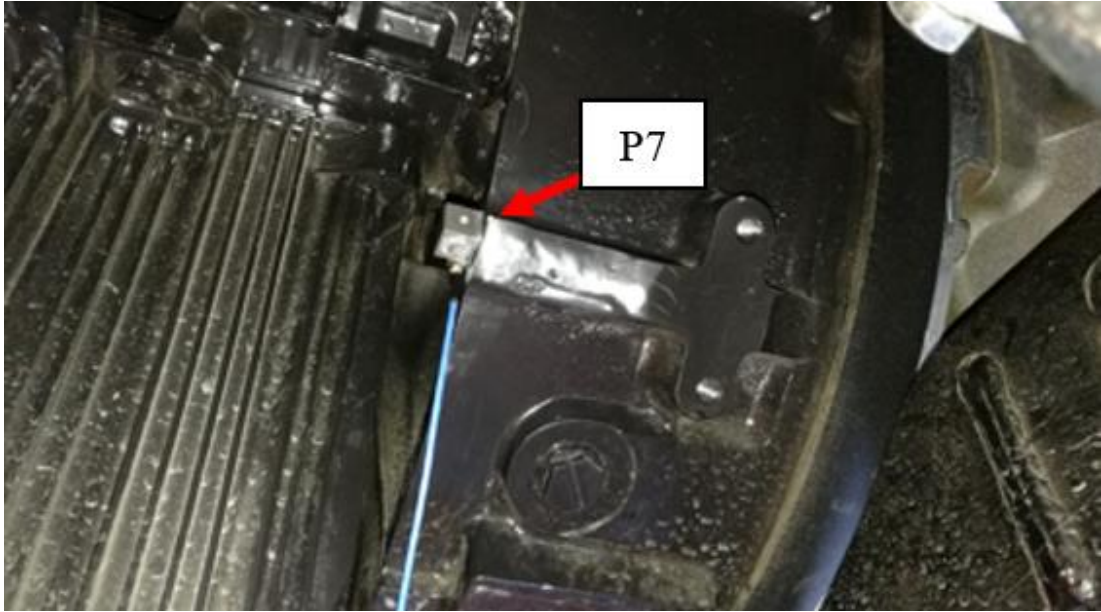


Figure 6.19: Accelerometer instrumentation for P₇

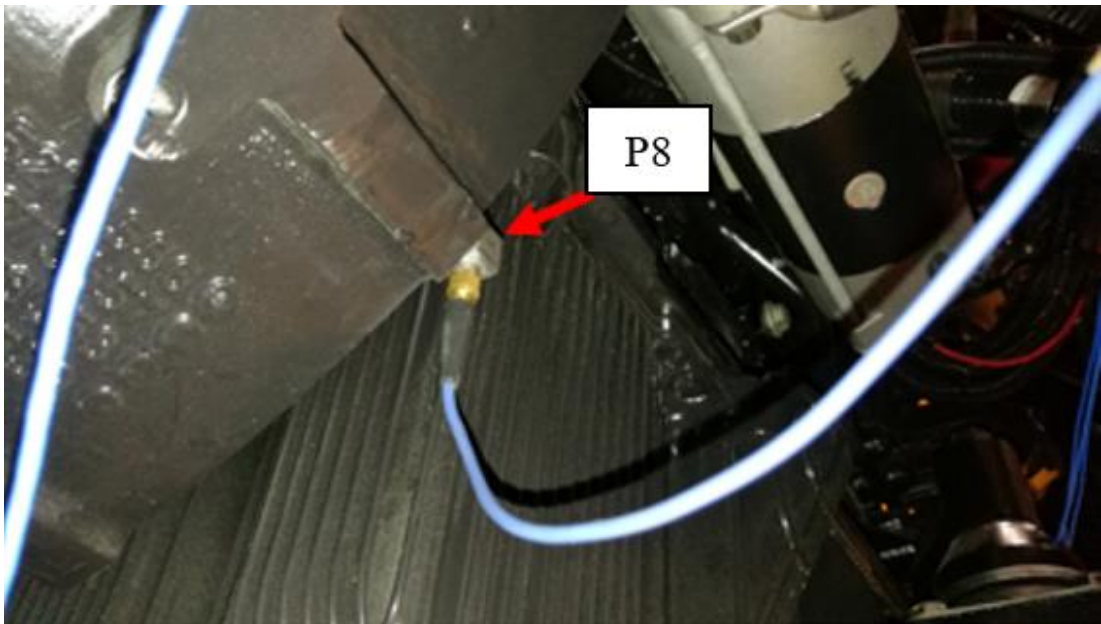


Figure 6.20: Accelerometer instrumentation for P₈

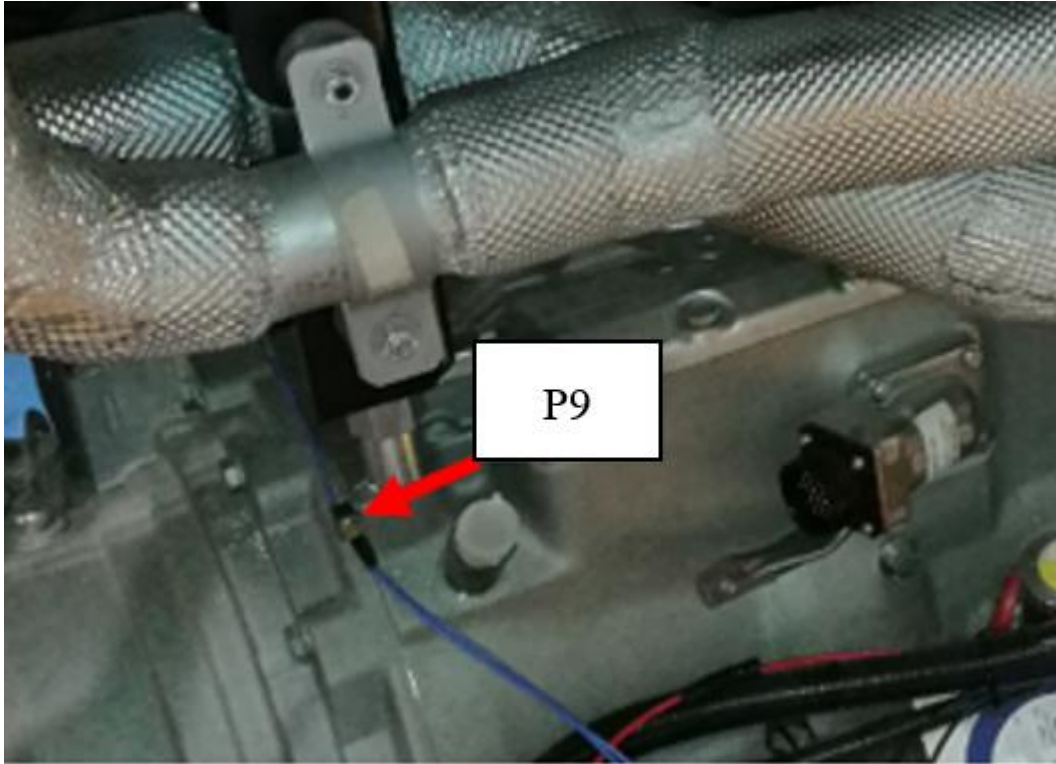


Figure 6.21: Accelerometer instrumentation for P₉

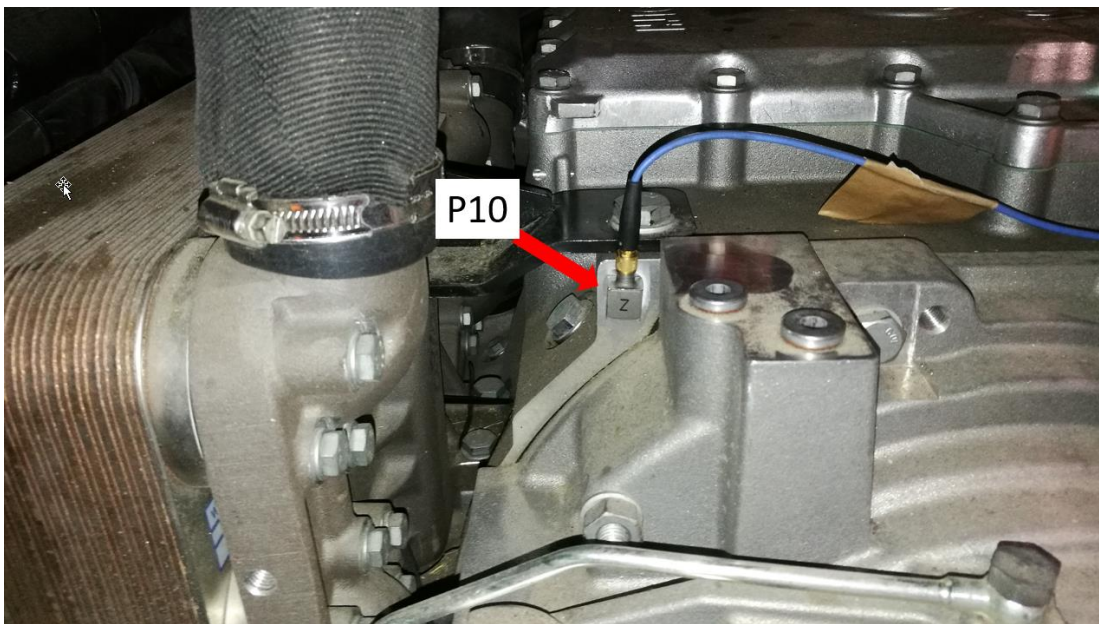


Figure 6.22: Accelerometer instrumentation for P₉

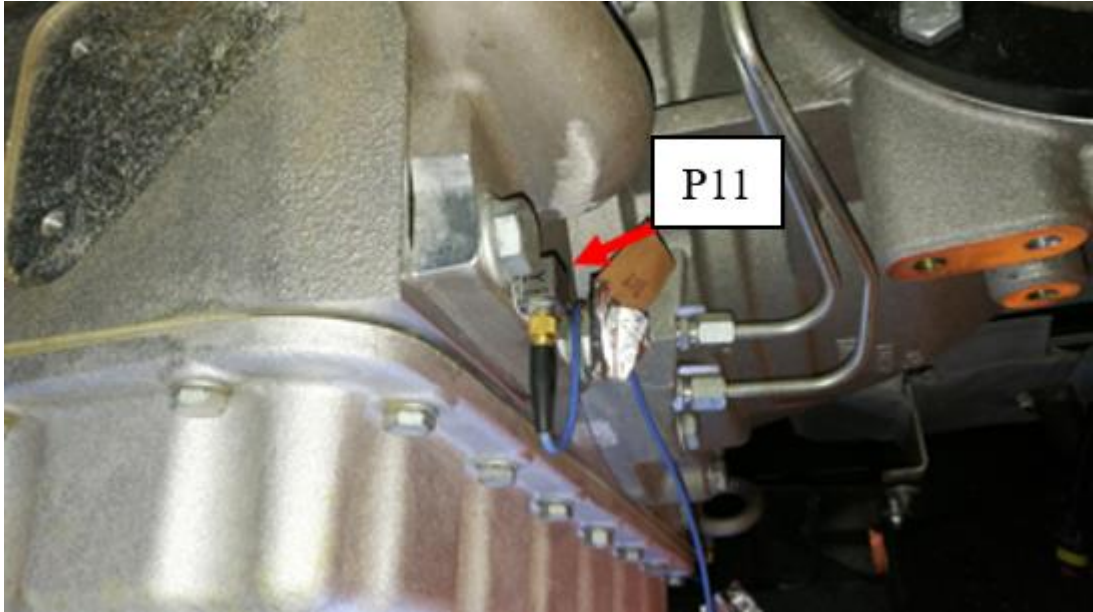


Figure 6.23: Accelerometer instrumentation for P₁₁

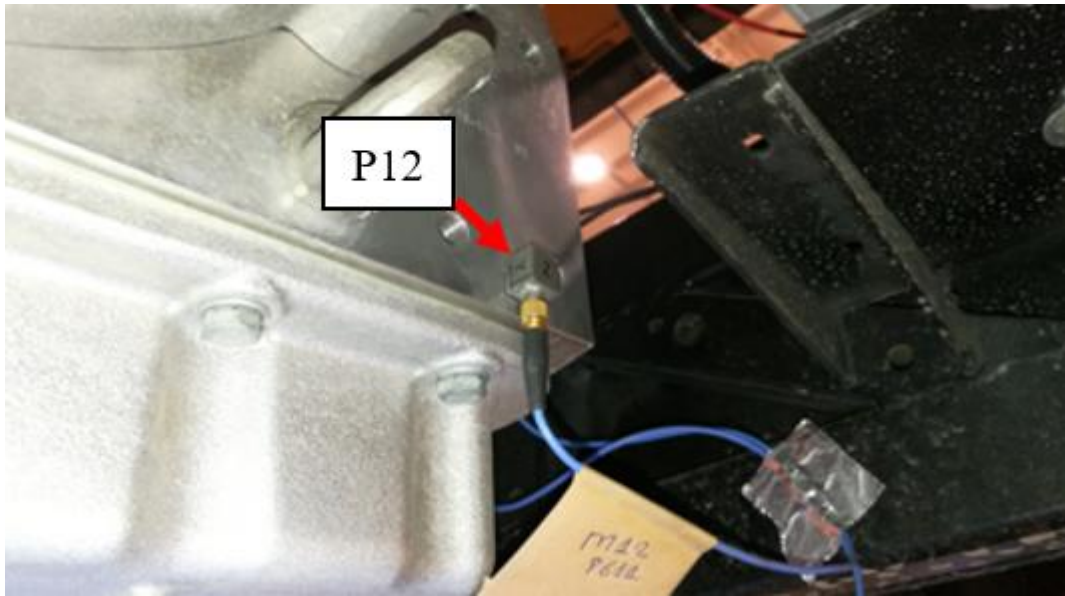


Figure 6.24: Accelerometer instrumentation for P₁₂

Modal test was performed using the impact hammer Type 8207 of Brüel & Kjær (Figure 6.25) [44]. Although single-point measurement was enough to evaluate FRFs, a second point was measured by hammer for a correction. Measured points were P₁₁ and P₁₂ triaxially.



Figure 6.25: Impact hammer used for modal test

All acceleration measurement points were visualized in Simcenter Testlab environment (Figure 6.26). Global coordinates of each measurement point were designated in Table 6.3.

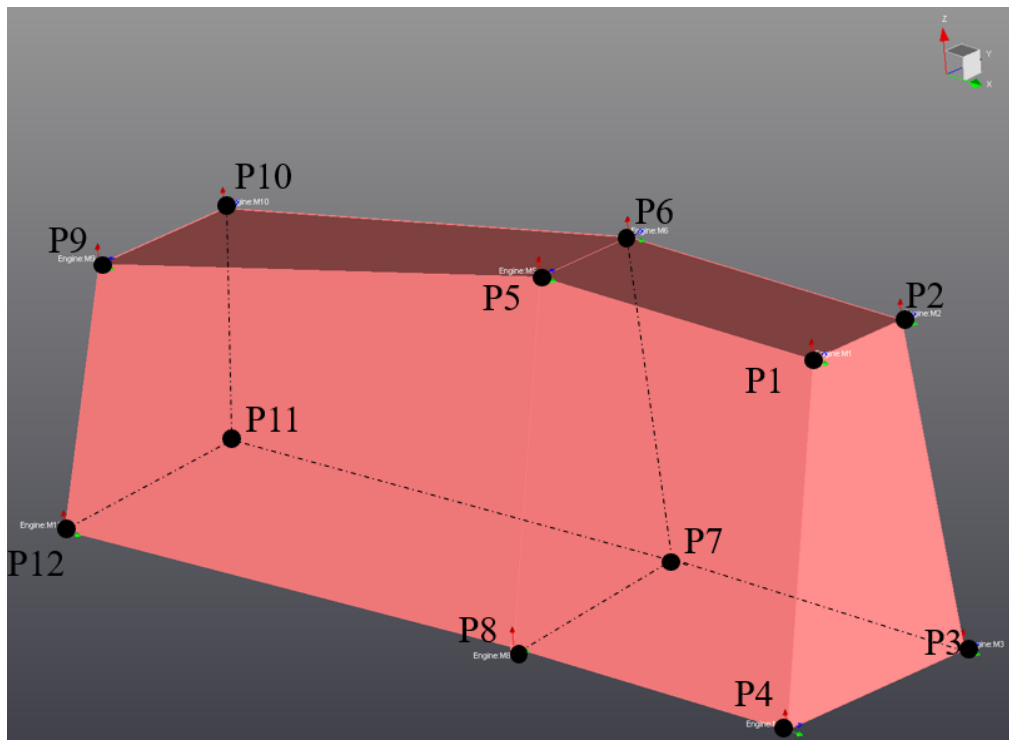


Figure 6.26: Calibration points for modal measurements

Table 6.3: Coordinates of calibration points for the modal test

Point #	X [mm]	Y [mm]	Z [mm]
P ₁	1300	150	500
P ₂	1300	320	500
P ₃	1300	390	0
P ₄	1300	50	0
P ₅	790	150	500
P ₆	790	320	500
P ₇	790	390	0
P ₈	790	50	0
P ₉	0	100	350
P ₁₀	0	340	350
P ₁₁	0	440	0
P ₁₂	0	0	0

6.2.2 Pre-optimization Model Analysis for Conceptual PMS

After validation of the FE modelling methodology, another commercial bus having a 6-stroke engine with an idle speed of 700rpm was chosen –which was at the early stage of the product design process– for the positional optimization. The main difference between the reference powertrain and the powertrain system of the conceptual bus is that hardpoints of the PMS of the powertrain of the optimization bus is not known yet. Therefore, there was no valid design of the vehicle at the very early design stage and it was very vital to determine PMS configuration with positioning engine mount hardpoints while it was still allowed to change positions of hardpoints of engine mounts.

For the model to be studied, 4 rubberlike engine mounts were to be used. Mounts at engine side were called “Mount Type A” and mounts at transmission side were called “Mount Type B” (Figure 6.27). As previously stated in the beginning of this section,

the only design variable remained as positioning Cartesian coordinates of each engine mount hardpoint.

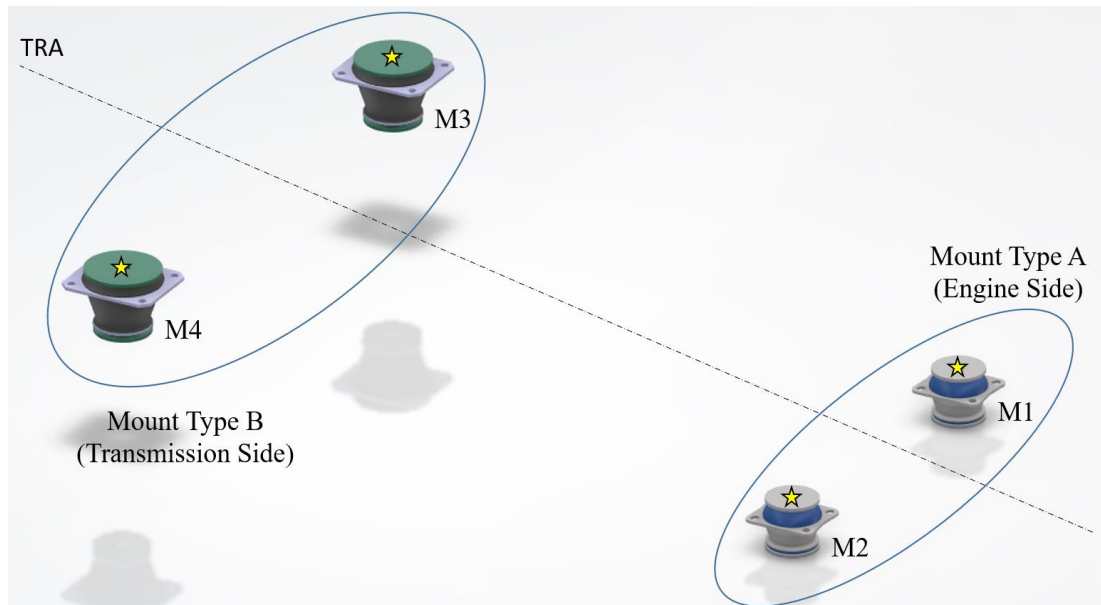


Figure 6.27: Nomenclature of PMS in optimization study

A control volume –which is a spatial limitation for each engine mount so that engine mount should not interfere with any other component of the vehicle– was defined for each engine mount (Figure 6.28). To define control volume, extremum points were determined by checking early conceptual design of the vehicle. Extremum points where each engine mount could be positioned without any interference to neighboring components of the vehicle.

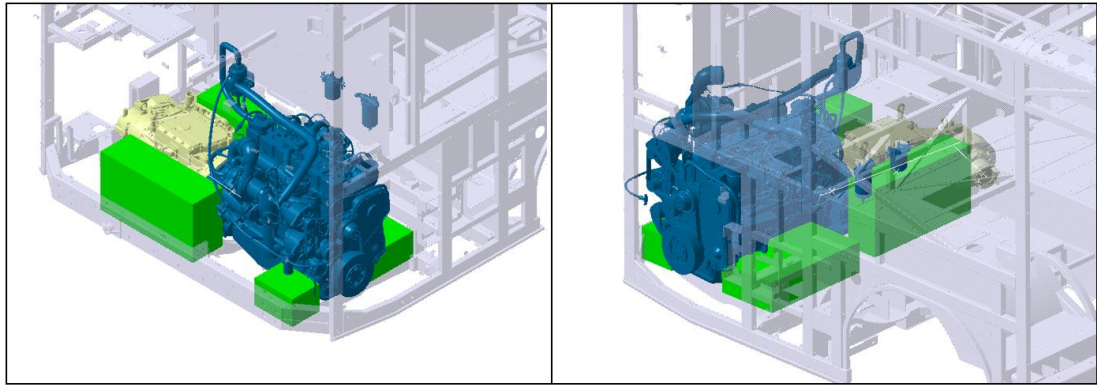


Figure 6.28 Determination of control volume according to conceptual design stage

Each control volume was named in accordance with the mount nomenclature (Figure 6.29).

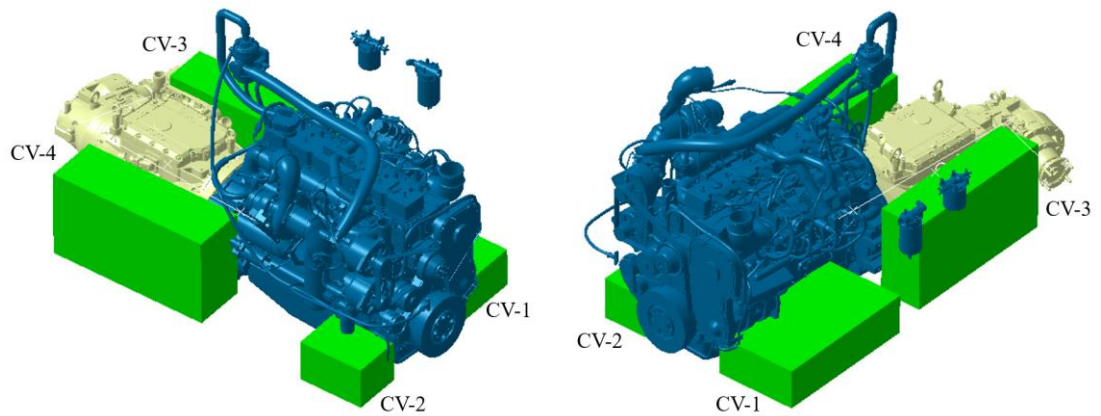


Figure 6.29: Nomenclature of control volume

Positional limits of each control volume can also be seen in Table 6.4.

Table 6.4: Positional limits of each control volume (units in mm)

Control Volume #	X_{\min}	X_{\max}	Y_{\min}	Y_{\max}	Z_{\min}	Z_{\max}
CV-1	-543.10	-158.10	-196.30	502.70	-418.70	-231.70
CV-2	228.90	456.90	190.70	502.70	-418.70	-221.70
CV-3	-543.10	-339.10	-1085.30	-320.30	-361.70	36.30
CV-4	209.90	456.90	-1085.30	-320.30	-361.70	36.30

For the pre-optimization, engine mounts within the introduced PMS was positioned randomly (Table 6.5).

Table 6.5 Mount initial coordinates of selected hardpoints

Mount #	X [mm]	Y [mm]	Z [mm]
M_1	-301.60	306.60	-402.00
M_2	368.40	265.70	-402.00
M_3	-482.70	-951.80	-89.20
M_4	330.80	-1018.20	-89.20

Mechanical properties of engine and the transmission of the optimization bus are given in Table 6.6. Local Cartesian coordinate system was located at the CG of the engine. The engine used in the conceptual bus had 6 stroke and its idle speed is 700rpm, which means the idle frequency according to the third firing order where the greatest disturbance occurs at 35Hz.

Table 6.6: Mechanical properties of engine and transmission for the optimization model

Component	Moment of Inertia [kg.m ²]	CG [mm]			Weight [kg]
		X	Y	Z	
Engine	$\begin{bmatrix} 37.00 & & \\ & 84.00 & \\ & & 63.00 \end{bmatrix}$	0	0	0	747.00
Transmission	$\begin{bmatrix} 14.00 & & \\ & 38.00 & \\ & & 35.00 \end{bmatrix}$	-120.60	-926.10	-209.50	520.00

Mechanical properties of rubberlike engine mounts are given in Table 6.7. In Table 6.7, only translational stiffnesses were given for the engine mounts. Damping ratio of the rubberlike specimen is taken 0.05 according to the literature.

Table 6.7: Mechanical properties of the engine mounts for the optimization model

Mount Type	Location	Number in Use	Static Stiffness [N/mm]			Dynamic Stiffness [N/mm]		
			Trans-X	Trans-Y	Trans-Z	Trans-X	Trans-Y	Trans-Z
Mount A	Engine	1+1	200	200	710	350	350	1230
Mount B	Transmission	1+1	2800	2800	1012	3900	3900	1600

Force vs. displacement graphs are given in Figures 6.30 and 6.31. According to these graphs, static reaction force must be within the elastic region in each translational direction. However, as the only existing stiffness graph for Mount A and Mount B is axial graph, radial evaluation was not taken into the account. Eventually, considering torque roll axis passing through the symmetry line of the model, the greatest impact within various loading cases was estimated to appear axially, which means stiffness data was sufficient to make a sensible rational discussion.

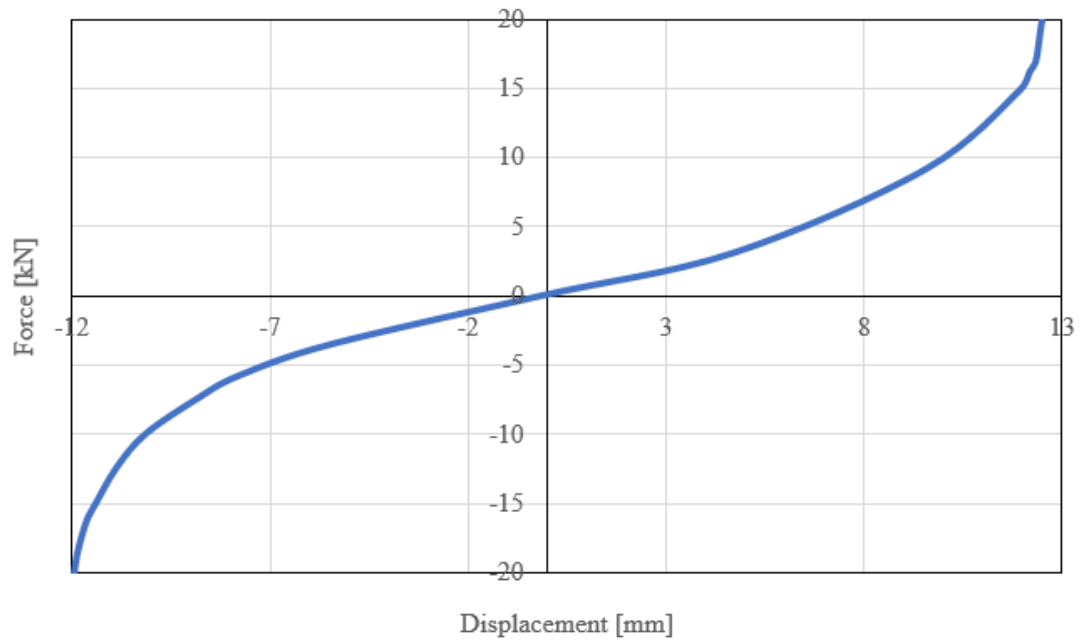


Figure 6.30: Axial static stiffness plot of the conceptual PMS for mount A of the engine side

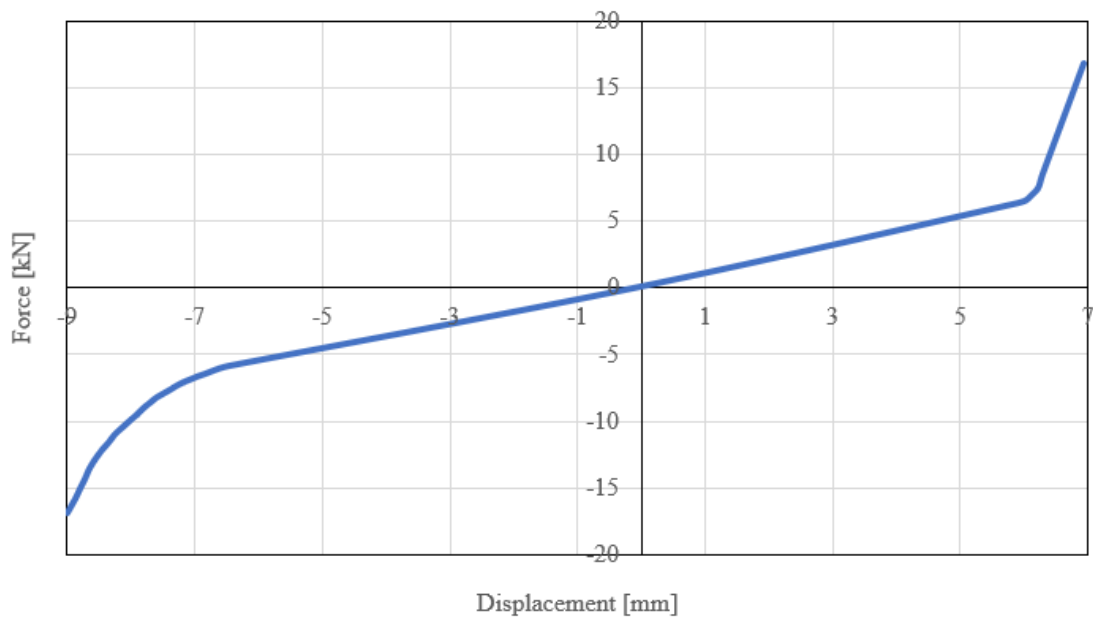


Figure 6.31: Axial static stiffness plot of the conceptual PMS for mount B of the transmission side

6.2.2.1 Static Analysis

Positioning the engine mounts in the right locations is an important subject regarding the lifetime of the engine mounts, the kinetic energy distribution reaching the axes, and accordingly keeping the forces and moments in the axes at the desired levels.

To keep each engine mount in their elastic deformation limits is important in regard to the life of the mount. Besides, engine mounts are subjected to loading scenarios both from the road and engine. In order that each mount should work within any of the loading scenarios, force reaction of the engine mounts should be controlled whether it is within elastic limits.

In this case, a set of static analyses are performed whose loading scenarios were denoted in Table 6.8. The first loading scenario was for the vehicle standing against the Earth gravity. Loading scenario number 2 represents the maximum torque applied by the engine through TRA.

Table 6.8: Loading scenarios for static analysis

#	Loading Scenario	Vehicle Longitudinal [g]	Vehicle Transversal [g]	Vehicle Vertical [g]
1	Standing	0	0	-1
2	Engine Max Torque	8 kNm + Gravity (9.81kg/s ²)		

To build the FE model of static analyses in Hypermesh 2021.1 (Figure 6.32-33), a local Cartesian coordinate system was introduced at the beginning. Engine and transmission are assumed as point masses. CONM2 point mass elements were defined according to CGs introduced in Table 6.6. Afterwards, each engine mount was created using CBUSH elements according to the feasible length of each engine mount and coordinates of the hardpoints of each engine mount were given in Table 6.5 and stiffness values in Table 6.7.

TRA is introduced and the torque to be used is applied at the end of the transmission shaft through +X direction according to the local Cartesian coordinate system.

Considering that engine and transmission are mechanically fixed to each other and engine brackets of PMS were considered rigid at this early design stage, all components were connected by RBE2 rigid 1D elements such that CG of the engine was the center of the RBE2 spider. Consequently, the bottom of each engine mount was fixed to the ground as the bus body (Figure 6.32 and 6.33).

The result file was written in H3D format. The output was supposed to be within the elastic limits of each engine mount.

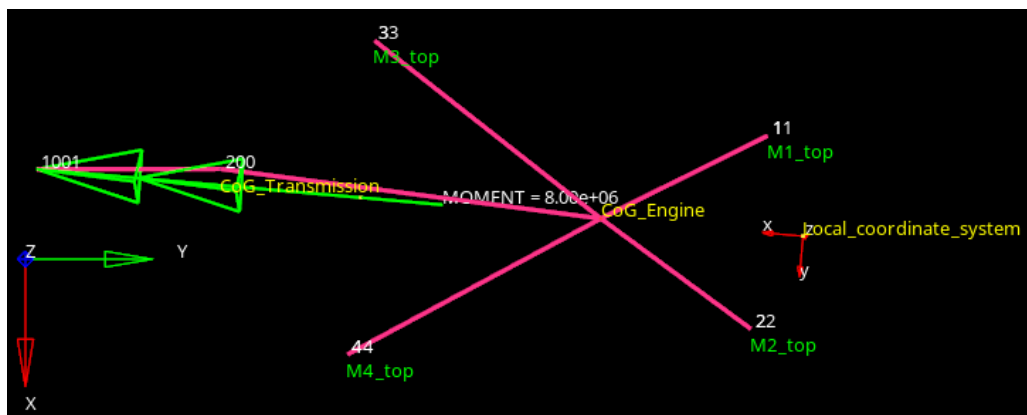


Figure 6.32: FE model for static analysis

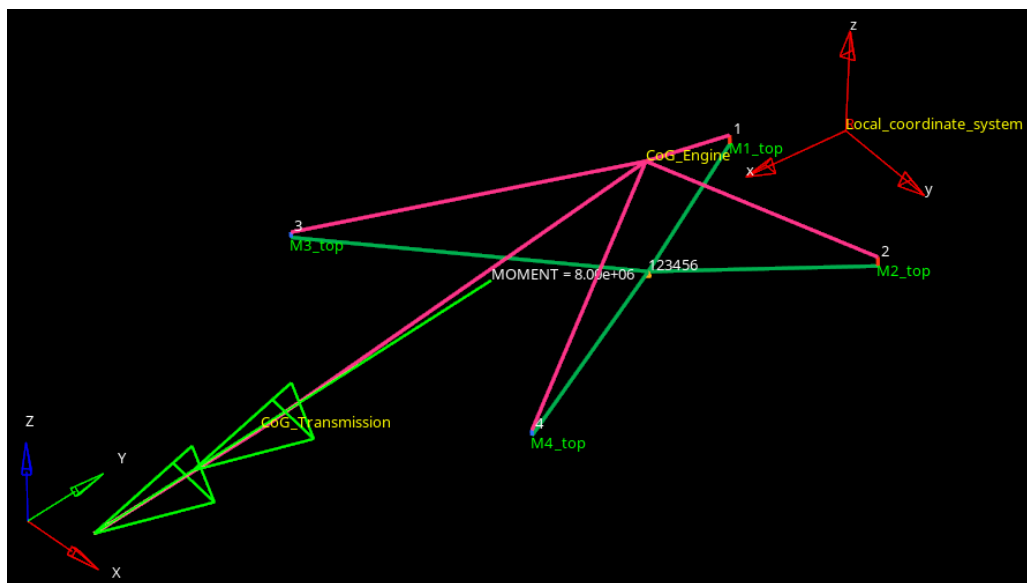


Figure 6.33 FE model for static analysis 2

6.2.2.2 Modal Analysis

A modal analysis was set up applying Lanczos method for normal mode analysis having a frequency range of 0–50Hz. All 6 modes were required to be seen. The result file was printed out in H3D file format. The output was evaluated such that the greatest natural frequency at TRA should be less than 24.75Hz which comes from equation 2.38, where the idle frequency for the engine is 35Hz.

Analogical to the FE model of static analysis, FE model of the modal analysis was set up in a similar way. The greatest difference was that there is a Lanczos modal analysis load collector and load step cards defined instead of static analysis loading set-up (Figure 6.34).

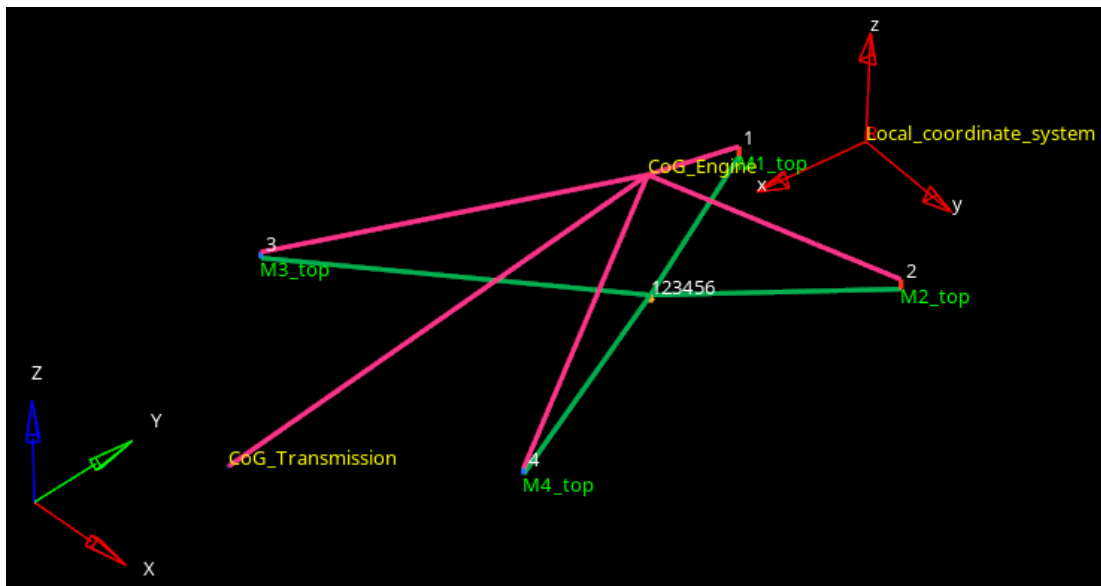


Figure 6.34: FE model for modal analysis

6.2.2.3 Transmissibility Analysis

An FE model similar to the previous FE model was set up to perform an FRF analysis (Figures 6.35 and 6.36). The aim of this analysis model was to inspect the vibration isolation value of the PMS configuration. To inspect this value, unlike the previous analysis, a dynamic excitation node was introduced at the ground, by which an

excitation can be given. Having defined the dynamic excitation node at the node where fixed support was located, the system was rotated 1 radian about the X-axis according to the local Cartesian coordinate system. The measurement was taken at the CG of the engine, where all elements were interconnected at that node.

The result file was written in H3D format. The output of the analysis was evaluated by means of the angular acceleration around X-axis of the local Cartesian coordinate system.

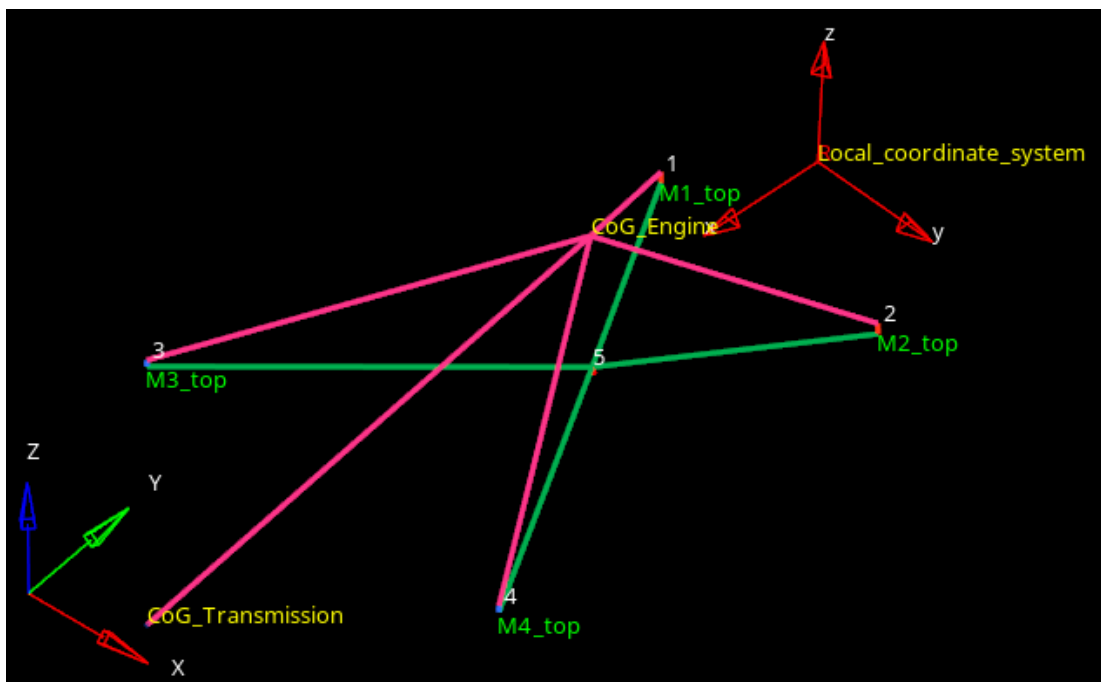


Figure 6.35: FE model for FRF transmissibility analysis: Dynamic excitation node is shown with number 5

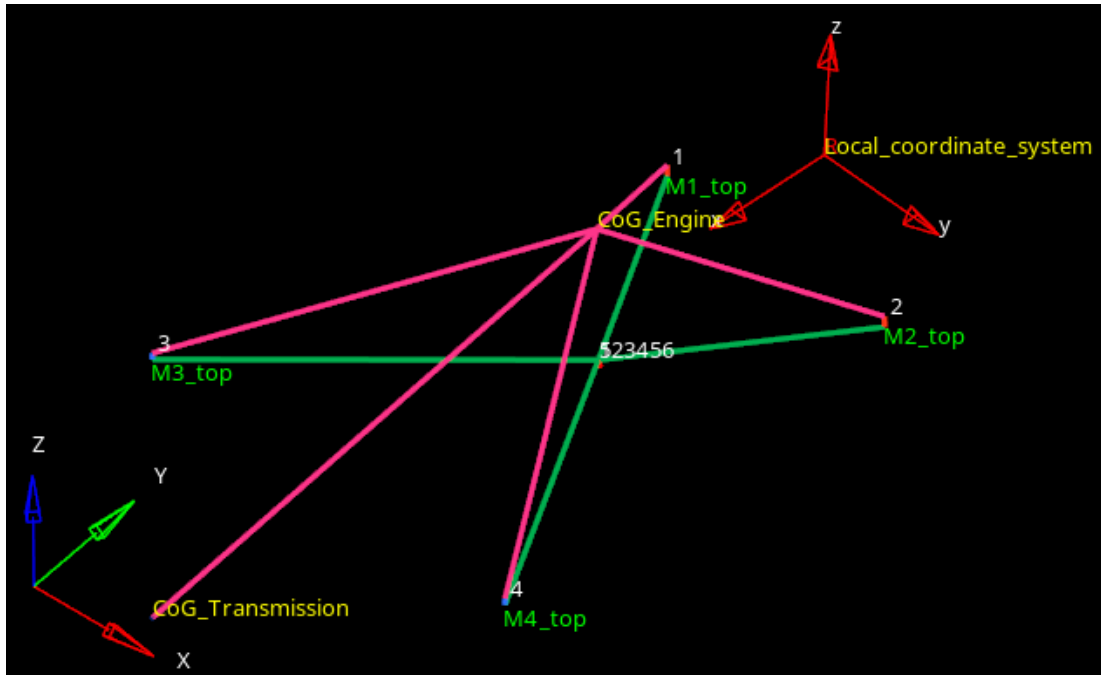


Figure 6.36: FE model for FRF transmissibility analysis

6.2.3 DoE and Optimization Studies

After performing pre-optimization analysis of the conceptual powertrain mounting system using the validated finite element model, a DoE study was performed in order to screen the behavior of each parameter and investigate correlations of parameters with each other.

6.2.3.1 DoE Study

DoE study was performed via Altair Hyperstudy 2021. The set-up procedure was as follows:

Initially, the FE pre-optimization with initial coordinates was introduced to the software as “.tpl” file. All translational coordinates of each node of each mount became a parameter with respect to control volume limit coordinates (Figure 6.37). For instance, x_1 of mount 1 became a parameter adding minimum and maximum limits of control volume 1 for mount 1.

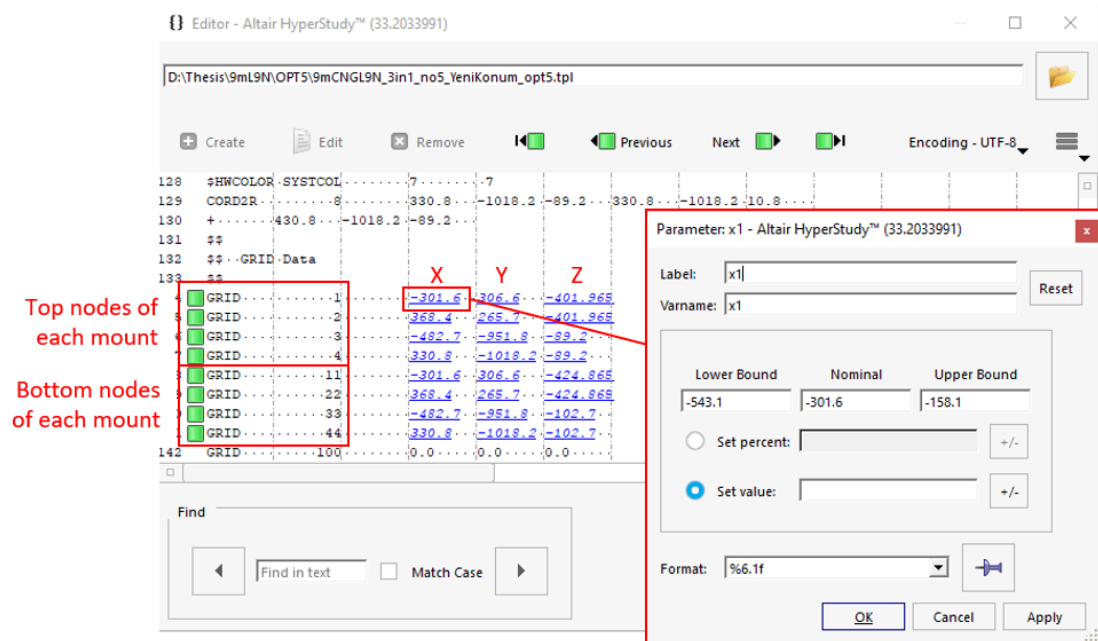


Figure 6.37: Parameter definition in Hyperstudy software

Afterwards, each bottom node was associated with the corresponding top node so that each mount can be represented without any skewness in CBUSH elements (Figure 6.38). Taking M_1 for instance, $x_{11} = x_1$, $y_{11} = y_1$, $z_{11} = z_1 - 22.9\text{mm}$ where 22.9mm is the length of the mount A. By this relationship, M_1 , M_2 , M_3 and M_4 become independent, thus they can move with no outer dependency within their control volumes (Figure 6.38).

	Active	Label	Varname	Data Type	Expression
1	<input checked="" type="checkbox"/>	x1	x1	Real	...
2	<input checked="" type="checkbox"/>	y1	y1	Real	...
3	<input checked="" type="checkbox"/>	z1	z1	Real	...
4	<input checked="" type="checkbox"/>	x2	x2	Real	...
5	<input checked="" type="checkbox"/>	y2	y2	Real	...
6	<input checked="" type="checkbox"/>	z2	z2	Real	...
7	<input checked="" type="checkbox"/>	x3	x3	Real	...
8	<input checked="" type="checkbox"/>	y3	y3	Real	...
9	<input checked="" type="checkbox"/>	z3	z3	Real	...
10	<input checked="" type="checkbox"/>	x4	x4	Real	...
11	<input checked="" type="checkbox"/>	y4	y4	Real	...
12	<input checked="" type="checkbox"/>	z4	z4	Real	...
13	<input checked="" type="checkbox"/>	x11	x11	Real	x1
14	<input checked="" type="checkbox"/>	y11	y11	Real	y1
15	<input checked="" type="checkbox"/>	z11	z11	Real	z1-22.9
16	<input checked="" type="checkbox"/>	x22	x22	Real	x2
17	<input checked="" type="checkbox"/>	y22	y22	Real	y2
18	<input checked="" type="checkbox"/>	z22	z22	Real	z2-22.9
19	<input checked="" type="checkbox"/>	x33	x33	Real	x3
20	<input checked="" type="checkbox"/>	y33	y33	Real	y3
21	<input checked="" type="checkbox"/>	z33	z33	Real	z3-13.5
22	<input checked="" type="checkbox"/>	x44	x44	Real	x4
23	<input checked="" type="checkbox"/>	y44	y44	Real	y4
24	<input checked="" type="checkbox"/>	z44	z44	Real	z4-13.5

Figure 6.38: Internal relations among parameters defined in Hyperstudy software

The following response functions were identified; (Figure 6.39) transmissibility ratio (r_{trans}), the highest natural frequency (r_{modal}), and force reaction in Z-axis for maximum torque loading case (r_{tork1} , r_{tork2} , r_{tork3} and r_{tork4}).

	Active	Label	Varname	Expression	Value	Goals
1	<input checked="" type="checkbox"/>	r_{trans}	r_{trans}	$ds_trans[numpts(ds_trans)-16]$	0.6081980	Multiple
2	<input checked="" type="checkbox"/>	r_{modal}	r_{modal}	$max(ds_modal)$	24.590570	Multiple
3	<input checked="" type="checkbox"/>	r_{tork1}	r_{tork1}	$mag(ds_tork1)$	6924.8872	Multiple
4	<input checked="" type="checkbox"/>	r_{tork2}	r_{tork2}	$mag(ds_tork2)$	1030.3041	Multiple
5	<input checked="" type="checkbox"/>	r_{tork3}	r_{tork3}	$mag(ds_tork3)$	9566.7646	Multiple
6	<input checked="" type="checkbox"/>	r_{tork4}	r_{tork4}	$mag(ds_tork4)$	3019.7493	Multiple

Figure 6.39: Response functions

Objective functions were identified and associated with response functions (Figure 6.40). By this operation, transmissibility ratio was to be minimized and to be less than

0.40 rad/s², the highest natural frequency was to be minimized and be less than 24Hz, force reactions for each mount in maximum torque loading case was to be minimized and be less than 15kN for mount type A and 10kN for mount type B, which were elastic limits of each mount type.




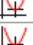















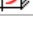

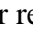


	Active	Label	Varname	Apply On	Type	... 1 2 ...
1	<input checked="" type="checkbox"/>	g_trans1	g_trans1	 r_trans (r_trans)	 Minimize	N/A	N/A
2	<input checked="" type="checkbox"/>	g_modal1	g_modal1	 r_modal (r_modal)	 Minimize	N/A	N/A
3	<input checked="" type="checkbox"/>	g_tork1_1	g_tork1_1	 r_tork1 (r_tork1)	 Minimize	N/A	N/A
4	<input checked="" type="checkbox"/>	g_tork2_1	g_tork2_1	 r_tork2 (r_tork2)	 Minimize	N/A	N/A
5	<input checked="" type="checkbox"/>	g_tork3_1	g_tork3_1	 r_tork3 (r_tork3)	 Minimize	N/A	N/A
6	<input checked="" type="checkbox"/>	g_tork4_1	g_tork4_1	 r_tork4 (r_tork4)	 Minimize	N/A	N/A
7	<input checked="" type="checkbox"/>	g_trans2	g_trans2	 r_trans (r_trans)	 Constra...	<=	▼ 0.4000000
8	<input checked="" type="checkbox"/>	g_modal2	g_modal2	 r_modal (r_modal)	 Constra...	<=	▼ 24.000000
9	<input checked="" type="checkbox"/>	g_tork1_2	g_tork1_2	 r_tork1 (r_tork1)	 Constra...	<=	▼ 15000.000
10	<input checked="" type="checkbox"/>	g_tork2_2	goal_10	 r_tork2 (r_tork2)	 Constra...	<=	▼ 15000.000
11	<input checked="" type="checkbox"/>	g_tork3_2	g_tork3_2	 r_tork3 (r_tork3)	 Constra...	<=	▼ 10000.000
12	<input checked="" type="checkbox"/>	g_tork4_2	g_tork4_2	 r_tork4 (r_tork4)	 Constra...	<=	▼ 10000.000

Figure 6.40: Objective functions for responses

Plackett-Burman design was chosen to make DoE screening in an economical way by means of computational time. For the DoE study having 12 design variables, Plackett-Burman historic design had 16 runs to investigate the behavior of each design variable. DoE study was carried out so that targets can be achieved.

6.2.3.2 Parametric Optimization

For parametric optimization set-up, the same procedure was followed as shown in Figure 6.37-6.40. The set-up of the optimization was linked to the DoE study in Hyperstudy.

Multi-Objective Genetic Algorithm (MOGA) was chosen as the optimization algorithm, which is a global explorative method without gradients. Using MOGA, minimum number of iterations was set as 25 and maximum number of iterations as 50. The population size was 148. Mutation rate was selected as 0.01.

6.2.3.3 Post-Optimization Analysis

After performing DoE study and parametric optimization with MOGA, the best value was chosen. The chosen values for the 12 defined design variables were applied to FE model. After the new coordinates for each mount were described in Hypermesh environment, same procedures in Section 6.2.2 were carried out. The aim of this section was to check the outputs of optimization in FEM environment.

Chapter 7

Results and Discussion

7.1 Validation Results of the Reference Powertrain System

7.1.1 FEA Results of the Reference PMS

7.1.1.1 Results of the Static Analysis

Regarding X-axis of global Cartesian coordinate system, minimum displacements within PMS are 0.018mm on M3.2 and M4.2, and maximum displacements are 0.032mm on M3.1 and M4.1; as shown in Figure 7.1.

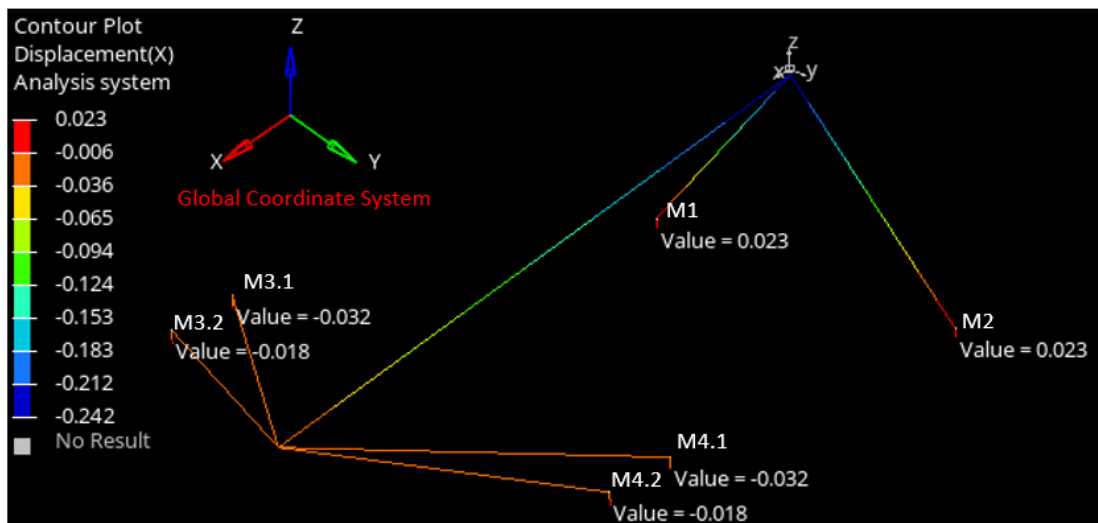


Figure 7.1: Static analysis result for global X-axis of the reference PMS

Regarding Y-axis of global Cartesian coordinate system, minimum displacements within PMS are 0.160mm on M3.1 and M3.2; and maximum displacement is 0.377mm on M1; as shown in Figure 7.2.

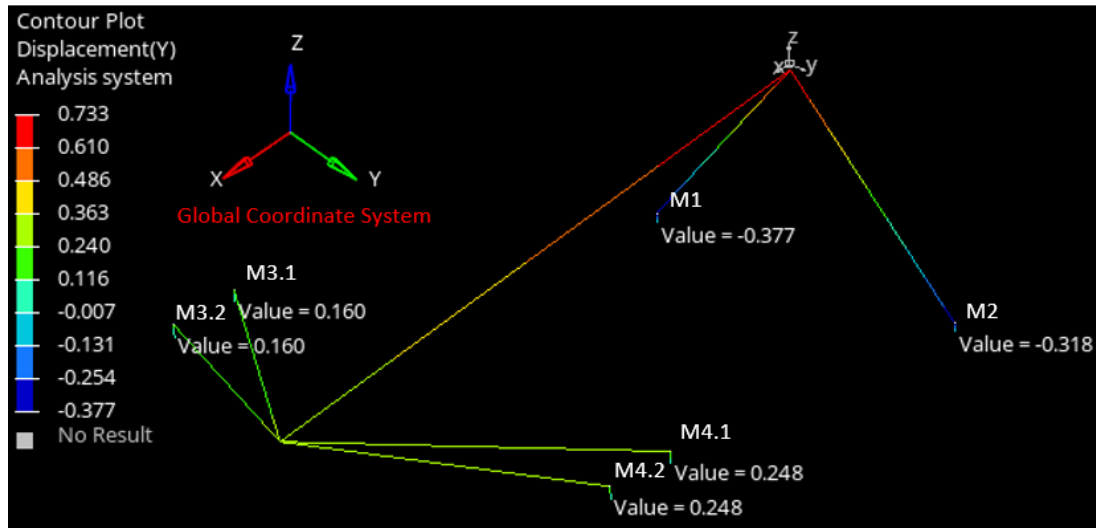


Figure 7.2: Static analysis result for global Y-axis of the reference PMS

Regarding Z-axis of global Cartesian coordinate system, minimum displacements within PMS are 0.4.444mm on M4.1 and maximum displacement is 8.038mm on M1; as shown in Figure 7.3.

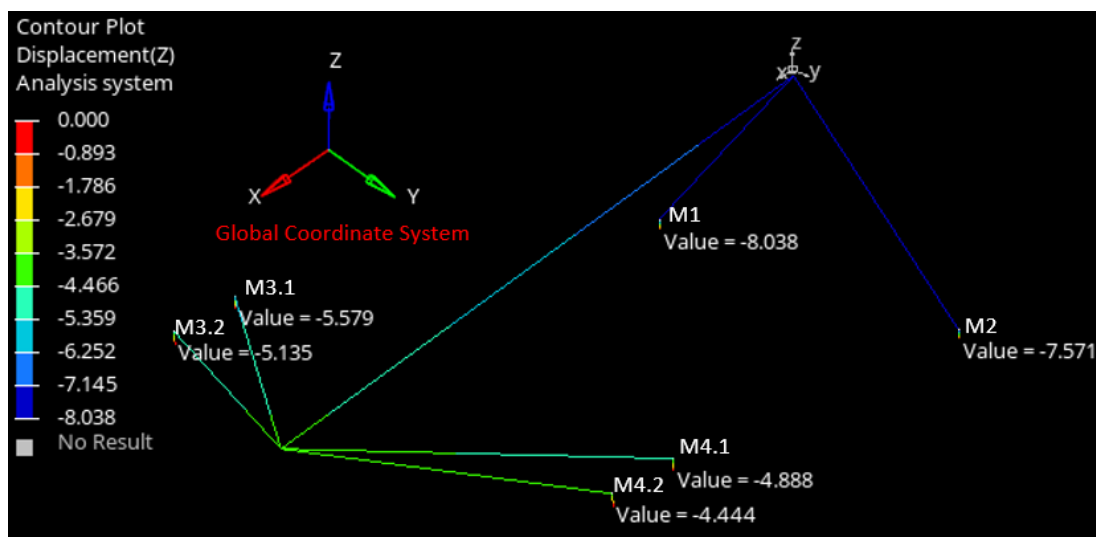


Figure 7.3: Static analysis result for global Z-axis of the reference PMS

Displacement results by mount name are given in Table 7.1.

Table 7.1: Absolute displacement results for standing loading case

Mount #	X [mm]	Y [mm]	Z [mm]
M1	0.02	0.38	8.04
M2	0.02	0.32	7.57
M3.1	0.03	0.16	5.58
M3.2	0.02	0.16	5.14
M4.1	0.03	0.25	4.89
M4.2	0.02	0.25	4.44

Comparing axial displacements using Figures 6.8 and 6.9, all displacements for mount types A and B are within the elastic deformation limits.

7.1.1.2 Results of the Modal Analysis

According to the system, all eigenvalues are distributed for each mode shape at once. Coming up with the first modal shape, pitch motion is seen at 4.45Hz regarding the local Cartesian coordinate system (Figure 7.4).

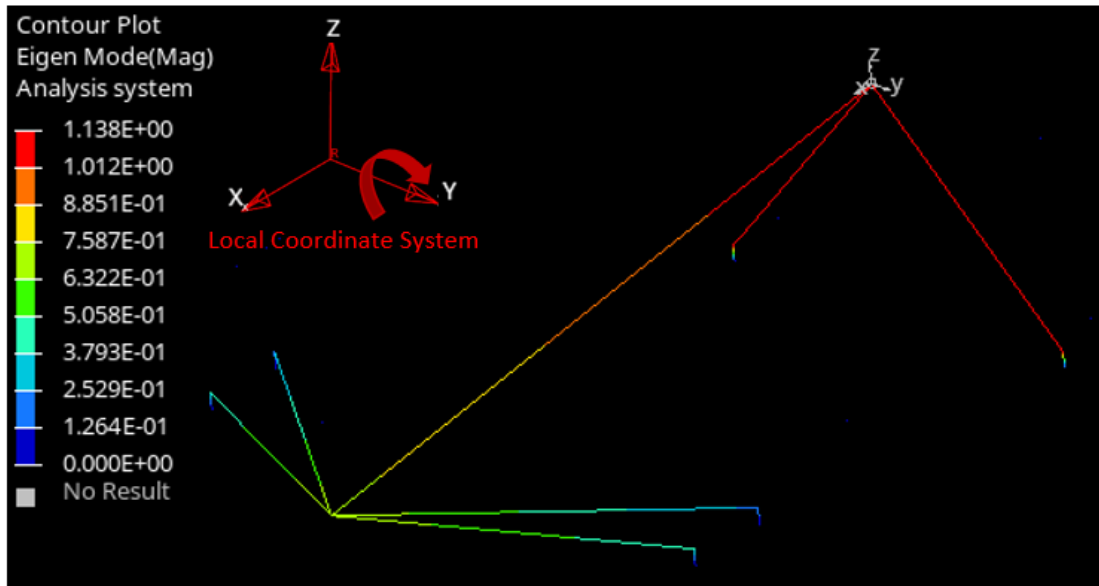


Figure 7.4: Mode 1, Pitch at 4.45Hz

At the second modal shape, translational motion along local Y-axis is seen at 6.58Hz regarding the local Cartesian coordinate system (Figure 7.5).

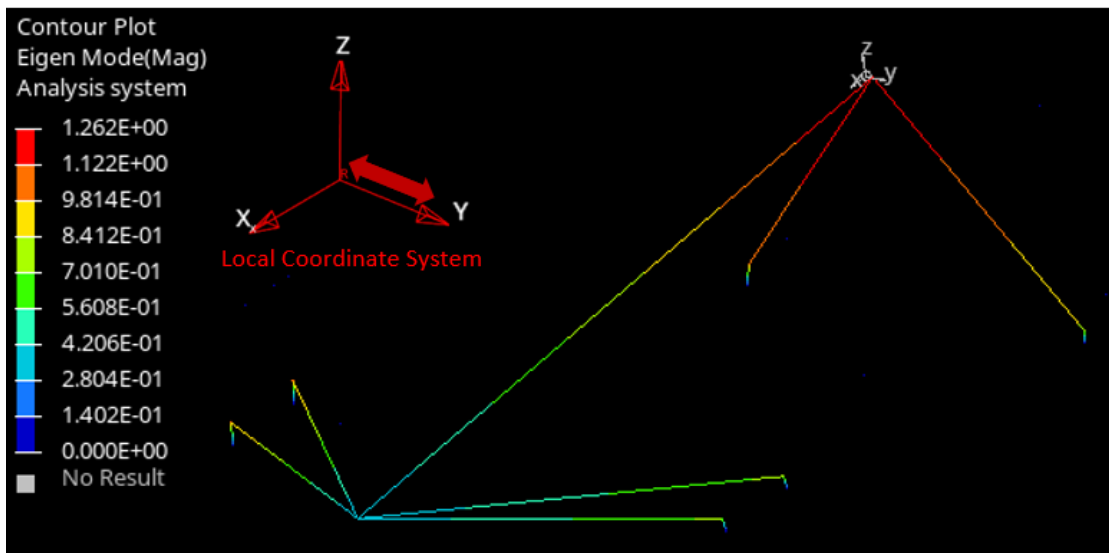


Figure 7.5: Mode 2, Trans-Y at 6.58Hz

At the third modal shape, bounce motion along local Z-axis is seen at 7.64Hz regarding the local Cartesian coordinate system (Figure 7.6).

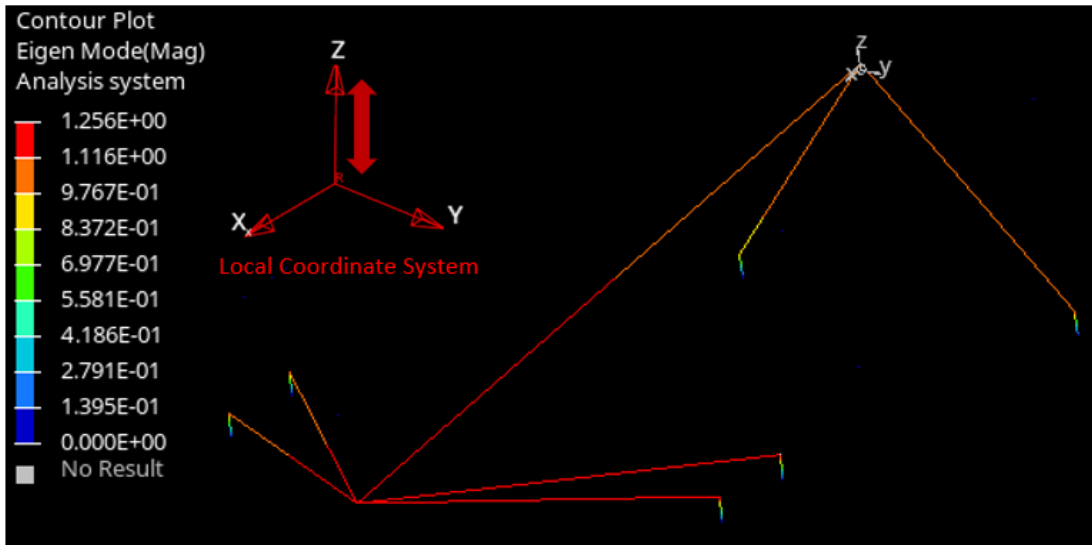


Figure 7.6: Mode 3, Bounce at 7.64Hz

At the fourth modal shape, translational motion along local X-axis is seen at 8.13Hz regarding the local Cartesian coordinate system (Figure 7.7).

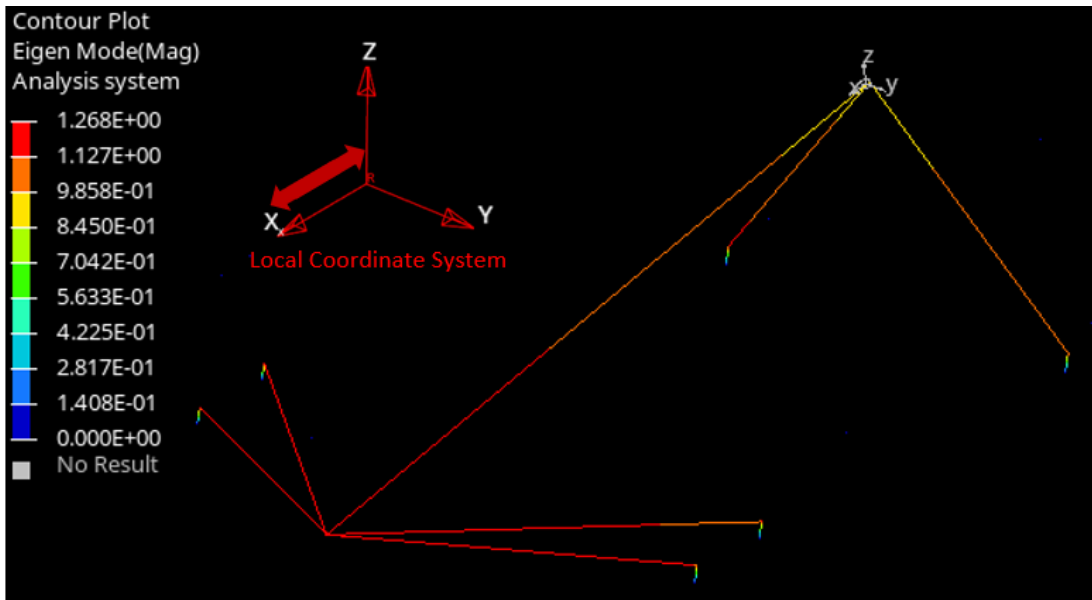


Figure 7.7: Mode 4, Trans-X at 8.13Hz

At the fifth modal shape, yaw motion around local Z-axis is seen at 10.03Hz regarding the local Cartesian coordinate system (Figure 7.8).

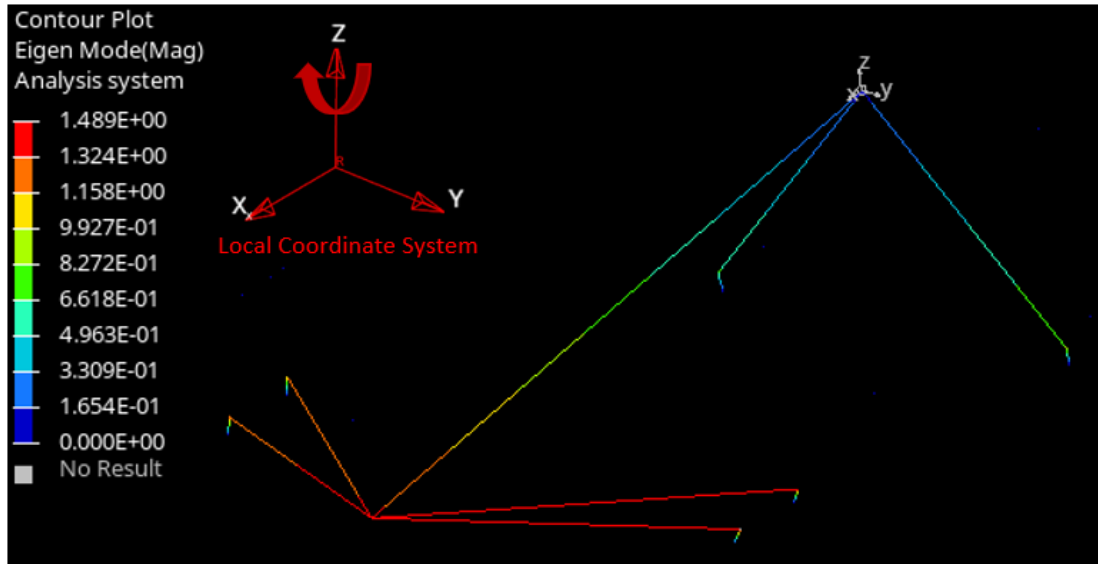


Figure 7.8: Mode 5, Yaw at 10.03Hz

At the sixth last modal shape, roll motion around TRA (local X-axis) is seen at 14.45Hz regarding the local Cartesian coordinate system (Figure 7.9).

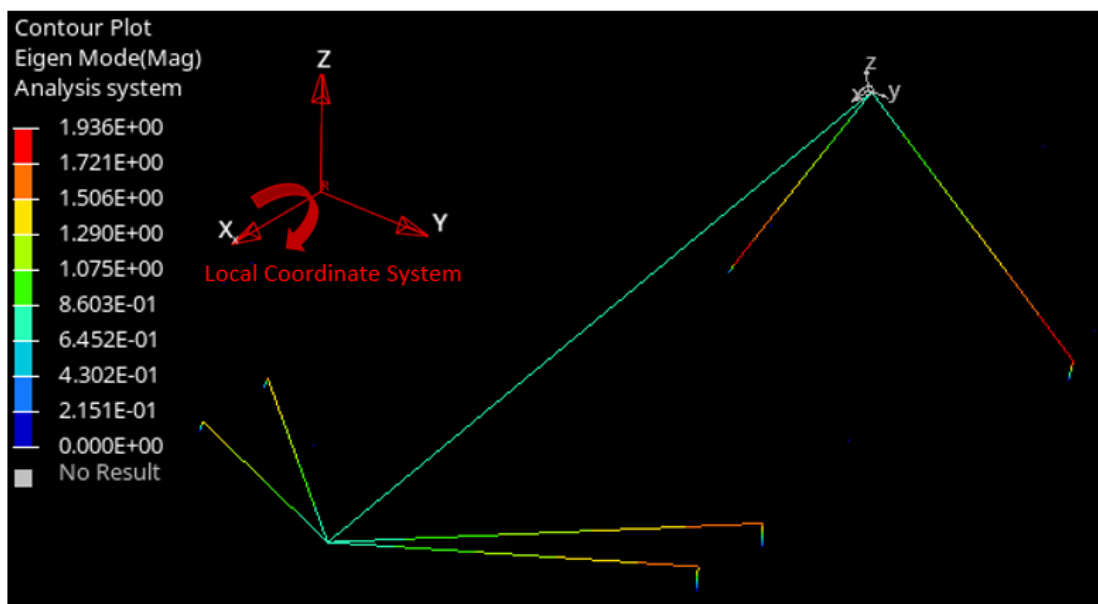


Figure 7.9: Mode 6, Roll at 14.45Hz

Natural frequencies and mode shapes of the PMS are demonstrated in Table 7.2.

Table 7.2: Modal analysis results for the reference PMS

Mode #	Natural Frequency [Hz]	Mode Shape	Local Axis
Mode 1	4.45	Pitch	Rotational Y
Mode 2	6.58	Fore-Aft	Translational Y
Mode 3	7.64	Bounce	Translational Z
Mode 4	8.31	Fore-Aft	Translational X
Mode 5	10.03	Yaw	Rotational Z
Mode 6	14.45	Roll	Rotational X

Natural frequency of Mode 6 is the greatest and this is the most effective mode shape since the roll mode is distorted by the torque applied along TRA. Considering the modal analysis target of the reference PMS, the greatest natural frequency of PMS is found 38% less than 23.34Hz.

7.1.2 Physical Test Results

Static deformation test was performed on PMS of the standing vehicle. Results are compared with analysis results in Table 7.3. % Error is calculated as

$$\frac{(Z_{test} - Z_{analysis})}{Z_{analysis}} \times 100.$$

Table 7.3: Comparison of test results with analysis outputs

Mount #	$Z_{analysis}$ [mm]	Z_{test} [mm]	% Error
M1	8.04	7.10	13.21
M2	7.57	6.55	15.59
M3.1	5.58	4.96	12.48
M3.2	5.14	4.82	6.54
M4.1	4.89	5.00	2.24
M4.2	4.44	4.92	9.67

Coming up with modal test results, there are only four mode shapes that can be found. This happened due to the fact that two modes were almost coupled and the vehicle envelop let only P_{11} and P_{12} to apply modal test. Physical measurements are evaluated using Siemens Test Lab software, 4 observed mode shapes and their natural frequency values are shown in Figure 7.10. As shown in the figure, the pitch mode frequency is 7.19 Hz, bounce mode frequency 10.85 Hz, yaw mode frequency 13.86 Hz, and roll mode frequency 14.71 Hz.

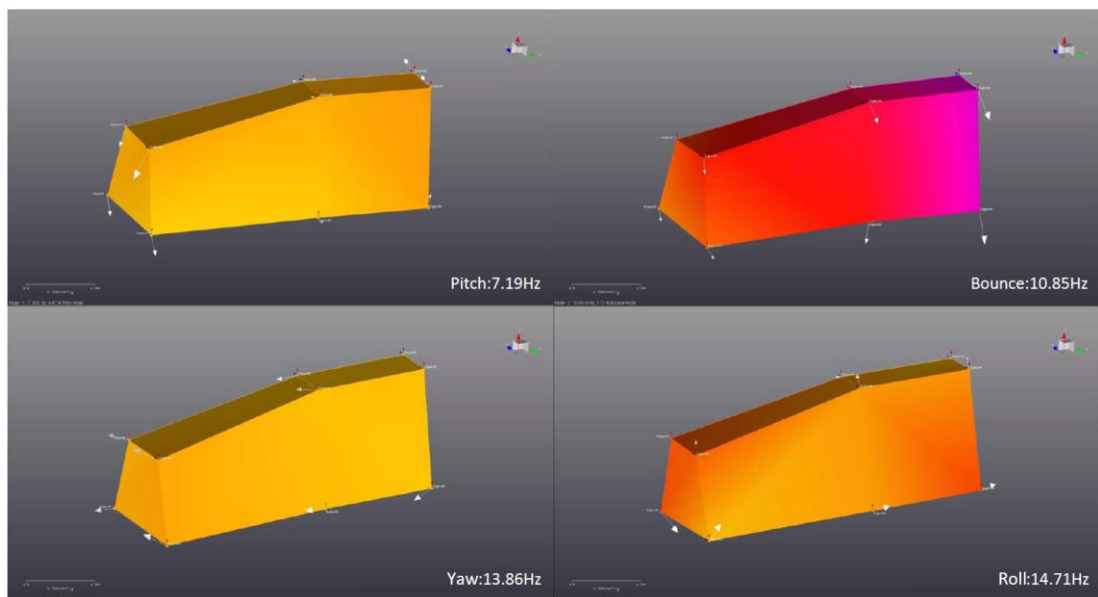


Figure 7.10: Modal test results

Finite element modal analysis and physical modal test results are shown in Table 7.4. The number of mode shapes of the test are 4 due to the fact that there are coupled mode shapes which also involved “Fore-Aft Y” mode shape and “Fore-Aft X” mode shape within other mode shapes. Therefore, since the main focus of the study is to reduce roll mode shape along TRA, all modal frequencies can be reduced by reducing the greatest eigenvalue of the system.

Table 7.4: Comparison of modal analysis and modal test results

Mode #	f_{analysis} [Hz]	FEA Mode Shape	f_{test} [Hz]	Test Mode Shape	% Error
Mode 1	4.45	Pitch	7.19	Pitch	38.11
Mode 2	6.58	Fore-Aft Y	-	-	-
Mode 3	7.64	Bounce	10.85	Bounce	29.59
Mode 4	8.31	Fore-Aft X	-	-	-
Mode 5	10.03	Yaw	13.86	Yaw	27.63
Mode 6	14.45	Roll	14.71	Roll	1.77

The critical eigenvalue of the system is Mode 6 (Roll Mode) for both physical test and analysis results. It is 14.45Hz at modal FE analysis and is 14.71Hz at modal test. The comparison reveals 1.77% error between these two-roll mode shape results.

7.2 Pre-optimization Results of the Conceptual PMS

7.2.1 Results of the Static Analysis

The static analysis result for the gravity loading case is shown in Figure 7.11. According to the results, the total force reaction of each mount is equal to the force stemming from the cumulative weight of engine-transmission coupling.

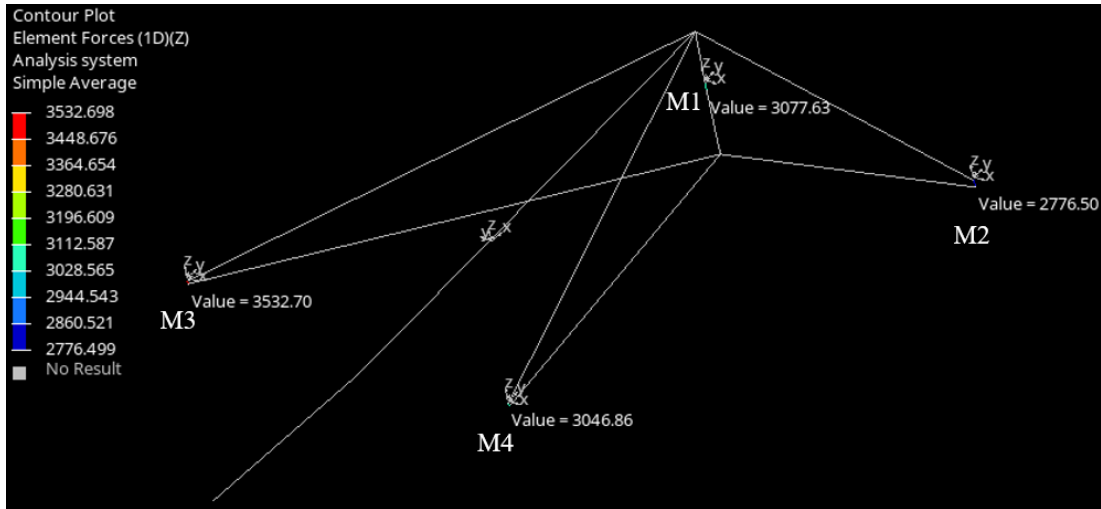


Figure 7.11: Results for gravity loading case

Coming up with the static analysis result for maximum torque case (including gravity) (Figure 7.12), it is seen that the applied torque is clock-wise around X-axis. Reaction forces are $M_1 = -6924.89\text{N}$ (compression), $M_2 = -1030.30\text{N}$ (tension), $M_3 = -9566.76\text{N}$ (compression), $M_4 = 3019.75\text{N}$ (tension).

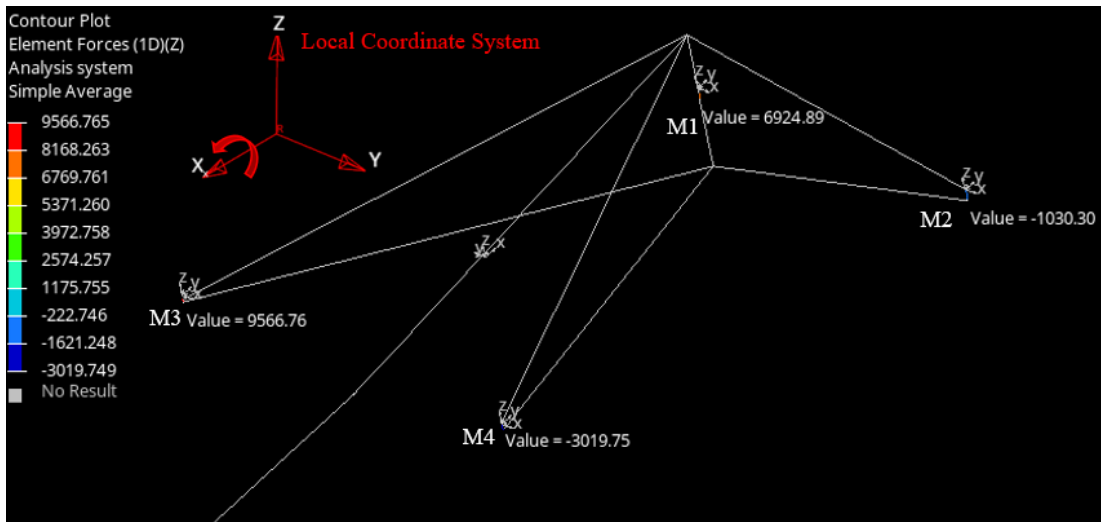


Figure 7.12: Results for maximum torque loading case

Static analyses results are also given in Table 7.5. Evaluating reaction forces according to stiffness diagrams of mount type A& B according to Figure 6.30 and 6.31, gravity

loading case are fully within the elastic working limits; however, the reaction force at M_3 is almost at the elastic deformation limit. Therefore, it should be reduced and this configuration cannot be safely used for PMS.

Table 7.5: Static analysis results

	Gravity [N]	Evaluation	Max Torque [N]	Evaluation
M_1	3077.63	OK	6924.89	OK
M_2	2776.5	OK	-1030.3	OK
M_3	3532.7	OK	9566.76	NOK
M_4	3046.86	OK	-3019.75	OK

7.2.2 Results of the Modal Analysis

Modal analysis results are shared. All six eigenvalues and each rigid body mode shape regarding these eigenvalues are calculated.

The first mode shape is the Fore-Aft along local Y-axis at 7.81Hz. Translational deflection is identified (Figure 7.13).

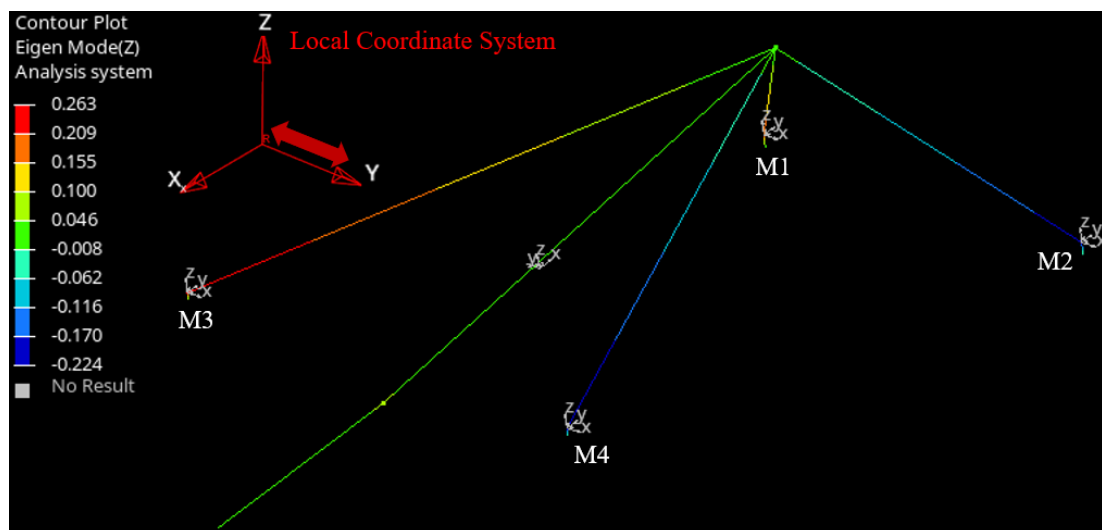


Figure 7.13 Mode 1, Fore aft on Y-axis at 7.82Hz

The second mode shape is the Bounce along local Z-axis at 10.49Hz. Deflection is translational (Figure 7.14).

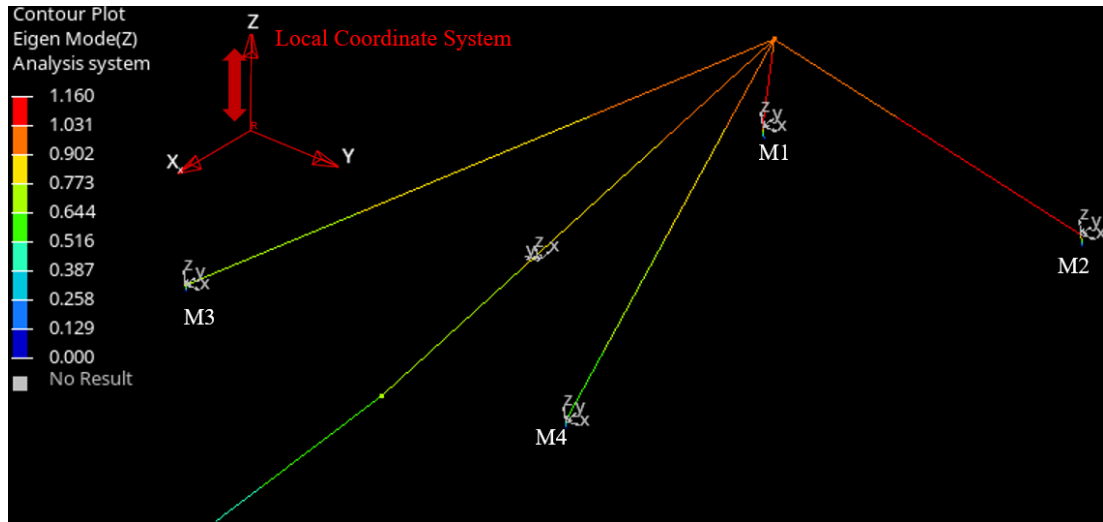


Figure 7.14 Mode 2, Bounce on Z-axis at 10.49Hz

The third mode shape is identified as Pitch around local Y-axis at 12.82Hz. The deflection is rotational (Figure 7.15).

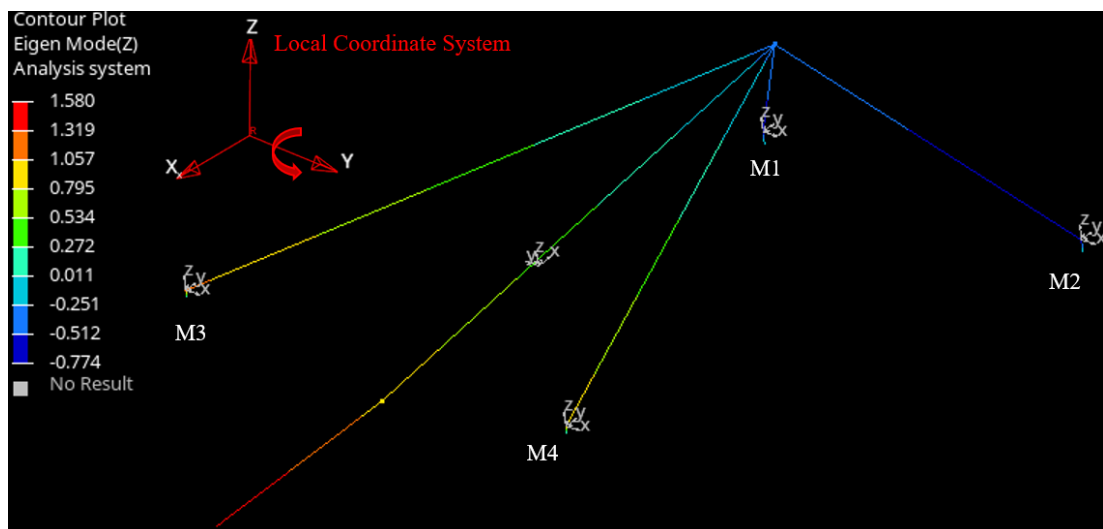


Figure 7.15: Mode 3, Pitch around Y-axis at 12.82Hz

The fourth mode shape is identified as Fore-Aft along local X-axis at 13.25Hz. The deflection is translational (Figure 7.16).

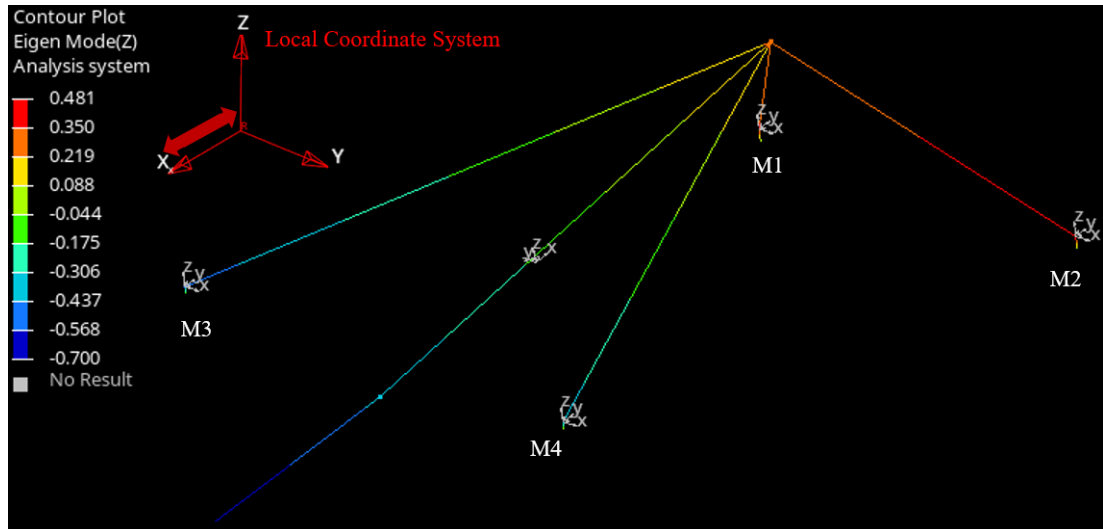


Figure 7.16: Mode 4, Fore-Aft on X-axis at 13.25Hz

The fifth mode shape is identified as Yaw around local Z-axis at 17.37Hz. The deflection is rotational (Figure 7.17).

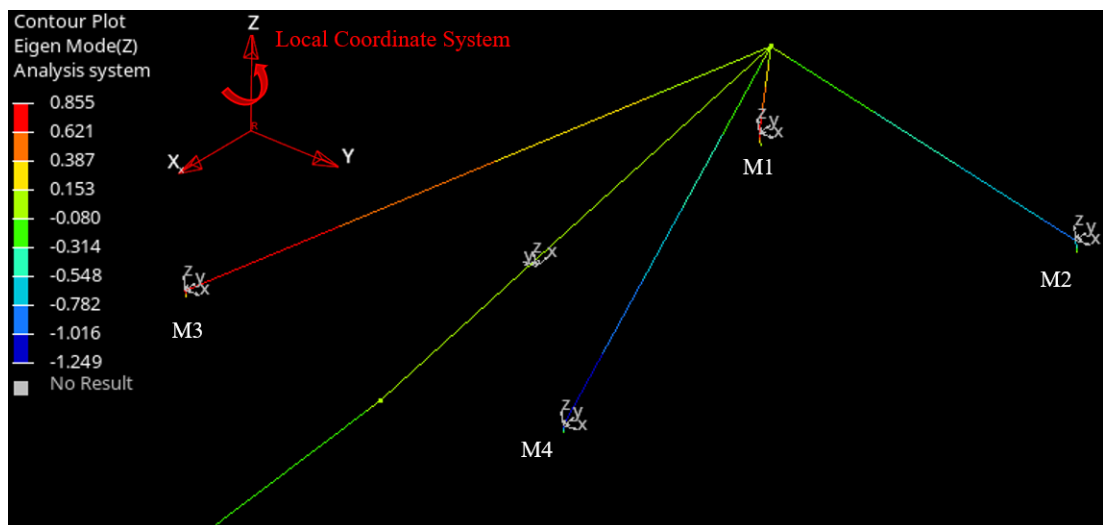


Figure 7.17: Mode 5, Yaw around Z-axis at 17.37Hz

The sixth and the last mode shape is roll around X-axis at 24.59Hz. Rotational deflection is observed (Figure 7.18). As the applied torque is also almost through the local X-axis, which is also called Torque Roll Axis (TRA), the roll-mode around TRA is the most remarkable mode shape as well as it is the greatest eigenvalue of the system.

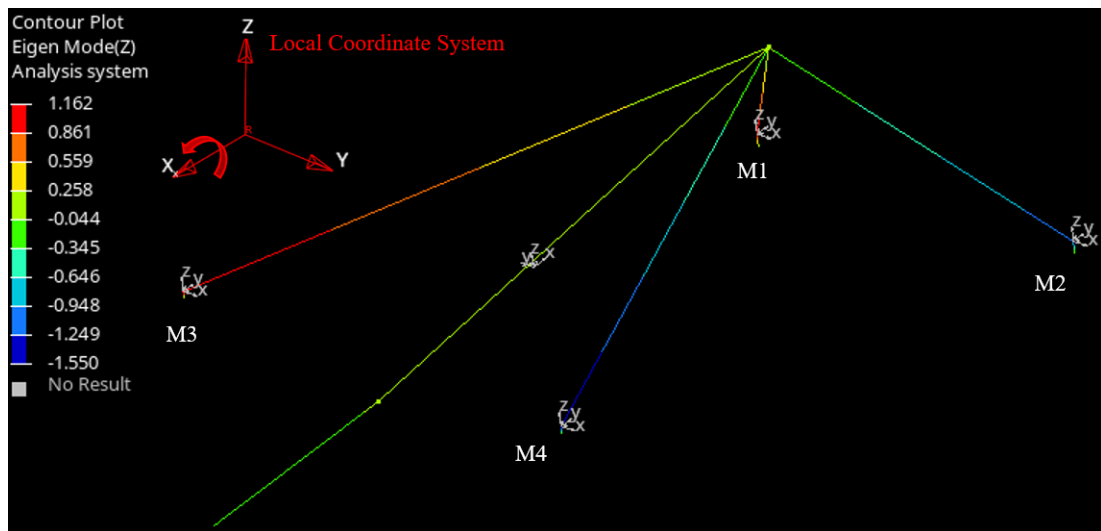


Figure 7.18 Mode 6, Roll around X-axis at 24.59Hz

All eigenvalues and mode shapes are also given in Table 7.6. Knowing that the greatest eigenvalue of the system should be less than 24.75Hz determined from equation (2.38), the sixth eigenvalue is observed slightly less than the target frequency, which is conditionally safe for the system.

Table 7.6: Modal analysis results

	Natural Frequency [Hz]	Mode Shape	Axis
Mode 1	7.82	Fore Aft	Trans-Y
Mode 2	10.49	Bounce	Trans-Z
Mode 3	12.82	Pitch	Rot-Y
Mode 4	13.25	Fore Aft	Trans-X
Mode 5	17.37	Yaw	Rot-Z
Mode 6	24.59	Roll	Rot-X

7.2.3 Results of the Transmissibility Analysis

Remembering that the system is excited by an angular acceleration of 1 rad/s^2 applied from the ground and the measuring node was the CG of the engine at the origin, the transmissibility ratio is found measuring transmitted angular acceleration through the PMS on TRA for the frequency interval between 1-50Hz. The resulting data is visualized by a transmissibility ratio vs. frequency plot given in Figure 7.19.

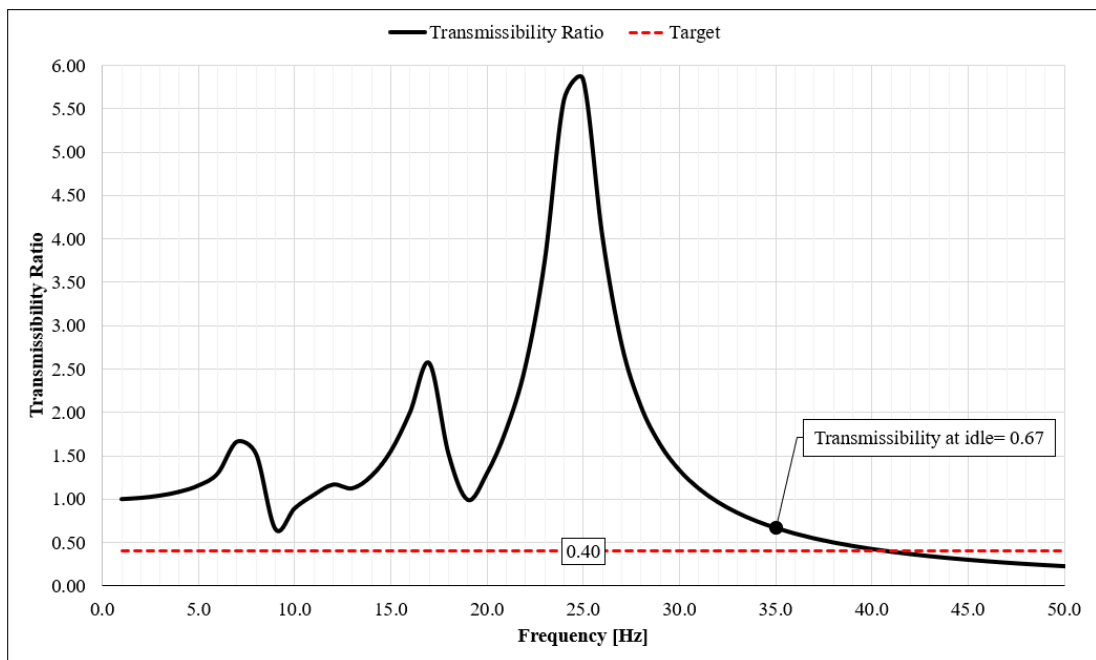


Figure 7.19: Transmissibility ratio vs. frequency plot

As shown in Figure 7.19, the target transmissibility ratio is given as 0.40 demonstrated by a dashed red line on the horizontal axis. Remembering that the idle frequency of the engine was 35Hz, and the transmissibility ratio is below 0.40 at idle frequency, the current transmissibility ratio is found 0.67 at the system. In other words, the PMS could isolate the vibration only 33% while 60% isolation is desired.

Moreover, deviations on the plot (Figure 7.19) in terms of transmissibility axis stems from the eigenvectors affecting local rotational X axis. By this, it is also seen that the peak value corresponds to the roll mode shape around TRA which was 24.59Hz. The second peak corresponds to the yaw mode shape deflected through local rotational X axis as well.

Furthermore, it is seen that excitation would be amplified if the excitation force approached the resonance frequency of the system, see 25Hz on Figure 7.19.

7.3 DoE and Parametric Optimization Results

7.3.1 DoE Results

Plackett-Burman design performs 16 iterations that provided a screening behavior of inputs and outputs to this study. The screening results in Plackett-Burman design in this study should not be expected as optimal results.

Initially, correlation between design variables and responses is investigated. Correlation values in Table 7.7 are marked greenish if the comparison is proportional to each other or positively correlated, and marked reddish if the comparison is inversely proportional or negatively correlated.

Referring Figure 6.27, M_1 and M_3 are on the right-hand side of the TRA, and M_2 and M_4 were on the left-hand side of the TRA.

For the right-hand side of the TRA, coming closer to engine-transmission group along global $-X$ direction provides a greater percentage of vibration isolation. On the other hand, for the left-hand side of the TRA, travelling away from the engine-transmission group provides a better vibration isolation value.

Considering coordinates for y-axis, travelling along global $+Y$ direction has almost no significant effect on dynamic responses which are modal and transmissibility responses. However, for mounts at transmission side it is revealed that M_3 would be better travel along $+Y$ direction and M_4 should be vice versa.

Table 7.7: Correlation table between design variables and response functions

	Coordinates M_1			Coordinates M_2			Coordinates M_3			Coordinates M_4		
	x_1	y_1	z_1	x_2	y_2	z_2	x_3	y_3	z_3	x_4	y_4	z_4
Transm.	-0.30	-0.03	-0.04	0.14	0.09	-0.04	-0.27	0.19	0.19	0.27	-0.18	-0.07
Modal	-0.34	-0.05	-0.12	0.08	0.20	0.02	-0.19	0.31	0.15	0.16	-0.28	-0.36
Torque M_1	0.14	-0.22	0.14	0.22	-0.31	-0.11	0.32	-0.58	-0.23	-0.02	0.29	0.18
Torque M_2	-0.04	-0.18	0.04	0.02	0.00	-0.14	0.32	0.31	0.10	0.06	-0.17	-0.13
Torque M_3	0.11	0.37	-0.11	-0.07	0.21	0.12	-0.19	0.43	0.17	-0.09	-0.21	-0.22
Torque M_4	0.65	-0.10	0.30	-0.16	-0.39	-0.14	-0.02	-0.68	-0.43	0.46	0.51	0.43

The correlation network within the response functions are also investigated (Table 7.8). Results shows that the roll mode frequency was highly and positively correlated (0.82) with transmissibility ratio. In other words, the smaller the eigenvalue of the roll mode shape is, the higher the vibration isolation is.

Secondly, reaction force at mount number 3 is found to be highly and positively correlated (0.86) with reaction force at mount number 2 for the maximum torque loading case.

Table 7.8: Correlation table within response functions

Transm.	1.00					
Modal	0.82	1.00				
Torque M ₁	-0.23	-0.45	1.00			
Torque M ₂	-0.31	-0.04	-0.53	1.00		
Torque M ₃	-0.14	0.22	-0.67	0.86	1.00	
Torque M ₄	-0.48	-0.33	0.17	0.27	0.27	1.00
	Transm.	Modal	Torque M ₁	Torque M ₂	Torque M ₃	Torque M ₄

As it is expected, no correlation was found between the design variables since those are independent coordinates.

7.3.2 Parametric Optimization Results

Results of the parametric optimization which is performed by applying MOGA revealed 3308 positional configurations for 4-mounted PMS within introduced control volumes. However, only 591 positional configurations are found to satisfy the constraining functions. Each optimal result is found as constraining functions is introduced into the optimization study. However, as the number of optimal positional configurations is very high to easily select the best one value, more evaluation is needed.

Since the target of the study is primarily on vibration control, parametric optimization results according to transmissibility and modal analysis are investigated first of all. Secondly, reaction forces are taken into consideration.

All optimal positional configurations are shown as blue dots in Figure 7.20. Blue dots can be compared by checking transmissibility ratio on the vertical axis and by the natural frequency value of the roll modes on the horizontal axis. Natural frequencies of the roll modes are ranged between 15.66 – 22.30 Hz along the horizontal axis, while

transmissibility ratios are ranged between 0.16 – 0.40 Hz along the vertical axis. In this regard, all of the 591 positional conditions met the dynamic targets of modal and transmissibility analyses. As demonstrated in DoE study, transmissibility ratio is found to be proportional with the natural frequency of the roll mode. That is why distribution of blue dots seem to be a $y=x$ polynomial.

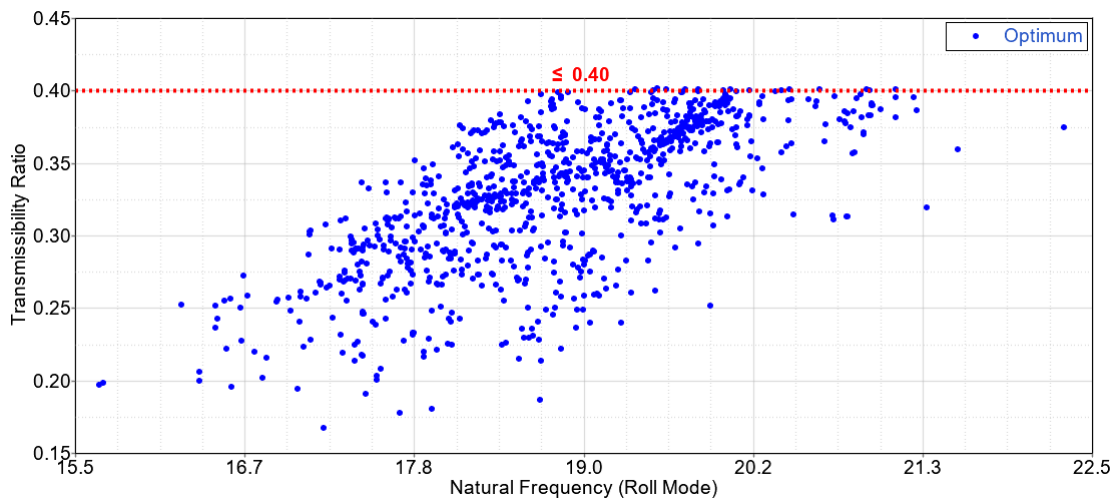


Figure 7.20: Transmissibility ratio vs. natural frequency of the roll mode

It is also known that reaction force due to the torque of the engine should be minimized since the reaction force may cause a plastic deformation on PMS. This reaction force can be either tensile or compressive force. Regardless of in which direction the reaction force is located, the sum of each absolute reaction force –which is called the absolute cumulative reaction force– towards Z-axis should be minimized. By this means, dots shown in Figure 7.20 are modified with bubble shapes and a new graph is created (Figure 7.21). In Figure 7.21, blue bubbles designate the cumulative reaction force caused by torque input of the engine. Diameter of bubbles are proportional with the absolute cumulative reaction force from 0 to 32.46kN.

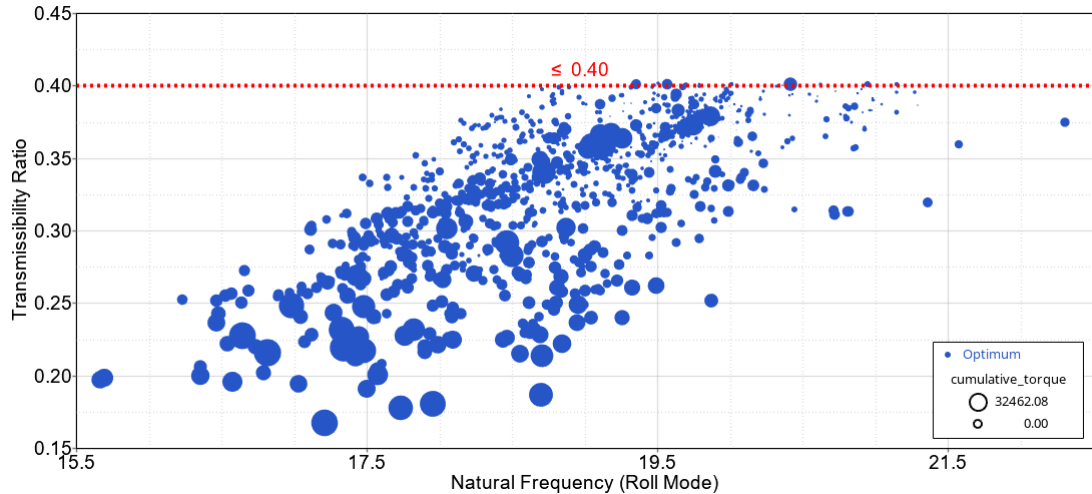


Figure 7.21: Comparison of optimal results according to all responses

Figure 7.21 states that transmissibility ratio seems to be inversely proportional to absolute cumulative reaction force. Smaller bubbles are located at the upper area on the graph while low transmissibility ratio refers to the downer area on the graph. In this consideration, Figure 7.21 states that a higher vibration isolation causes higher overall reaction forces on PMS.

Reaction forces are not desired to be at the edge of the elastic limits of engine mounts even though they satisfy the constraining functions and objective functions. Therefore, each reaction force on each engine mount (M_1 , M_2 , M_3 , and M_4) should be investigated. To do this, bubbles in Figure 7.21 are colorized from blue to red, and Figure 7.22, 7.23, 7.24 and 7.25 are created. In these figures, a bubble being closer to reddish means an increased absolute reaction force on corresponding engine mount. Doing this, transmissibility ratio, natural frequency values, and absolute cumulative reaction forces can also be seen in Figure 7.22 to 7.25.

Absolute reaction force at Z-axis for M_1 ranges from 5.2kN to 14.5kN. Lower reaction forces point out respectively a higher transmissibility rate (between 0.30 – 0.40) (Figure 7.22).

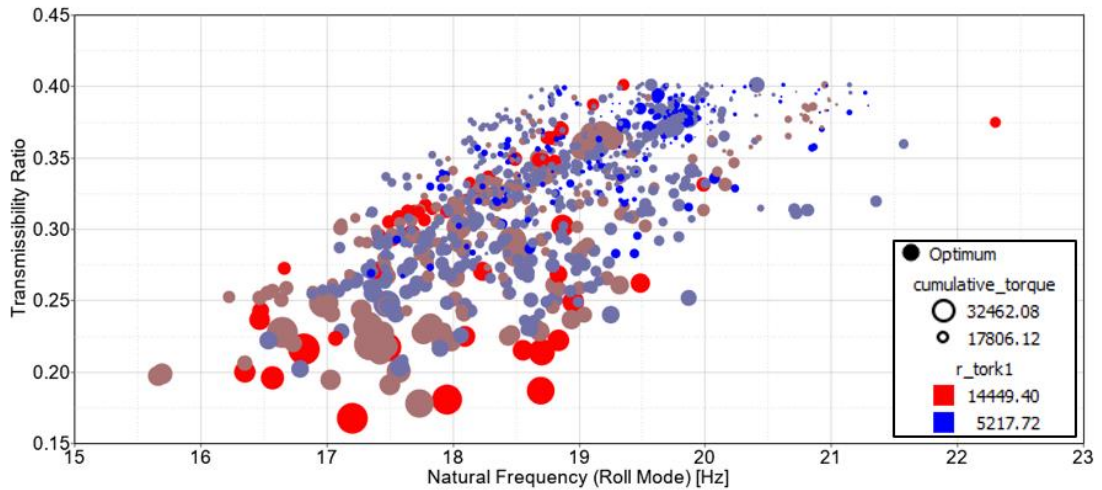


Figure 7.22: Comparison of vibration isolation in terms of cumulative force reaction and the force reaction received by M_1

Absolute reaction force at Z-axis for M_2 ranges from zero to 5.3kN. Lower reaction forces point out respectively a lower transmissibility rate (between 0.16 – 0.30) (Figure 7.23).

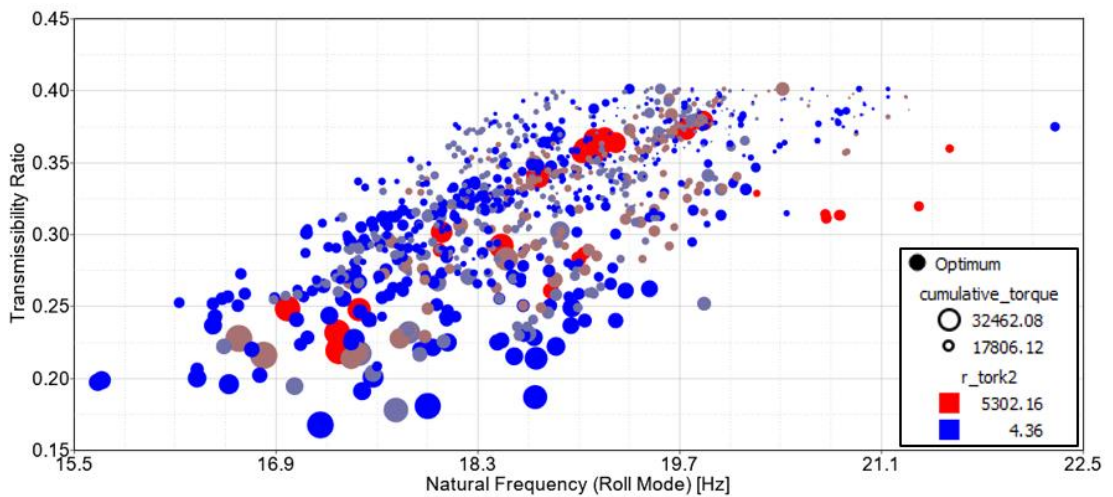


Figure 7.23: Comparison of vibration isolation in terms of cumulative force reaction and the force reaction received by M_2

Absolute reaction force at Z-axis for M_3 ranges from 3.4kN to 10kN. Lower reaction forces point out mid-rates of transmissibility (between 0.30 – 0.35) (Figure 7.24).

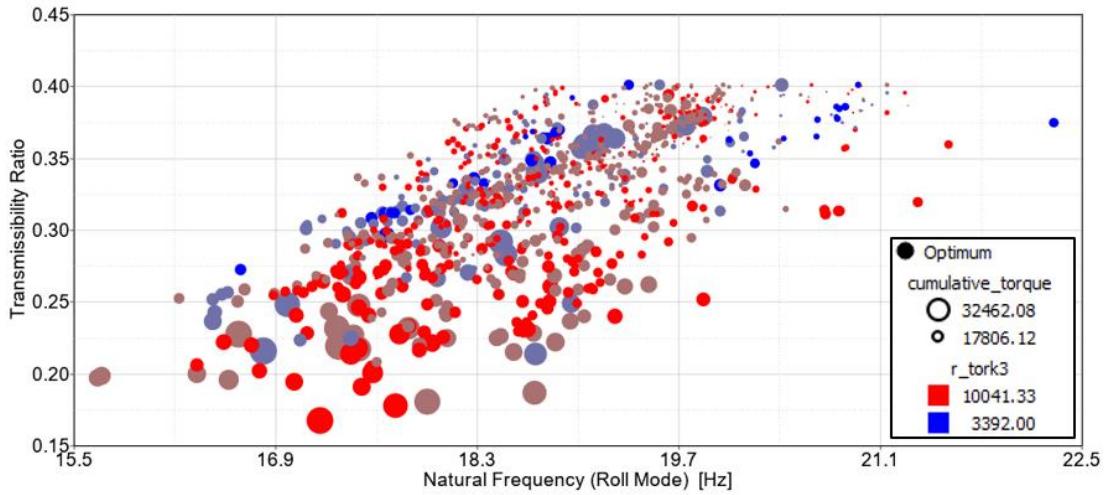


Figure 7.24: Comparison of vibration isolation in terms of cumulative force reaction and the force reaction received by M_3

Absolute reaction force at Z-axis for M_4 ranges from 0.2kN to 10kN. Lower reaction forces point out mid-rates of transmissibility (between 0.25 – 0.40) (Figure 7.25).

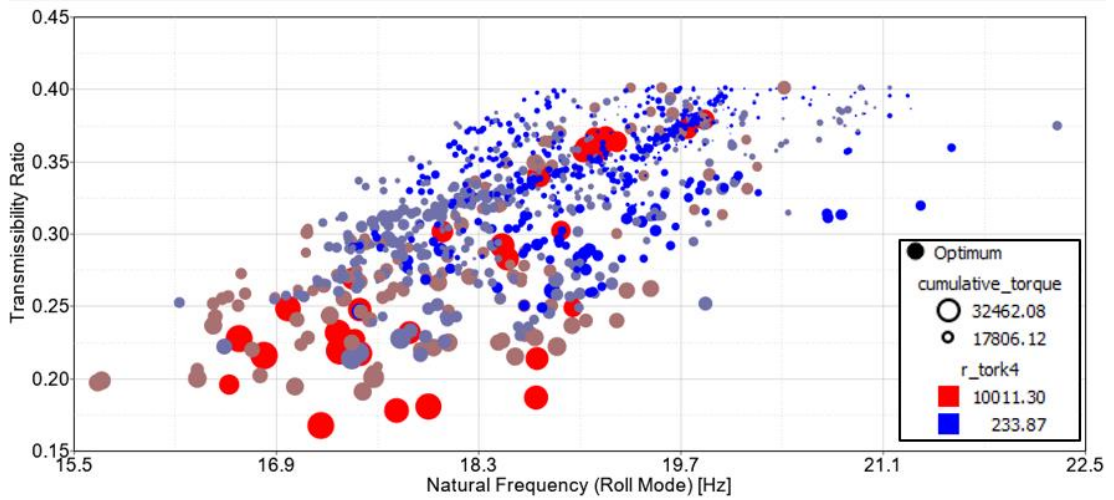


Figure 7.25: Comparison of vibration isolation in terms of cumulative force reaction and the force reaction received by M_4

In order to find the most appropriate and balanced positional configuration according to absolute reaction forces shown in Figure 7.22, 7.23, 7.24, and 7.25, a probability distribution for each engine mount is created by histogram plotting. Histogram plots

provide an understanding on results by answering these questions: “How often?” and “In what range?”.

To do that, each absolute reaction force results for M_1 , M_2 , M_3 , and M_4 are evaluated separately first of all. For example, absolute reaction forces on M_1 in optimal configurations are distributed into uniform range (Figure 7.26) on the horizontal axis and each absolute reaction forces are put into each bar in order to answer the question “What is the most frequent absolute reaction force on M_1 ?”. Moreover, the mean value and standard deviation for absolute reaction force on M_1 are evaluated and then designated on histogram plots. This operation is done for M_2 in Figure 7.27, for M_3 in Figure 7.28, and for M_4 in Figure 7.29.

Bubble plots are associated with histogram plots such that Figure 7.26 refers to Figure 7.21, Figure 7.27 refers to Figure 7.23, Figure 7.28 refers to Figure 7.24, and Figure 7.29 refers to Figure 7.25.

A probability density function provides a simple description of the probabilities associated with a random variable. A histogram is an approximation for a probability density function. For each interval of the histogram, the area of the bar equals the relative frequency (proportion) of the measurements in the interval. The relative frequency is an estimate of the probability that a measurement falls in the interval.

Reaction force of M_1 among all optimization results is distributed using histogram plot as shown in Figure 7.26. The mean of reaction forces on M_1 is found as 8795.97N while the mean of all feasible reaction forces on M_1 was 9181.78N. Among the entire iterations, the greatest P value –which designates the most frequent reaction force– is found as 0.38 at 9233.68N.

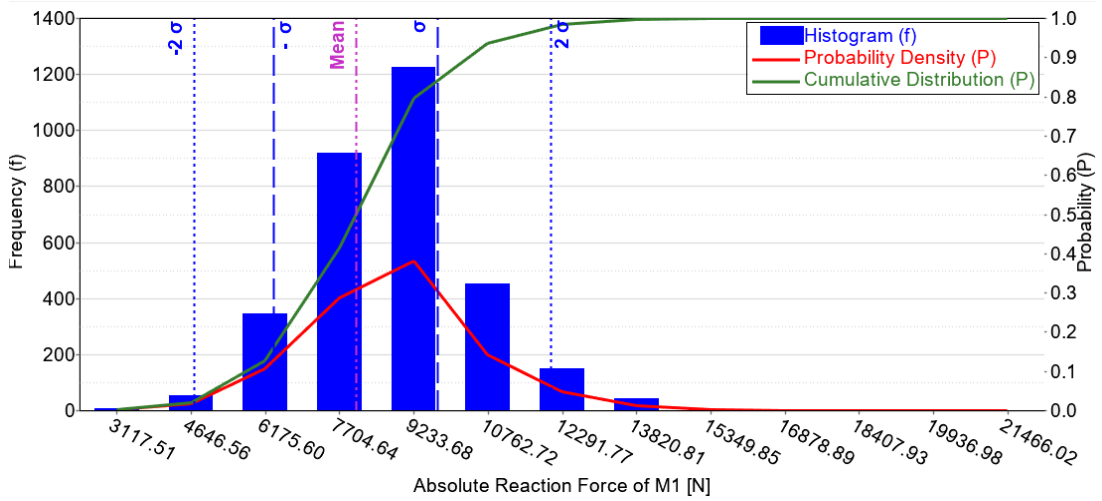


Figure 7.26: Absolute reaction force distribution of M_1

Reaction force of M_2 among all optimization results is distributed using histogram plot as shown in Figure 7.27. The mean of reaction forces on M_2 is found as 1781.52N while the mean of all feasible reaction forces on M_2 is 1706.16N. Among the entire iterations, the greatest P value is found as 0.16 at 1259.04N.

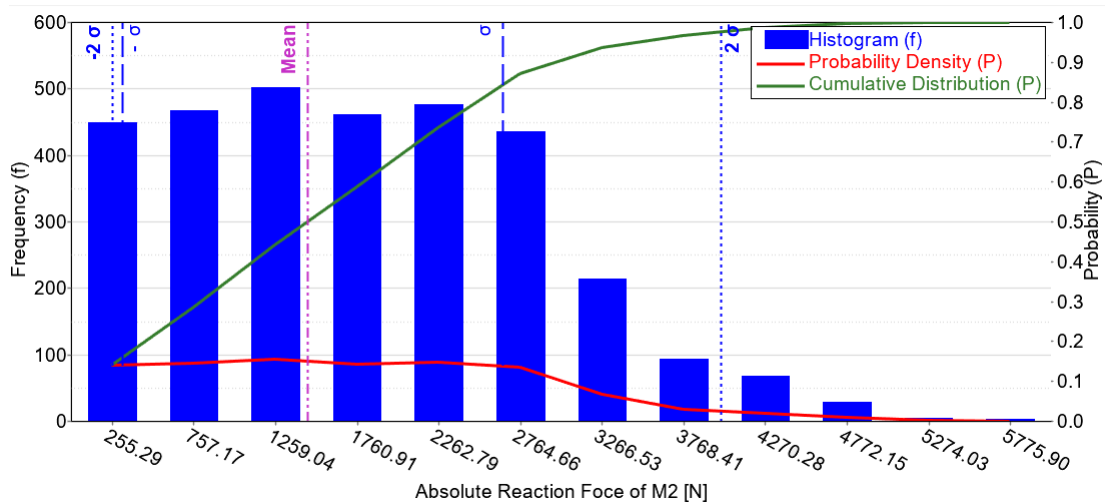


Figure 7.27: Absolute reaction force distribution of M_2

Reaction force of M_3 among all optimization results is distributed using histogram plot as shown in Figure 7.28. The mean of reaction forces on M_3 is found as 8279.73N

while the mean of all feasible reaction forces on M_3 is 7704.44N. Among the entire iterations, the greatest P value is found as 0.25 at 7898.86N.

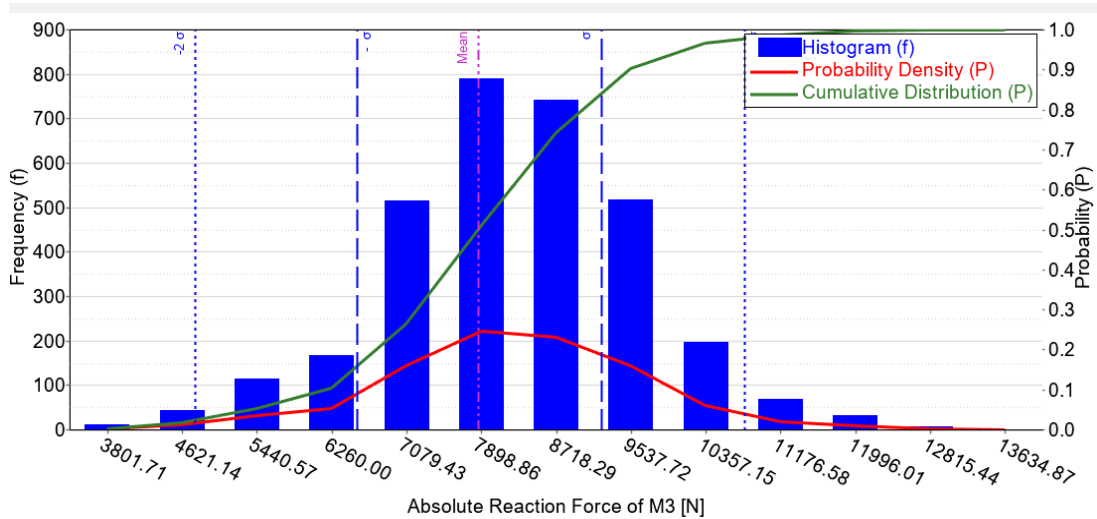


Figure 7.28 Absolute reaction force distribution of M_3

Reaction force of M_4 among all optimization results is distributed using histogram plot as shown in Figure 7.29. The mean of reaction forces on M_3 is found as 3514.51N while the mean of all feasible reaction forces on M_3 is 3194.38N. Among the entire iterations, the greatest P value is found as 0.19 at 2279.64N.

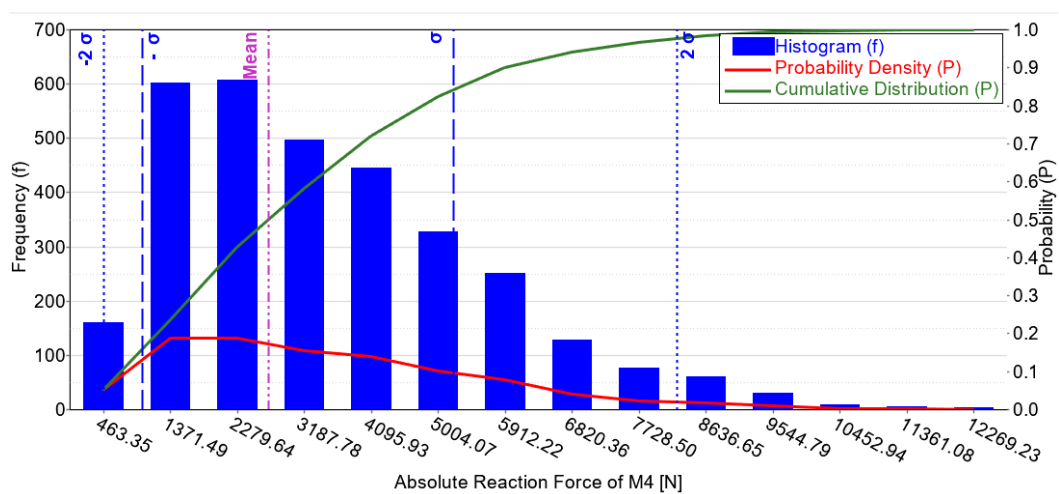


Figure 7.29: Absolute reaction force distribution of M_4

After investigating the probability distribution of absolute reaction forces on each mount, responses of all optimal positional configurations are filtered according to acquired statistical information shown in Figure 7.26, 7.27, 7.28, and 7.29. The most appropriate and balanced positional configuration is selected as shown in Table 7.9.

Table 7.9: Coordinates of the best positional configuration of the PMS according to specs and scope of the study

Mount #	X [mm]	Y [mm]	Z [mm]
M ₁	-192.26	500.89	-418.47
M ₂	316.75	289.02	-233.01
M ₃	-339.23	-1085.25	-359.74
M ₄	210.01	-321.3	36.12

By means of the parametric optimization, dramatic changes are observed in the system (Table 7.10). Vibration isolation rate at the PMS of the vehicle is enhanced from 33% to 72%. The natural frequency of the roll mode shape reduced 25% from 24.59Hz to 18.33Hz. Reaction forces at M₁ and M₂ faced with dramatic increases which are 25.61% and 50.32% respectively. On the contrary, A reduction in reaction forces is obtained at M₃ and M₄ which were 21.11% and 24.79% respectively.

Table 7.10: Percent change in responses by means of parametric optimization

Criteria	Pre-optimization Results	Optimization Results	% Change
Transmissibility Ratio	0.67	0.28	57.55
Eigenvalue of the Roll Mode [Hz]	24.59	18.33	25.47
Reaction force at M ₁ [N]	6924.89	8698.63	-25.61
Reaction force at M ₂ [N]	-1030.3	-1548.71	-50.32
Reaction force at M ₃ [N]	9566.76	7546.90	21.11
Reaction force at M ₄ [N]	-3019.75	-2271.03	24.79

Moreover, the transmissibility ratio of the optimal configuration is investigated in post-optimization process (Figure 7.30). At the peak location demonstrated the roll mode shape whose eigenvalue is 18.33Hz. Consequently, the transmissibility ratio at idle frequency of 35Hz is found to be 0.28.

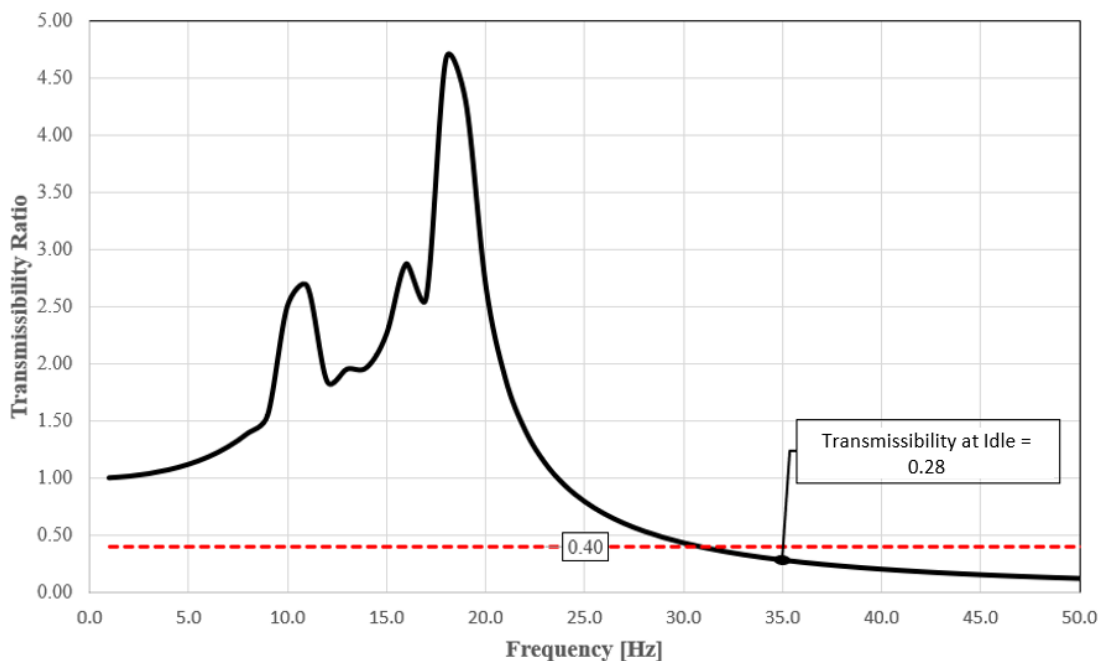


Figure 7.30: Transmissibility ratio of the post-optimization analysis

Chapter 8

Conclusion

This study revealed a comprehensive methodology with a procedural point of view in terms of vibration isolation. The optimization methodology was performed through a validated FE model. Therefore, any type of commercial vehicle can be analyzed by this validation. The only problem during the validation process was that the modal test could not reveal all decoupled modal shapes since two of the modes were almost coupled. However, as the key-point for the study was to decrease the natural frequency of the roll mode, the test was satisfactory to validate the FE model. Static FE analysis and static physical test for the reference powertrain system were close to each other, which verified the validation outputs.

Mount location coordinates were randomly selected in the control volume at the beginning for the optimization model of the powertrain. In order to get initial results from randomly selected locations, a pre-optimization analysis was performed for static, modal and transmissibility outputs. Afterwards, a DoE study was done based on the results of pre-optimization analysis. Plackett-Burman design provided the study comprehensive correlations both between design variables and response function, and among response functions. Screening results demonstrated how initial coordinates of the optimization model would change based on the pre-optimization results. By Plackett-Burman design, the system showed the response changes according to each change in coordinates. It also revealed the inter-relationship among response functions. Those clarified us how parameters responded and how responses affected each other.

Finally, a parametric optimization was performed using MOGA. According to the outputs of parametric optimization based on MOGA, 591 configurations were determined that satisfied each constraining function. However, since the number of optimal points were high and the configurations having coordinates such that output

of response functions were at their limits, a probabilistic distribution in terms of torque loading case for each mount was analyzed. For the confidence level $\sigma = \pm 1$ of the probabilistic distribution, configurations having the smallest reaction force were determined. Among them the best configuration was selected regarding dynamic characteristics of configurations. Eventually, the configuration having 0.28 transmissibility ratio was selected, which provided 72% vibration isolation. Therefore, the vibration isolation was enhanced 57.55% with respect to the initial isolation rate which was 33%.

In a further study, engine brackets –which are the components to fix powertrain to the chassis– can be studied according to selected PMS hardpoints. Knowing the locations of those brackets fixed to engine and transmission, a topology optimization can be performed since all hardpoints would be discrete in this further study.

References

- [1] Tair R, Machado CB, Chiementin X, Bernardo-Filho M. Whole Body Vibrations: Physical and Biological Effects on the Human Body. CRC Press; 2018.
- [2] Hostens I, Ramon H. Descriptive analysis of combined cabin vibrations and their effect on the human body. *Journal of Sound and Vibration* 2003; 266: 453-464. doi.org/10.1016/S0022-460X(03)00578-9
- [3] ISO/TC 108/SC 4 - Human exposure to mechanical vibration and shock [Internet]. ISO. 2021 [cited 27 October 2021]. Available from: <https://www.iso.org/committee/51514.html>
- [4] Jazar RN. *Vehicle dynamics: theory and application*. New York: Springer; 2008.
- [5] Mahajan SR, Rajopadhye RD. Transportation noise and vibration-sources, prediction and control. *International Journal of Soft Computing and Engineering* 2013; 3(5): 2231-2307.
- [6] Lichty L. *Combustion Engine Process*. New York: McGraw Hill; 1967.
- [7] Karagöz M, Tuncay B. An engine mount design and vibration analysis. *International Journal of Automotive Science and Technology* 2020; 4(3): 164-170.
- [8] Erdelyi HE, Roesems D, Toso A, Donders S. Powertrain mounting system layout for decoupling rigid-body modes in the vehicle concept design stage. *SAE Technical Paper Series* 2013-01-1706. doi.org/10.4271/2013-01-1706
- [9] Yunhe Y, Naganathan NG, Dukkipati RV. A literature review of automotive engine mounting systems. *Mechanism and Machine Theory* 2001; 36(1): 123-142. doi.org/10.1016/S0094-114X(00)00023-9

- [10] Courteille E, Leotoing L, Mortier F, Ragneau E. New analytical method to evaluate the powerplant and chassis coupling in the improvement vehicle NVH. *European Journal of Mechanics-A/ Solids* 2005; 24(6): 929-943.
- [11] Sui J, Hoppe C, Hirshey J. Powertrain mounting design principles to achieve optimum vibration isolation with demonstration tools. SAE Technical paper 2003-01-1476. doi: 10.4271/2003-01-1476.
- [12] Sano T. Engine mount simulation tool by ease of use. SAE Technical paper 2004-32-0066. doi: 10.4271/2004-32-0066.
- [13] Courteille E, Mortier F, Leotoing L, Ragneau E. Multi-objective robust design optimization of an engine mounting system. SAE Technical paper 2005-01-2412. doi: 10.4271/2005-01-2412.
- [14] El Hafidi A, Martin B, Loredó A, Jégo E. Vibration reduction on city buses: Determination of optimal position of engine mounts. *Mechanical Systems and Signal Processing* 2010; 24(7): 2198-2209. doi.org/10.1016/j.ymsp.2010.04.001
- [15] Shital P, Ghosh C, Talwar H, Gosain A, Dayal P. A study of engine mount optimisation of three-cylinder engine through multi-body dynamic simulation and its verification by vehicle measurement. SAE Technical Paper Series 2015-26-0126. doi.org/10.4271/2015-26-0126
- [16] Ooi L, Ripin Z. Optimization of an engine mounting system with consideration of frequency-dependent stiffness and loss factor. *Journal of Vibration and Control* 2014; 22(10): 2406-2419.
- [17] Naseri R, Ohadi A, Fakhari V, Talebi HA. Optimal characteristics determination of engine mounting system using TRA mode decoupling with emphasis on frequency responses. *Journal of Theoretical and Applied Vibration and Acoustics* 2017; 3(2): 111-126
- [18] Jeong T, Singh R. Analytical methods of decoupling the automotive engine torque roll axis. *Journal of Sound and Vibration* 2000; 234(1): 84-114. doi.org/10.1006/jsvi.1999.2860

- [19] Xu X, Su C, Dong P, Liu Y, Wang S. Optimization design of powertrain mounting system considering vibration analysis of multi-excitation. *Advances in Mechanical Engineering* 2018; 10(9): 1-12. doi.org/10.1177/1687814018788246.
- [20] Liang J, Zhang D, Wang S. Vibration characteristic analysis of single-cylinder two-stroke engine and mounting system optimization design. *Science Progress* 2020; 103(3): 1-21. doi.org/10.1177/0036850420930631
- [21] Rossi de Sá W, Silveira H, Pederiva R. Influence of the positioning and characteristics of the cushions in the dynamic response of a four cylinders diesel engine. *SAE Technical Paper Series 2015-36-0325*. doi.org/10.4271/2015-36-0325
- [22] Rao S. *Mechanical Vibrations*. Upper Saddle River: Prentice Hall; 2011.
- [23] Rivin EI. *Passive Vibration Isolation*. New York: ASME Press; 2003.
- [24] Gatti PL. *Applied Structural and Mechanical Vibrations: Theory, Methods and Measuring Instrumentation*. CRC Press; 1999.
- [25] Zanwar DR, Deshpande VS, Modak JP, Gupta MM, Agrawal KN. Determination of mass, damping, coefficient, and stiffness of production system using convolution integral. *International Journal of Production Research* 2015; 53(14): 4351-4362. doi.org/10.1080/00207543.2014.998787
- [26] Braun S, Ewins D, Rao SS. *Encyclopedia of Vibration*. Cornwall: Academic Press; 2002.
- [27] Mead DJ. *Passive Vibration Control*. West Sussex: John Wiley and Sons Ltd; 2000.
- [28] CTP Rubber Mounts. [Internet]. [Date of Access 7.12.2021]. <https://www.costex.com/rubber-mounts/>
- [29] Wang Q, Wang L, Tan L. Automotive Vehicle Powertrain Mounting System Optimum Design and Simulation Analysis. *Proceedings of IAJC/ASEE*. 2011.

- [30] Ramachandran T, Padmanaban KP. Review on internal combustion engine vibrations and mountings. *International Journal of Engineering Sciences and Emerging Technologies* 2012; 3(1): 63-73.
- [31] Zhou J, Xiao Q, Xu D, et al. A novel quasi-zero-stiffness strut and its applications in six degree-of-freedom vibration isolation platform. *Journal of Sound and Vibration* 2017; 394: 59-74.
- [32] Krzyzynski T, Maciejewski I, Meyer L, Meyer H. *Modelling and Control Design of Vibration Reduction Systems: Methods and Procedures of Selecting Vibro-isolation Properties*. Springer International Publication; 2018.
- [33] Keshavarz A, Bayani Khaknejad M, Azadi S. Improving vehicle nvh behavior via tuning the engine mount stiffness using doe method. *SAE Technical Paper Series* 2011-05-1510. doi.org/10.4271/2011-01-1510
- [34] Mollenhauer K, Tschoke H. *Handbook of Diesel Engines*. Berlin: Springer; 2010.
- [35] Taylor CF. *The Internal Combustion Engine in Theory and Practice*. Massachusetts: Mit Press; 1985.
- [36] Mashadi B, Crolla DA. *Vehicle Powertrain Systems*. West Sussex: John Wiley and Sons Ltd; 2012.
- [37] Rivin EI. *Passive Vibration Isolation*. New York: ASME Press; 2003
- [38] Kumar Battula S, Rama Murty Raju P, Ratnam C. Engine isolation angular mount with different types elastomers. *Materials Today: Proceedings* 2018; 5(9): 19555-19564. doi.org/10.1016/j.matpr.2018.06.317
- [39] Tuncay, B. Otomobillerde kullanılan bir motor takozunun tasarımı ve analizi (master's thesis). Karabük: Karabük University; 2020. <https://tez.yok.gov.tr/>
- [40] Logan DL. *A First Course in the Finite Element Method, SI Edition (6th ed.)*. Cengage Learning; 2016. ISBN-13: 978-1-305-63734-4

- [41] Zienkiewicz OC, Taylor RL, Zhu JZ. The Finite Element Method: Its Basis and Fundamentals (6th ed.). Elsevier Butterworth-Heinemann; 2005. ISBN 0 7506 6320 0
- [42] Zolpakar NA, Lodhi SS, Pathak S, Sharma MA. Application of Multi-Objective Genetic Algorithm (MOGA) Optimization in Machining Process. In: Gupta K, Gupta M (eds) Optimization of Manufacturing Processes. Springer Series in Advanced Manufacturing. Springer, Cham; 2020. https://doi.org/10.1007/978-3-030-19638-7_8
- [43] PCB Piezotronics. Model:356A33 Accelerometer, ICP, Triaxial. [Internet]. [Date of Access 7.12.2021]. <https://www.pcb.com/products?model=356A33>
- [44] Brüel & Kjær. Modal Sledge Hammer, 1lb Head, Cable Included. [Internet]. [Date of Access 7.12.2021]. <https://www.bksv.com/en/transducers/vibration/impact-hammers/8207>
- [45] Konak A, Coit DW, Smith AE. Multi-objective optimization using genetic algorithms: A tutorial. Reliability Engineering & System Safety 2006; 91(9): 992-1007. <https://doi.org/10.1016/j.res.2005.11.018>.
- [46] He J, Fu Z-F. Modal Analysis. Oxford: Butterworth-Heinemann; 2004.

Curriculum Vitae

Name Surname : Sinan Yıldırım

Education:

2011–2016 İzmir Institute of Technology, Dept. of Mechanical Eng.
2018–2022 İzmir Kâtip Çelebi University, Dept. of Mechanical Eng.
2021– İzmir Institute of Technology, Dept. of Engineering
Management.

Work Experience:

2017 – 2018 Dirinler Sanayi Makinaları Endüstri ve Tic. A.Ş
2019 – BMC Otomotiv Sanayi ve Tic. A.Ş